Metabolomics Footprinting of Three Dimensional Bioreactors with Applications to In-Cell NMR

Christopher M. Seagle

A dissertation submitted to the faculty of the University of North Carolina at Chapel Hill in partial fulfillment of the requirements for the degree of Doctorate in the department of Biomedical Engineering.

Chapel Hill
2007

Approved by:

Professor Jeffrey M. Macdonald, Ph.D.

Professor Robert G. Dennis, Ph.D.

Professor Oleg V. Favorov, Ph.D.

Professor Shawn M. Gomez, Ph.D.

Professor Timothy A. Johnson, Ph.D.

Professor Mark Tommerdahl, Ph.D.

Abstract

CHRISTOPHER M. SEAGLE: Metabolomics Footprinting of Three Dimensional Bioreactors with Applications to In-Cell NMR
(Under the direction of Jeffrey M. Macdonald, Ph.D.)

Electrostatic devices for the manufacturing of cell encapsulations were constructed and used to form spherical alginate encapsulations containing hepatocytes, hepatic progenitor cells, mixed hepatic populations, and *Escherichia coli*. The encapsulations were tested for cell viability, cell functionality, respiration, and encapsulation architecture. A novel high through-put NMR method was used to test serial media extractions from multi-coaxial bioreactors to determine metabolic function of human hepatic cell encapsulations over a 30 day period. These tests revealed that by day five, lactate decreased below detection limits while glucose concentrations did not significantly change indicating aerobic metabolism. Evidence of system perturbation and recovery following ammonia spiking of superfused media was also observed along with glutamine metabolism indicating urea cycle activity. These NMR results are the first demonstration of an assay to monitor the full spectrum of metabolites found in *ex vivo* encapsulated hepatic cell culture media for determination of consumption and production rates.

Improvements to the NMR method were introduced to accommodate for evaporative loss and allow for more precise determination of actual metabolite consumption of media constituents and production of metabolites. This new approach was used to compare metabolism differences between three-dimensional

closed loop bioreactors and classic two-dimensional cultures to test the hypothesis that the more efficient 3D bioreactor will facilitate aerobic metabolism compared to 2D cultures. This will be reflected by consumption of aerobic nutrients, such as glutamine and alanine, and anaerobic production of lactate. Based upon differences in metabolism of glucose and other energy sources, these studies seek to also test the hypothesis that traditionally observed oxygen levels (95%) in 3D culture studies are excessive for hepatocytic function.

The tools of encapsulation based metabolomics were adapted to in-cell protein conformation studies using *Escherichia coli*. Preliminary findings, while inconclusive, suggest that encapsulation based studies can eliminate confounding extracellular signals in NMR studies.

Dedication

This work is dedicated first to my wife Carol for her support throughout my academic career and for showing me that this endeavor was an achievable goal through her own hard work in academic science. I should also thank, by way of dedication, my parents who as scientists first instilled in me the appreciation for the wonder of science.

Acknowledgements

This work could not have been carried out without the assistance and guidance I have received from so many outstanding individuals and laboratories. I therefore wish to acknowledge Connie Engle, Tim Johnson, Wayne Cascio, Barbara Muller-Borer, and Leonard Gettes for the training I received at the UNC-CH Experimental Cardiology Lab especially in the areas of confocal microscopy, experimental design, small animal surgery, instrument design, and electrical safety. Thanks to the many instructors in the Departments of Biomedical Engineering, Pathology, and Pharmacology their fine tutelage. Thanks to the Michael Chua and Wendy Salmon at the Michael Hooker Microscopy Core Facility for training, equipment usage, and consultation. Thanks to Bob Bagnell, Vicky Madden, and Elena Davis at the UNC Microscopy Service Laboratory for training, equipment usage, and consultation on electron microscopy. Thanks to David Gerber, Lisa Rice and Prakash Chandrasekaran of the UNC Transplant Surgery Lab for contributions to numerous to list. Thanks to Megan Christie, Mark Johnston, Randy McClelland and John Ludlow at Vesta Therapeutics and Admet Technologies for providing human cells, bioreactor maintenance, and financial underwriting for portions of this work. Thanks to Mark ter Horst for his patience and NMR training. Special thanks to all the collaborators I have had on the many projects undertaken in the seven years I spent at UNC—William Turner, Lisa Charlton, Gary Pielak, Rex Jeffries,

Jason Winnike, Tom O'Connell, Vinay Tannan, Mike Gamcsik, Oleg Favorov, and many others. Lastly, thanks to Jeff Macdonald for believing in and sticking with this project despite the many challenges.

Table of Contents

List of Tables

List of Illustrations

List of Abbreviations and Symbols

2D	two-dimensional
3D	three-dimensional
A	Amperes
ALT	alanine aminotransferase
ALP	alkaline phosphatase
AST	aspartate aminotransferase
AUC	area under the curve
BAL	bio-artificial liver
$CaCl_2$	calcium chloride
CI2	Chymotrypsin inhibitor 2
cm	centimeter
CPMG	Carr-Purcell-Meiboom Gill pulse sequence
DC	direct current
DMEM	Dulbecco's modified Eagle media
DNA	deoxyribonucleic acid
ECM	extracellular matrix
EDTA	ethylene diamine tetraacetic acid
EGTA	Ethylene glycol-bis-(2-aminoethyl)-N,N,N', N'-tetraacetic acid
GGT	gamma-glutamyltransferase
HBSS	Hanks' Balanced Salt Solution
HSQC	Heteronuclear Single Quantum Correlation

HTP	high through-put
IPTG	isopropyl-β-D-thiogalactosidase
kDa	kilodalton
KV	kilovolt
l	liter
LDH	lactate dehydrogenase
MCB	Multicoaxial Bioreactor
MHz	megahertz
MitoTracker® Green	Benzoxazolium, 2-[3-[5,6-dichloro-1,3-bis[[4-(chloromethyl)phenyl]methyl] -1,3-dihydro-2H-benzimidazol-2-ylidene]-1-propenyl]- 3-methyl-, chloride
MitoTracker® Red	1H,5H,9H,11H,15H-Xantheno[2,3,4-ij:5,6,7-i'j']diquinolizine, 9-[4-(chloromethyl)phenyl]-2,3,6,7,12,13,16,17-octahydro-
ml	milliliter
mm	millimeter
mmol	millimole
mol	mole
mRNA	messenger RNA
MW	molecular weight
n	transients, number of transients
nm	nanometer
nM	nanomolar
NOESY	Nuclear Overhauser Effect Spectroscopy
OCT	optimal cutting temperature

PBS	phosphate buffered saline
PC	pyruvate carboxylase
PDH	pyruvate dehydrogenase
ppm	parts per million
rDNA	recombinant DNA
SEM	scanning electron microscopy
SDS-PAGE	sodium dodecyl sulfate poly polyacrylamide gel electrophoresis
T_1	spin-lattice relaxation time
T_2	spin-spin relaxation time
TEM	transmission electron microscopy
TMRM	tetra-methyl rhodamine methyl ester perchlorate
TSP	3-(trimethylsily)propionic-2,2,3,3-d_4 acid sodium salt
V	volts

Greek Based Symbols

μA	microampere
μg	microgram
μl	microliter
μm	micrometer
μM	micromolar

1 Introduction and Background

1.1 Clinical and Research Challenges in Hepatology

The liver is the largest internal organ of the human body responsible for a set of complex tasks including synthesis of biochemicals (bile, cholesterol, amino acids, coagulants, filtration of the blood, metabolism and storage of energy sources (carbohydrates, proteins, fats, and lipids), storage of vitamins (vitamin A, D, and B_{12}), and building materials for tissues [1]. The complexity of these functions poses a tremendous challenge for researchers wishing to study the liver or any of its functions while maintaining the aggregate functionality of the organ within reasonable physiological parameters. Such research-oriented issues have historically been encountered in university and academic research settings but increasingly are being found in industries, including pharmaceutical research and development, where design of hepatic model systems for metabolic and toxicological testing of new drug compounds is becoming more prevalent.

From the clinical perspective, liver complexity presents a challenge second only to that of availability of transplantable organs. Improvements in automobile safety combined with increased life expectancy have led to a situation where 30,000 U.S. patients die of liver failure while waiting for a liver transplant annually [2]. In short, the present organ availability problem is an inability of supply to meet

demand. In this environment where availability of suitable livers is a clear limit in the clinical equation, it is important to consider that liver failure patients may be sustained with only 20% of a functioning liver which would be approximately 300 grams (g) [3]. In an effort to provide hepatic functionality to patients awaiting transplant organs, a variety of extracorporeal bio-artificial liver (BAL) devices have been considered and tested [2, 4-9]. The following discussion will elucidate methods and material designs relevant to furthering progress in both the research and clinical areas of hepatic research in BALs.

Using nuclear magnetic resonance (NMR) technology, metabolic analysis of media streams from BALs specifically monitoring chemical constituents and concentrations was conducted. The BALs were prepared with hepatic cells isolated from human cadaver livers in gels or encapsulations through use of an electrostatic encapsulation device developed as part of this project. The long-range goal for such encapsulations is the development of stable hepatic cultures that can perform a partial or full range of hepatic physiological functions for both research and clinical applications. Such encapsulations may provide long-term storage of hepatic cells, opportunities to amplify cells within a bioreactor environment, a reduction in mortality for patients experiencing liver failure, possible solution to the need for immunosuppressive therapy required with transplants, and a decrease in research costs associated with pharmaceutical development.

New industrial perspectives are forcing pharmaceutical management to rethink target selection and validation methods, especially emerging low-cost biological modeling systems [10]. This trend is the result of increasing research and development costs which have more than doubled from an average of $316 million

for the decade of the 1980s to $802 million for the decade of the 1990s in inflation adjusted dollars [11]. Furthermore, many in the pharmaceutical community, including the FDA, argue that diminishing submissions of New Molecular Entities (NME) are the combined result of these substantially higher research costs in an era when most experts agree that the less complicated solutions and those achieved at lower research costs have largely been exhausted [12]. Bioreactor modeling of disease states coupled with high-throughput metabolomic studies using NMR technology may prove to be a cost-effective screening resource for determining metabolism and toxicity effects of lead compounds in the search for new pharmaceutical products [13].

1.2 State of Bioartificial Liver Research

Several research groups have proposed different models for BALs. The designs include two-dimensional (2-D) plates with cells grown on matrix and many varieties of three-dimensional (3-D) bioreactors with superficially attached cells, sandwiched cells, and/or cells secured in gels or permeable compartments. 2-D bioreactors are effectively cultured hepatocyte monolayers with the addition of media or plasma flow across the cell surface or permeable membrane separating the flow and monolayer. While hepatocytes have performed for longer than two weeks in 2-D bioreactors, the large dimensions for a flat surface in order to generate sufficient surface area are a disadvantage when compared to 3-D systems [14]. An important design consideration for bioartificial liver devices must be the fact that hepatocytes maintain differentiation through attachment to extracellular matrix and

cell-to-cell interaction.[15] For this reason, success achieved in renal support devices using cell suspension devices do not translate to hepatic devices as determined by diminished oxygen consumption of suspended hepatocytes [16, 17].

1.3 Woven Hollow-Fiber Bioartificial Liver

One of the earliest successes in the field of 3-D liver bioreactors occurred in 1975 when Wolf and Munkelt successfully cultured hepatocytes in a hollow-fiber bioreactor system while monitoring bilirubin conjugation [18]. Contemporary developments in the hollow-fiber bioreactor field by Gerlach have resulted in systems having discrete fibers containing cells, nutrient flows, gas flows, and waste flows [19]. Such 3-D designs demonstrate attention to detail in the spatial arrangement to ensure adequate oxygen concentrations and nutrient concentrations but seem limited in the ability to scale-up to due to the need for elaborate networks of fiber tubules.

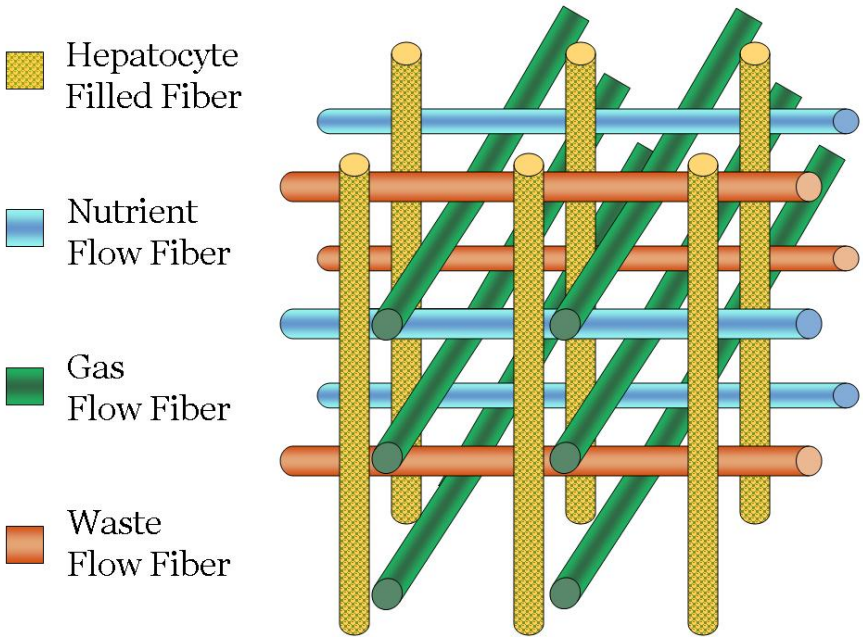

Figure 1-1
Hollow fiber bioreactor model

1.4 Coaxial Bioreactors for Bioartificial Liver

Coaxial bioreactors have geometries which mimic the dimensions of the liver acinus. The natural geometry of the liver includes a central venule, hepatocytes, and a collection of hepatic triads each having a portal venule, hepatic arteriole, and bile duct (see Figure 1-2, right side). Coaxial bioreactor designs utilize concentric cylinders that serve as semi-permeable membranes allowing for nutrient and gas exchange between compartments while retaining cells in a space having a 500 micron radial distance similar to the architecture of the liver. Coaxial bioreactor designs better approximate the structure of a liver acinus but are just as susceptible to fouling of semi-permeable membranes over time as compared to other bioreactor designs [4].

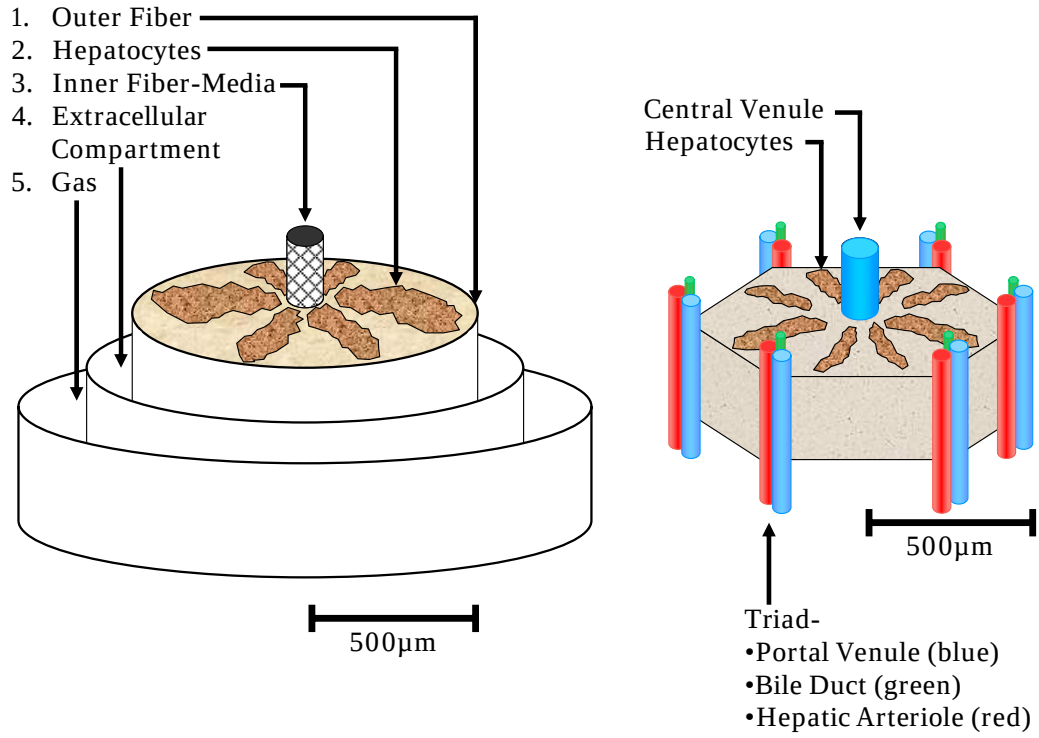

Figure 1-2
Structural comparison of coaxial bioreactor and liver acinus

The multicoaxial bioreactor (MCB) name is taken from the multi-tube architecture in which all tubes share the same axis of symmetry. The MCB mimics the acinus in dimension and can mimic the oxygen profile which exists as free oxygen drops from 10 mmHg in the vicinity of the triad to 3 mmHg at the central venule [20].

While other designs exist, the two described to this point illustrate the need for appropriately sized architecture and potential problems with scaling and membrane fouling. Ultimately, bioartificial liver designs should satisfy three points for consideration as practical tools for both clinical and basic science use:

1. Bioreactors should provide stable environments for

2. physiological function of the tissues supported in a
3. scalable model to allow for organ-sized constructs.

1.4.1 Traditional Clinical Methods for Determination of Liver Function

No single laboratory test is sufficient to provide a complete estimate of the function of the liver for every clinical situation. An array of biochemical tests are employed clinically, therefore, to assess the many functions of the liver and to evaluate patients with suspected or established liver disease. Liver function panels usually consist of aspartate aminotransferase (AST), alanine aminotransferase (ALT), alkaline phosphatase (ALP), lactate dehydrogenase (LDH), gamma-glutamyltransferase (GGT), bilirubin (total and conjugated), albumin, transthyretin (prealbumin), and prothrombin time [21, 22]. ALT and AST are both indicators of liver cell death. While ALT is largely found in the liver and kidney, ALT is not found exclusively in the liver and also may be found in the heart and other muscle tissue. Therefore, blood tests using ALT must be considered as total systemic measures [23]. LDH measures are less specific in terms of assessing liver damage, except in cases of ischemic liver injury where LDH levels are quite elevated [24]. In all cases, the most common liver function tests are limited to measures of injury or cell death. What may prove more beneficial for both clinical and basic science use in the future are functional assays which explore specific metabolic function by assessing the concentration of a host of chemical species related to liver health in parallel. These tests would rely clinically on blood, serum, or urine analyzed by NMR resulting in

systemic measures of the compounds of interest. However, through the use of bioreactors, the basic science use of such tests may exploit the isolated function of liver cells or other tissue types to determine organ specific metabolic activity.

1.5 Endnotes

1. Guyton, A.C., Hall, J.E., *Textbook of Medical Physiology*. 10 ed. 2000, Philadelphia: W.B.Saunders. 1064.

2. Tilles, A.W., et al., *Bioengineering of liver assist devices.* Journal of Hepato-Biliary-Pancreatic Surgery, 2002. **9**(6): p. 686-696.

3. Hughes, R., Williams, R., *Use of bioartificial and artificial liver support devices.* Semin. Liver Disease, 1996. **16**(4): p. 435-444.

4. Macdonald, J.M., et. al., *Chapter 21 Bioartificial Livers*, in *Cell Encapsulation Technology and Therapeutics (Tissue Engineering)*, W.M. Kuhtreiber, Lanza, R.P., and Chick, W.L., Editor. 1999, Birkhäuser: Boston. p. 450.

5. Ijima, H., et. al., *Development of a hybrid artificial liver using a polyurethane foam/hepatocyte-spheroid packed-bed module.* Int. J. Artif. Organs, 2000. **23**(6): p. 389-97.

6. Fremond, B., et. al., *Cell-based therapy of acute liver failure: the extracorporeal bioartificial liver.* Cell Biol. Toxicol., 1996. **12**(4-6): p. 325-329.

7. Gerlach, J., Ziemer, R., Neuhaus, P., *Fulminant liver failure: relevance of extracorporeal hybrid liver support systems.* Int. J. Artif. Organs, 1996. **19**(1): p. 7-13.

8. Arkadopoulos, N., et. al., *Liver assist systems: state of the art.* Int. J. Artif. Organs, 1998. **21**(12): p. 781-787.

9. Wolfe, S.P., Hsu, E., Reid, L.M., Macdonald, J.M., *A novel multi-coaxial hollow fiber bioreactor for adherent cell types. Part 1: Hydrodynamic studies.* Biotechnology and Bioengineering, 2002. **77**(1): p. 83-90.

10. Butcher, E.C., *Can Cell Systems Biology Rescue Drug Discovery?* Nature Reviews Drug Discovery, 2005. **4**(6): p. 461-467.

11. Grabowski, H., *Are the Economics of Pharmaceutical Research and Development Changing? Productivity, Patents and Political Pressures.* PharacoEconomics, 2004. **22, Suppl. 2**: p. 15-24.

12. U.S. Department of Health and Human Services, F.D.A., *Innovation or Stagnation: Challenge and opportunity on the Critical Path to New Medical Products*. 2004.

13. Bollard, M., Stanley, E., Lindon, J., Nicholson, J., Holmes, E., *NMR-based metabonomic approaches for evaluating physiological influences on biofluid composition.* NMR in Biomedicine, 2005. **18**(3): p. 143-162.

14. Ichihara, A., Nakamura, T., Tanaka, K., *Biochemical functions of adult rat hepatocytes in primary culture.* Ann. New York Academy of Sciences, 1980. **349**: p. 77-84.

15. Dixit V, G.G., *Artificial liver support: state of the art.* Scand J Gastroenterol Suppl., 1996. **220**: p. 101-114.

16. Margulis, M., Erukhimov, E., Andreiman, L., Viksna, L., *Temporary organ substitution by hemoperfusion through suspension of active donor hepatocytes in a total complex of intensive therapy in patients with acute hepatic insufficiency*. Resuscitation, 1989. **18**(1): p. 85-94.

17. Matsumura, K., Guevara, G., Huston, H., Hamilton, W., Rikimaru, M., Yamasak,i G., Matsumura, M., *Hybrid bioartificial liver in hepatic failure: preliminary clinical report.* Surgery, 1987. **101**(1): p. 99-103.

18. Wolf, C., Munkelt, B., *Bilirubin coujugation by an artificial liver composed of cultured cells and synthetic capillaries.* Transactions of the American Socity of Artificial Internal Organs, 1975. **21**: p. 16-27.

19. Gerlach, J., Schnoy, N., et. al., *Comparison of hollow fibre membranes for hepatocyte immobilisation in bioreactors.* Int. J. Artif. Organs, 1996. **19**(10): p. 610-616.

20. McClelland, R.E., MacDonald, J.M., Coger, R.N., *Modeling O2 transport within engineered hepatic devices.* Biotechnology and Bioengineering, 2003. **82**(1): p. 12-27.

21. Astegiano, M., Sapone, N., Demarchi, B., Rossetti, S., Bonardi, R., Rizzetto, M., *Laboratory evaluation of the patient with liver disease.* Eur Rev Med Pharmacol Sci, 2004. **8**(1): p. 3-9.

22. Knight, J., *Liver Function Tests: Their Role in the Diagnosis of Hepatobiliary Diseases.* Journal of Infusion Nursing, 2005. **28**(2): p. 108-117.

23. Quinn, P., Johnston, D., *Detection of chronic liver disease: costs and benefits.* Gastroenterologist, 1997. **5**(1): p. 58-77.

24. Gitlin, N., Serio, K., *Ischemic hepatitis: widening horizons.* Am J Gastroenterol, 1992. **87**(7): p. 831-836.

2 Development of Encapsulator and First NMR Methods for Media Analysis

2.1 Rationale and Goals

Experiments were conducted with a focus on developing a matrix encapsulation system that could be used to mass produce spheres containing functioning cells. Encapsulations may provide stable microenvironments for cellular growth, proliferation, and differentiation while shielding the contained cells from shear forces associated flow environments and may provide an immuno-protective barrier to recipients of cells implanted in encapsulated form. Organized in 3D systems, such encapsulates can be studied by measuring metabolites in the media effluents from traditional culture plates and bioreactors.

The encapsulations used in experiments described in this chapter included either cells from murine hepatic isolation or Umix® human hepatic cell mix (Vesta Therapeutics, Durham, NC). Functional testing was conducted on the media streams taken from MCBs containing encapsulations using NMR methods developed in the course of this project. Imaging of encapsulations was also performed to observe bead stability, cell migration, and cell viability as a function of time.

Specifically, the goals of this research were to accomplish the following:

1. Develop an inexpensive system for the encapsulation of large quantities of cells into spherical matrix.
2. Demonstrate that encapsulated hepatocytes and/or cell mixes containing hepatocytes have similar metabolic function when compared to hepatocytes and/or cell mixes containing hepatocytes grown in conventional matrices.
3. Establish the time course of survival of encapsulated hepatocytes and/or cell mixes containing hepatocytes.
4. Establish a high through-put NMR metabolomic method for analyzing liver function as compared to traditional testing methods which tend to focus on measures of liver death.

2.2 Development of Electrostatic Encapsulation Device

In these studies, encapsulation of the cells was utilized for maintaining large numbers of cells within a confined hydrogel architecture which would provide protection from shear forces while still allow for diffusion into and out of the construct. The guidelines for encapsulation materials and geometry were initially established as the following:

1. Matrix material should be biocompatible. No materials should be used that would be toxic to contained cells or tissues that encapsulations may be implanted into/onto.

2. Encapsulation geometry should be spherical. Spherical geometry should allow for encapsulations to stack in regular patterns while providing space between adjacent encapsulations for media flow.
3. Encapsulate radius should be no greater than maximal gas diffusion distance into the encapsulation. This standard should prevent necrotic and apoptotic products resulting from an anoxic or hypoxic core from affecting more superficial viable cells in the encapsulation.

2.2.1 The value of spherical encapsulations in a limited diffusion distance environment

One of the inherent difficulties in the development of bioartificial organs is designing structures that provide environments that mimic *in vivo* conditions. Diffusion distance in bioartificial tissues and systems is one such challenge. While scalability of a system is often viewed as one of the success measures in tissue engineering, size and scalability are often restricted by the maximum distance that nutrients can diffuse or penetrate into tissue or matrix from a media flow. The nutrient possessing the smallest diffusion coefficient, therefore, determines the maximum measurement available for determining distances between cells and nutrient sources in a bioartificial tissue or organ design. In the case of the liver, natural architecture reveals that convective flow channels are separated by a distance of no more than 100 microns (μm) [1]. This relatively tight packing of hepatocytes in a highly channeled structure ensures adequate blood flow to the liver which is

essential when considering that in rats, for example, the liver uses between 1/5 and 1/3 of total body oxygen consumption [2].

Historically, the problem presented by the oxygen diffusion coefficient has resulted in bioreactor designs with distance suitable to provide appropriate oxygen concentrations to cells but challenged where scalability is concerned. A possible solution that provides reasonable proximity between cells and nutrient rich media while also allowing for greater ease of scalability utilizes spherical encapsulations of cells in permeable hydrogels superfused with media. Such a system would employ uniformly sized spheres such that a three-dimensional array of spheres would allow for media flows to pass through the spaces created between adjacent spheres. As is the case with any bioartificial system with a linearly flowed media system, nutrient concentrations drop as media traverses over or through the matrix. This most certainly would occur in a stacked sphere system. The rate at which nutrient depletion would occur is directly related to the number of cells per unit volume that reside in the spheres. A unique difference exists for systems that use spherical encapsulations. Because the cells are contained within the hydrogel rather than loaded on the surface, cells are not subjected to the shear forces presented by the moving flow of media. Because of this isolation from flow, encapsulated systems may utilize higher flow rates than those employed by superficially mounted cell systems. Higher flow rates would allow for higher nutrient concentrations at all distances from the flow source as compared to traditional low flow of stagnant systems. Figure 2-1 illustrates how uniform spherical encapsulations would stack and also demonstrates the aforementioned trend regarding concentration as a function of distance and flow rate.

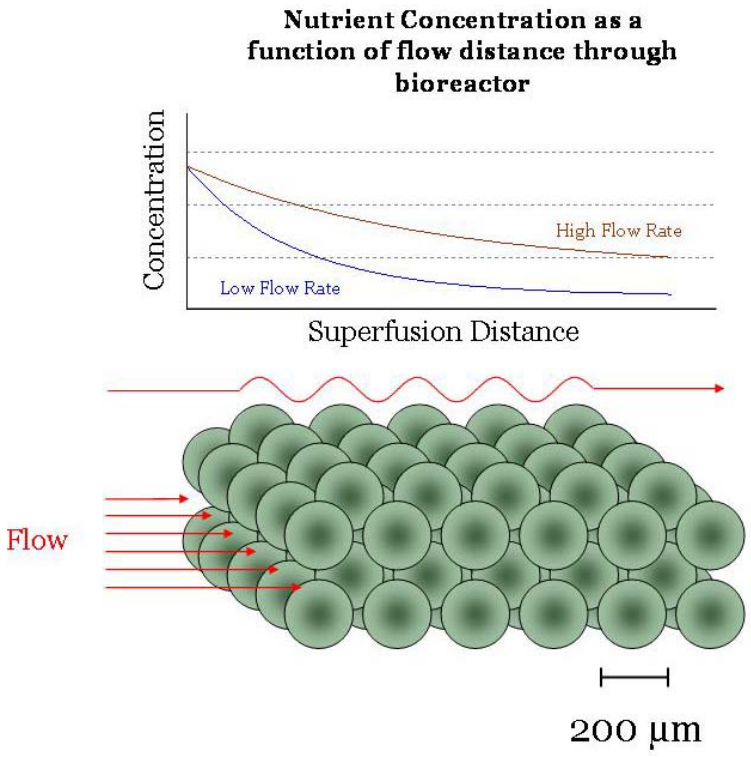

Figure 2-1
Three dimensional spherical encapsulation stack with nutrient concentration trend as a function of distance and media flow rate

2.2.2 Encapsulation Design Parameters

The first phase of this project focused on designing and manufacturing an encapsulation system. The requirements for the encapsulation system were as follows:

1. The system should be able to deliver spherical or other reasonably shaped geometry encapsulations containing cells in a permeable hydrogel.

2. The system should ensure viability of encapsulated cells. The system should minimize cell exposure to adverse chemical, pressure, shear, thermal, and hypoxic environments.
3. The system should be able to reproduce encapsulation size and viability under controlled conditions.

2.2.3 Preliminary Designs

The initial encapsulation system developed employed compressed nitrogen as the driver in an aerosol spray device consisting of a stainless steel spray head, syringe pump for delivery of the cell stock, and gas system to develop the aerosol spray. This design was selected on the basis of low cost, operator safety, and ability to completely build the system in less than two weeks. The aerosol system failed to deliver the desired spherical encapsulation and instead created large clumps of alginate with irregular geometries and diameters (or smallest measure in the case of irregular globular shapes) of greater than 800 microns. As continuing studies illustrated the need for higher gas flow through the aerosol nozzle in order to achieve sub-millimeter diameter encapsulations, concern over pressures in the aerosol nozzle and shear forces through the narrow annulus of the nozzle ultimately resulted in abandonment of this system. A parallel study undertaken in the David Gerber laboratories at UNC-CH sought to develop encapsulations by blowing air over the end of a small ejection port through which alginate cell stock was being pumped. This system produced encapsulates having few, if any, live cells. This system is

believed to result in cell death due to pressure and shear force applied to the cells during processing.

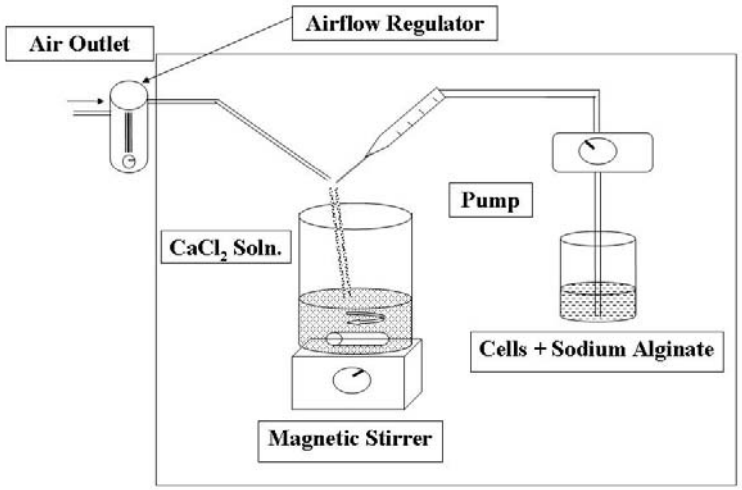

Figure 2-2
Chandrasekaran/Gerber encapsulation system

2.2.4 Electrostatic Encapsulation Device

The final system explored for this project was ultimately an electrostatic encapsulation device employing high voltage direct current (DC) as the driving force for consistent encapsulation size control. This system and its development are described in greater detail later in this work.

2.2.5 Selection of alginate as a matrix encapsulator

Sodium alginate was used to form the semi-permeable membrane on the exterior of the encapsulations. Alginate polymerizes in the presence of plus two

charged cations and can therefore be added to aqueous cell stock to form hydrogel coatings following ejection into a receiving bath containing barium, calcium, or magnesium. Similar techniques have been employed for several decades to encapsulate hepatocytes and islet cells isolations [3-5]. Alginate does not induce immune responses when used as an implant and can maintain structural and material properties for extended periods of time when used in culture [6-9]. Furthermore, alginate encapsulations of hepatocytes have been shown to provide more efficient cytochrome P450 induction as compared to other culture systems due to the porous nature of the alginate allowing for the exchange of biologically active molecules into and out of the encapsulations [10].

2.2.6 Validation of Encapsulated Hepatocytes

The second phase of this project encompassed characterizing encapsulations and monitoring the biological activity of encapsulated cells. First, it was necessary to assess viability over a time course of up to twenty-eight days. Fluorescent molecular probes were used to report cellular respiration in tandem with confocal microscopy to monitor cell viability for encapsulations cultured in two-dimensional (2D) plates. Confocal microscopy makes use of both laser and conventional light sources to produce images with resolutions below 10 microns through raster scanning to allow for optical thin-sectioning of samples with the need to fix or slice the specimen.

Transmission electron microscopy (TEM) was used to observe the definition of ultra-structure of fixed cells in encapsulations. TEM uses an electron beam directed at samples in a vacuum chamber which therefore requires significant

sample preparation and dehydration. TEM imaging can allow for magnifications greater than 100,000x with an imaging resolution in the single nanometer range.

Scanning electron microscopy (SEM) was used to image surface details of the alginate shell surrounding the hydrogel encapsulations. SEM is similar to TEM in its use of an electron beam as the interrogation modality and the requirement of extensive sample preparation and dehydration to allow for specimens to be placed in the vacuum chamber of the instrument. Unlike TEM, SEM does not require specimen slicing and instead makes use of conductive surface applications (typically gold, palladium, or mixed alloy) to the sample to allow for resolving of external surface details at magnifications in greater than 1,000x and imaging resolution in the single micron range.

2.2.7 Metabolic Analysis of Media Streams

Media collections were taken from bioreactors at 48 hour intervals. These samples were studied using NMR spectroscopy to determine chemical constituents and concentrations. Biofluid analysis has been a growing field of interest since 1983 when Jeremy Nicholson published the first studies in the field of "metabonomics" [11]. The term "metabolomics" first appeared in the plant metabolic field in the early 1980s. Since that time, the majority of published research has been directed at plant metabolism. In the later part of the 1990s, this focus began to shift to human and animal systems [12]. Early work in this field sought to exploit the power of NMR disaggregation of complex solutions when applied to blood, urine, and other biofluids. This concept is expanded in the research contained herein to include

media samples taken from bioreactors serving as *in vitro* models for physiological systems. In particular, the media samples represent non-hemoglobin proxies for blood in the bioreactors.

Prior studies have analyzed media streams from systems containing porcine hepatocytes [13]. However, little conclusive metabolic insights were obtained. The outlined goals above should serve as a guide in the development of a more robust method for observing metabolic activity over a broad range of indicators (glutamine, lactate, glucose, leucine, isoleucine, and others) resulting in a more complete picture of liver function using a 9.4 tesla magnet commonly found in laboratories throughout the research community.

The described studies are intended as a demonstration of a method and do not attempt to fully characterize hepatocyte metabolic activity within the MCB environment. Furthermore, total metabolic profiling by way of media studies cannot capture all metabolites as some charged species such as glutamate are unable to pass across the cell membrane and can therefore not be measured. Suggested methods for observing these species are described in the future works section later in this dissertation.

2.3 Methods and Materials

2.3.1 Cell Isolation Techniques

2.3.1.1 Cell Isolation from Murine Liver

Liver cells were isolated using a modification of the two-stage liver perfusion technique described by Seglen [14]. The hepatic progenitor cells were separated from mature hepatocytes using gravity separation and centrifugation. Full details of the isolation and characterization of the hepatic progenitor cells have been previously described [15].

Mice where anesthetized using ketamine. Following a reverse-T skin incision and transabdominal incision, the portal vein was catheterized using a 20 gauge angiocatheter. The inferior vena cava was severed allowing for blood to flow out. The diaphragm was breached allowing access to the heart which was cut to terminate blood flow. A buffered solution containing 0.5 mmol Ethylene glycol-bis-(2-aminoethyl)-N,N,N',N'-tetraacetic acid (EGTA) in KRH (see chart below for solution reagents and concentrations) was perfused into the liver for five minutes followed by perfusion with a buffered solution containing collagenase for 8 to 12 minutes as determined by observation of the liver for capsule swelling at which time the second perfusion was terminated and the liver was removed from the specimen. Liver cells were then collected and filtered using a buffered KRH solution containing 2 mmol $CaCl_2$ and 6 grams/liter BSA. Following filtering and centrifugation using the third buffer solution, cells were collected in low glucose Dulbecco's modified Eagle medium (DMEM).

KRH Buffer Solution	
HEPES	25 mmol
NaCl	115 mmol
KCL	5 mmol
KH_2PO_4	1 mmol

2.3.1.2 Cell Isolation from Human Liver

Adult human liver cells were isolated from donated cadaveric livers not suitable for orthotopic liver transplant. The organs were obtained from federally designated organ procurement organizations with informed consent having been given by appropriate next of kin regarding use of tissues for research purposes. Livers were perfused through the portal vein and hepatic artery with an EGTA buffer containing Liberase (Roche, Switzerland), a purified collagenase. Following digestion, organs were mechanically dissociated in a collection buffer maintained at 37˚C. The resultant cell stock was filtered and concentrated by low speed centrifugation.

Figure 2-3
Human liver cell isolation-perfusion (a), digestion (b-c), mechanical separation (d)

2.3.2 Encapsulation Device

2.3.2.1 History

The earliest documentation of an electrostatic bead device is found in US Patent 3,160,686 from 1964. In this patent, Doyle describes a system which uses heat to liquefy low melting point polyethylenes, resins, or wax which when combined with other liquid agents may be propelled out of an annular port by electrostatic force. The polyethylene, resin, or wax gels when making contact with a cooler receiving bath [16].

Such a design is suitable for the encapsulation of chemical and pharmaceutical agents which are not affected by the requisite heat of the process. Cells, however, are not suitable for use in this system due to cell death induced by the heat required to liquefy the gelling agent. Moreover, the resultant encapsulations using polyethylene, resin, or wax would not provide sufficient diffusion needed for gas, nutrient, synthesis products, and wastes exchanged across the outer membrane of the encapsulation.

Attention should be given to the application of the positive electrode in the Doyle design at the furthest point in the solution path from the ejection point. This design in theory will maintain the entire conductive fluid body at a selected voltage above ground. However, for small samples of viscous liquid potentially having air bubbles, such a design may allow for disruption of the electrostatic field. A solution ensuring more consistent electrostatic field maintenance is described later.

2.3.2.2 Design Concept

Spherical beads possessing a permeable external coating can be manufactured by use of a single tip electrostatic spraying system without the need for high temperatures as described by Doyle. The system, which is comprised of a high voltage DC power supply, syringe pump for delivery of media, and a receiving bath that catalyzes bead gelling, can reproducibly cast beads with diameters of 100 μm to 1mm ±8% at operating temperatures as low as 0˚C. Bead size is determined by a combination of four factors:

1. flow rate of the syringe pump,
2. diameter of the ejection port (typically a 24 gauge angiocatheter),
3. electric potential, and
4. distance between the receiving bath and ejection port.

Beads have successfully been cast using cell densities of $1x10^6$ to $2x10^7$ cells/ml. The typical bead gelling matrix is a 1:1 mix of low glucose D-MEM and aqueous alginate solution such that the final concentration of the gelling solution is 1% alginate. The gelling solution is combined with mature hepatocytes, hepatic progenitor cells, or a mixture containing multiple cell types. Human and murine cells were used in the experiments described herein. The solution containing cells is loaded into a syringe fitted with a 24 gauge angiocatheter modified to include the high voltage positive electrode. A grounding electrode is placed into a 125 mmol calcium chloride ($CaCl_2$) solution which serves as the receiving bath and catalyzes the polymerization of alginate in the gelling matrix as beads are cast into the bath.

Both the bath and gelling solution containing cells can be maintained at any temperature above their melting points allowing for cell degradation due to hypoxia to be minimized.

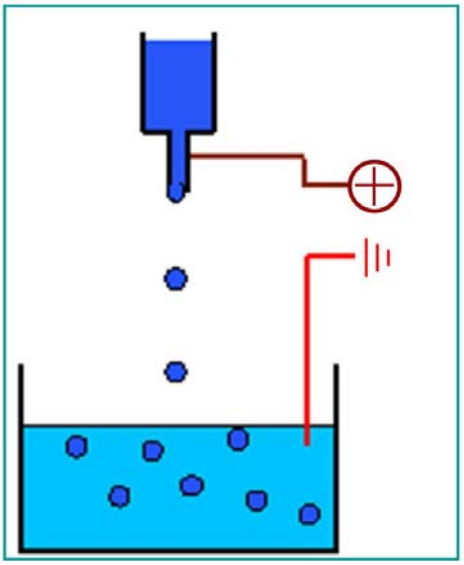

Figure 2-4
Electrostatic bead spray design

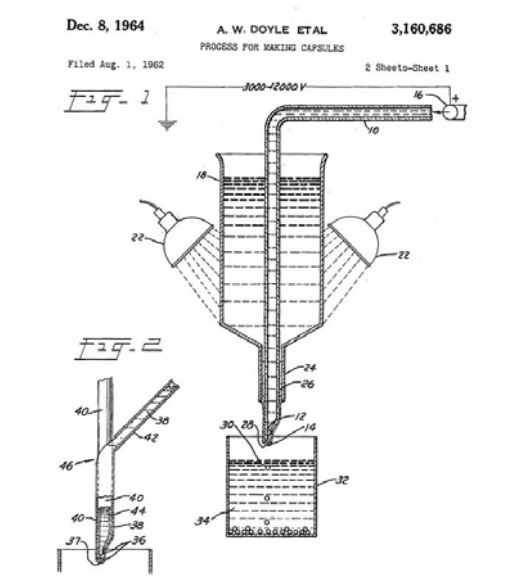

Figure 2-5
Doyle electrospray design, 1964 (U.S. Patent 3,160,686)

Early trials revealed the need to control ejection port size, flow rate, distance from tip to receiving bath, and voltage in order to achieve spherical beads. In tests with lower flow rates (0.25 ml/min to 0.5 ml/min), resultant beads consistently showed irregular geometry. These encapsulations typically had a spherical body with a long, conical tail tapering away from the body of the bead. Such tails were observed to line up in two-dimensional culture such that the tail of one bead would it between the spherical bodies of two adjacent beads preventing media flow through the matrix of encapsulations. Increasing the flow rate to 0.714 ml/min resulted in spherical beads without tails. Figures 2-6 and 2-7 illustrate the difference between

encapsulations having tails and those that do not. Of particular interest are the inter-encapsulation channels present in Figure 2-7. Without these channels, media would be unable to flow between the encapsulates.

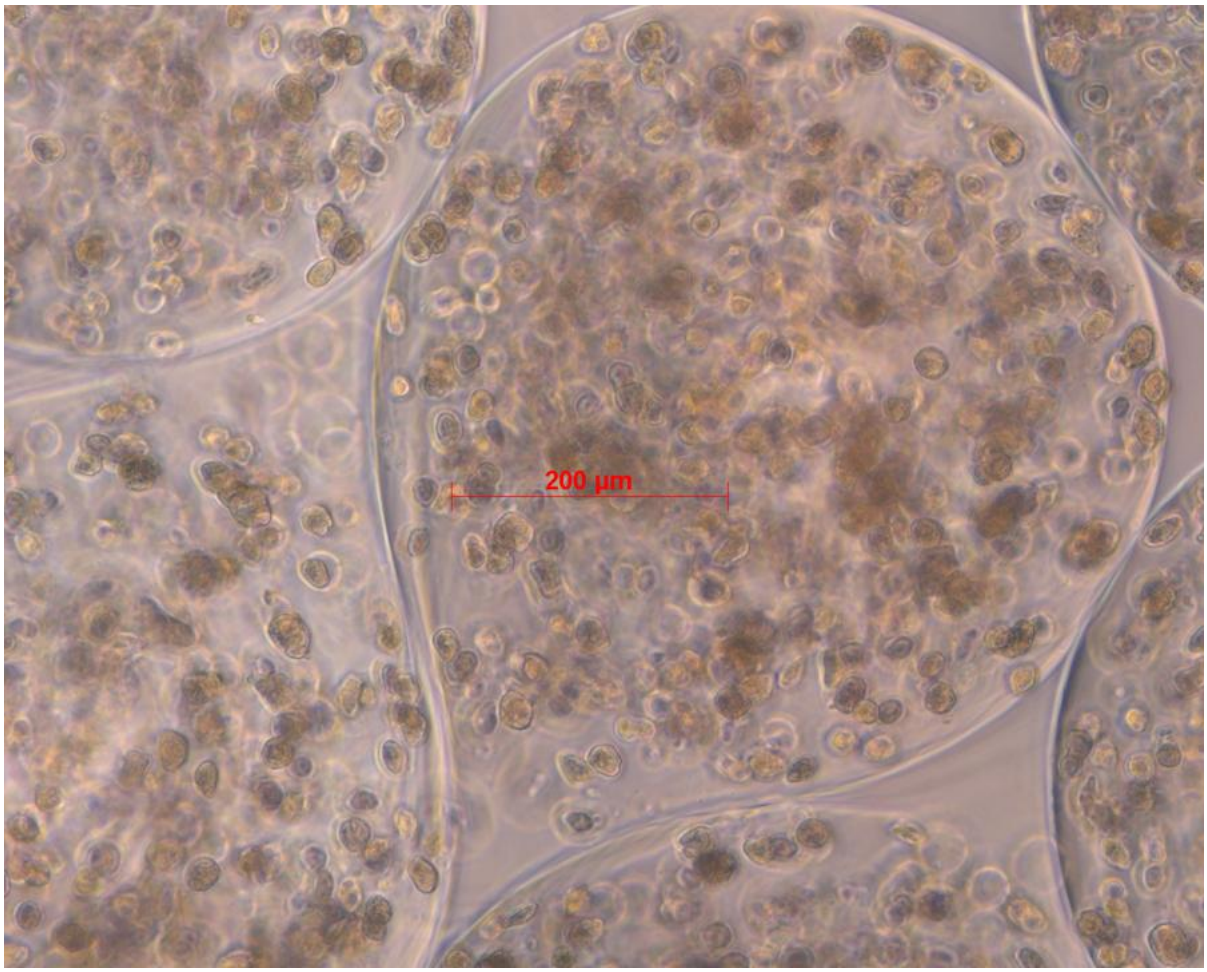

Figure 2-6
Murine HPC encapsulations with irregular conical tails

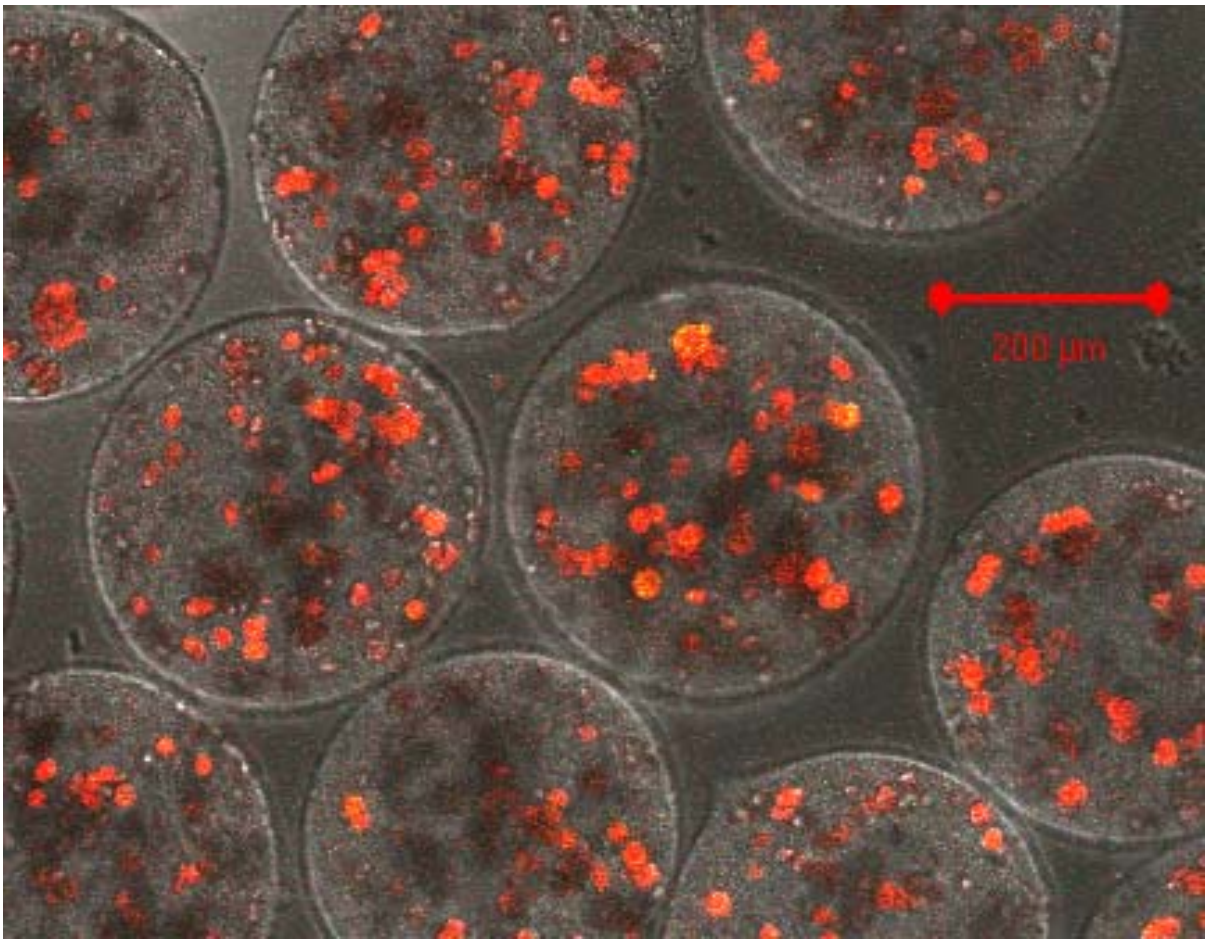

Figure 2-7
Mature hepatocyte encapsulations showing spherical geometry and inter-bead superfusion channels

2.3.2.3 Safety Considerations

Due to the high-voltage required to establish the electrostatic spray condition, a polycarbonate (Lexan®) case was designed and constructed to house the electrostatic spray equipment while providing reasonable protection to equipment operators. The housing was designed to have two compartments. The lower compartment was designed to hold a high-voltage power supply and magnetic stir-

bar plate stacked vertically. Particular attention was given to isolating the high-voltage supply from liquids used in the experiment. The upper compartment was designed to support stands for maintaining appropriate distances and alignments of the electrostatic spray ejection port and receiving bath. The delivery pump for gelling stock delivery was located in this area upper area of the cage to minimize flow distances from pump to ejection port. The initial design for the cage included a frontal plate to prevent users from incurring electric shock by accidental introduction of body parts into a line of continuity between the high-voltage DC source and any reasonable ground in the room. Early attempts to use the electrostatic device proved challenging with the frontal plate blocking the controls of the pump, stir plate, and power supply. Because of these complications with addressing the control systems during encapsulations, the cage was ultimately rotated 180˚ allowing for free access to all controls. In response to this change, the "one-hand-in-a-pocket" rule was employed to avoid provision of electrical paths that could cause shock, electric burns, or other serious injuries [17]. Additionally, safety measures recommended by the National Institute for Occupational Safety and Health were undertaken such that no encapsulations were performed by an individual operator [18].

While the electrostatic process by definition occurs at zero amperage, the high voltage delivered by the Spellman power supply could register sub-milliamp currents when provided with appropriate grounding. Such currents in the operational voltage range would be able to induce ventricular fibrillation [17, 19]. In Figures 2-8 and 2-9, the high voltage source and stir plate are isolated below the operational deck of the

safety cage away from the liquid gelling stock and aqueous receiving bath as an additional safety measure.

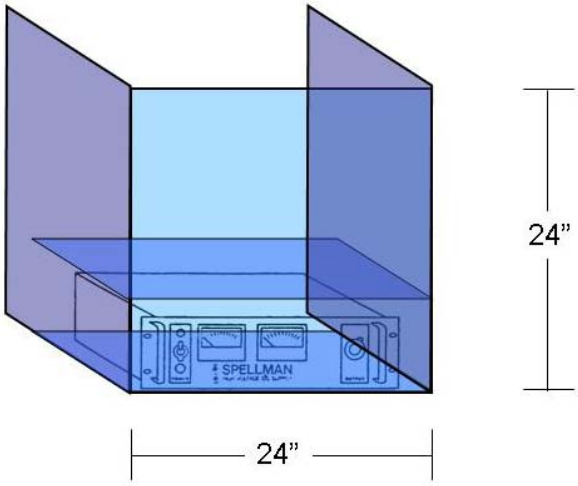

Figure 2-8
Schematic for Lexan safety case

Figure 2-9
Open front safety cage setup

To achieve the high-voltage, electrostatic field required to drive the electrospray device, a high-voltage DC source (Spellman model RHR30PF30, Hauppauge, NY) was used with voltages in the range of 3.8 to 6 kilovolt (KV). The positive electrode was established 2 cm above the ejection port by piercing the angiocatheter with a 22 gauge needle connected to the Spellman high-voltage source. This ensured that the electrostatic field was maintained throughout an experiment without disruption caused by small air bubbles that may exist in the fluid body causing loss of continuity. This design enhancement was undertaken after initial attempts to use the Doyle design for electrode placement resulted in formation of

long strands of alginate extruded into the $CaCl_2$ bath under zero voltage potential due to continuity disruption.

2.3.2.4 Grounding

The ground electrode for the high-voltage source was attached to benchtop plumbing by copper wire and a one inch hose clamp. This method was employed as conventional grounding plugs in 120 volt laboratory wiring may be unsuitable in for grounding voltages greater than specified usage. This plumbing based grounding scheme was recommended by the Spellman Company, manufacturers of the high voltage source used in these studies.

2.3.2.5 Liquid Delivery

Media stocks containing cells, alginate, and/or Matrigel were delivered through the encapsulation system by syringe pump. Typically, a 1 or 3 cc syringe was loaded into a syringe pump (Braintree Scientific BS-8000, Braintree, MA) arranged in the z-axis such that the expressed solution would exit the ejection port at the bottom of the pump and fall orthogonally onto the surface of a 150 ml receiving bath of 125 mmol $CaCl_2$ in a 250 ml Pyrex beaker. Pump flow rates were set in the range of 0.75 to 1.5 ml/min. The pump was mounted on an insulated riser to provide electrical isolation from possible spills on the operational deck of the safety cage.

This also minimized the null volume required to pump gelling solution from the pump to the spray nozzle resulting in more efficient encapsulation studies.

2.3.2.6 Ejection Ports

Initially, a variety of angle tipped needles were employed as ejection ports for the cell stock solutions delivered from the syringe pump. Uniformity in diameter of the tip was an important consideration which was easily satisfied by metal needles. Metal needles also offer excellent conductivity when an electrode is clamped to the exterior of the tip. Unfortunately, the angled tip failed to produce regular spherical encapsulations. Angle tipped needles were therefore abandoned in favor of flush cut angiocatheters. Preliminary trial and error led to the use of 24 gauge angiocatheters as the standard ejection port for all experiments. This selection was made based on the diameter of encapsulations which could be achieved at voltages that did not produce arcing. Arcing voltages were found above 6 kV. Using a 24 gauge angiocatheter, spherical encapsulations with diameters below 500 μm could be easily reproduced at voltages in the 4 to 5 kV range with the distance between the ejection port and the $CaCl_2$ bath in the range of 2.0 to 3.0 centimeters (cm).

2.3.3 Culture Environments

2.3.3.1 Multi-Coaxial Bioreactor

The Multicoaxial Bioreactor (MCB) is made of biocompatible materials engineered to proprietary specifications under design specifications provided by Jeff Macdonald [20]. All bioreactors used in studies described in this thesis were constructed onsite at ADMET Technologies, Inc. (Research Triangle Park, NC) from parts fabricated at the UNC Physics Instrument Shop (Chapel Hill, NC).

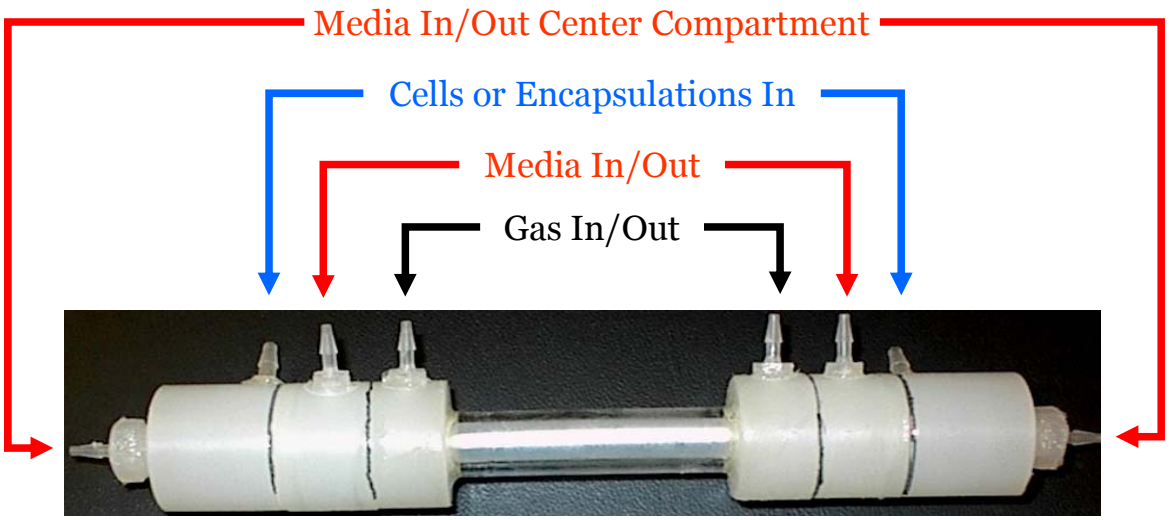

Figure 2-10
Bioreactor loading and flow diagram

Each MCB was primed and sterilized with ethanol under continuous flow provided by pump feed for twenty-four hours. Each MCB was next washed with cell culture media to remove ethanol from the entire system. After the completed MCB is flushed and activated with cell culture media, the MCB is inoculated with a human liver cell preparation (UMIX®) shown to contain hepatic stem/progenitor cells as

well as non parenchymal cells. Cells were inoculated in either in a mixed gel composed of collagen and Matrigel or in encapsulations containing 1% alginate, Matrigel, and DMEM. The cells or encapsulates were sandwiched between two media compartments. Multiple MCBs were set up in a single incubator for facile media sampling over regular time intervals.

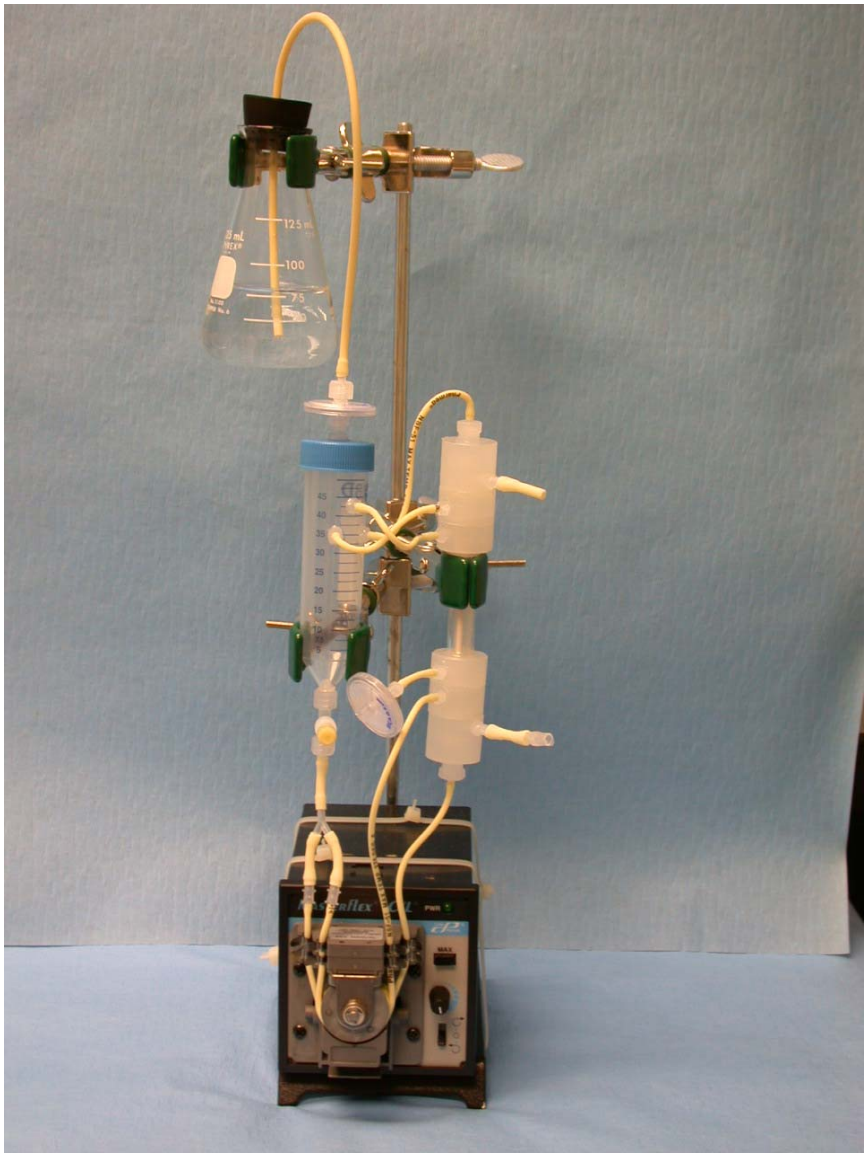

Figure 2-11
Multiple MCBs with gassing and media pumps

2.3.3.2 MCB Media Formulation

All bioreactors were circulated with a modified DMEM solution (Gibco, Carlsbad, California) having no phenol red and no glutamine. To this solution, additional ingredients listed in the table below were added.

DMEM Solution Additional Ingredients	
Pen/Strep Antibiotic	10 ml/L
Spite	10 ml/L
Albumax	2 g/L
HEPES	5.958 g/L
Niacinamide	600 mg/L
Beta mercapto	1 ml/L
2-13C/15N glycine	0.4 mmol
15N Glutamine	0.5 mmol

2.3.3.3 Two-Dimensional Plating

Three-dimensional encapsulations where incubated in two-dimensional plates allowing for a single layer of encapsulations to rest submerged in media. These plates allowed for easy access to encapsulations for microscopy studies. The alginate beads were suspended in DMEM plus 10% fetal bovine serum (FBS), 20 mmol HEPES, 10 mmol nicotinamide, 1 mmol ascorbic acid 2-phosphate, 1 μM dexamethasone, 0.5 mg/L ITS (insulin-transferrin-selenium) solution, 30 mg/L proline, 100 mg/L antibiotic solution, and 10 ng/ml epidermal growth factor (EGF) in 24- well plates or 35 mm covered culture plates at a density of $1x10^6$ to $20x10^7$ cells/ml of encapsulation stock. The plates were kept in a 5% CO_2/95% room air

incubator at 37°C. The media was changed every 3 days, and the supernatant was collected for analysis. As a control, hepatic progenitors were cultured on 24-well dishes at a cellular density of $5x10^5$ cells/well under the same culture conditions.

2.3.4 Sample Collection Methods

2.3.4.1 Media Collections

Media was removed from bioreactors every 48 hours and replaced with fresh media. Prior to media exchange, a sample of media was extracted from the bioreactor system using a syringe fitted with an 18 gauge needle utilizing aseptic technique. Media samples were maintained at -80˚C until completion of individual bioreactor studies. All samples from any single bioreactor experiment were thawed simultaneously and prepared in accordance with the metabolomic procedure described later in this work allowing for batch serial analysis. Control bioreactors possessing acellular encapsulations or gel were maintained under the same conditions and media change regimen as those containing hepatocytes in encapsulations or gel.

2.3.4.2 Matrix-Based Cell Collection

Samples contained in bioreactors were fixed for microtomy by injecting optimal cutting temperature (OCT) glycol/resin solution into the inner and outer chambers of the bioreactors before freezing. OCT was not introduced into the

central compartment of the bioreactor due to concerns that the viscous liquid might compress the encapsulations or other cell-bearing matrices. The bioreactors were then thin sectioned using a cryostat. Thin sections were placed onto slides for imaging with confocal microscopy.

2.3.4.3 Alginate Bead Disintegration by Sodium Citrate Wash

For studies that removed cells from encapsulations, a 75 mM sodium citrate solution was used to disintegrate the alginate encapsulation [21]. Citrate is a useful chelating ligand for divalent cations such as Ca^{+2} [22]. The chelation of calcium initiates the disintegration of the polymerized alginate. Encapsulations were placed in a 50 ml tube with the citrate wash and agitated manually until encapsulations were observed to disappear. Cells were pelleted using low speed centrifugation and resuspended in culture media.

2.3.5 Microscopy Techniques

2.3.5.1 Light Microscopy

The beads were visualized under a Zeiss Axiocarvert 100 (Carl Zeiss Inc., Thornwood, NY) inverted transmission microscope to ensure that 2D plates were not contaminated during time series studies. Inverted light microscopy was also used to study cell distribution inside the beads and also to determine bead size measurements.

2.3.5.2 Confocal Microscopy

Murine and human encapsulated samples were treated with 90 nanomolar (nM) solutions of MitoTracker® Red (Molecular Probes, M7512, Eugene, OR), a fluoroprobe that emits light when in the mitochondria of respiring cells. Preliminary studies suggested that incubations of 15 to 30 minutes in the fluoroprobe solution did not yield even staining within the encapsulations. Therefore, the fluoroprobe was loaded at a concentration of 90 nM directly in the liquid alginate/cell encapsulation stock prior to electrostatic encapsulation.

Encapsulations were visualized using a Zeiss LSM-510 or a Zeiss LSM-210 (Carl Zeiss Inc., Thornwood, NY) inverted confocal microscope to assess cellular viability distribution with in the three-dimensional structure of the bead. Beads were observed in DMEM in 35 mm glass bottom dishes.

2.3.5.3 Electron Microscopy Methods

2.3.5.3.1 Transmission Electron Microscopy (TEM)

Time series bead samples were fixed in a 2.5% glutaraldehyde solution with 0.2M sodium cacodylate with 0.01M $CaCl_2$ and stored at 4˚C until all were batch processed. Samples were treated with osmium tetroxide for 1 hour. Samples were dehydrated using a four-concentration process including 30%, 50%, 75%, and 100% ethanol immersion for 5 minute periods with three washes being performed at the

100% ethanol step. Samples were split into equal portions for final TEM and SEM preparation.

Transmission electron microscopy samples were then washed in propylene oxide followed by immersion in a 1:1 solution containing propylene oxide and epoxy resin. The TEM samples were embedded next in 100% epoxy and sectioned using ultra-microtomy techniques [23]. TEM Samples were observed using the LEO EM 910 (LEO Electron Microscopy, Thornwood, NY).

2.3.5.3.2 Scanning Electron Microscopy (SEM)

Following dehydration gradient ethanol series washing, critical point drying was applied to the scanning electron microscopy samples using high pressure carbon dioxide. SEM samples were then sputter coated with gold/palladium alloy to increase sample conductivity [23]. SEM samples were observed using the Cambridge S200 (Carl Zeiss Inc., Thornwood, NY).

2.3.5.4 NMR Techniques

2.3.5.4.1 Sample Preparation

Media samples were combined 1:1 with a phosphate buffered deuterium oxide solution containing sodium formate for use as a concentration reference. As all samples were buffered media solutions, there was no need to titrate samples to correct for pH.

2.3.5.4.2 Reference Selection

The use of 3-(trimethylsily)propionic-2,2,3,3-d_4 acid sodium salt (TSP) as a reference for chemical shift due to the fact that the chemical shift for TSP is a singlet at 0 parts per million (ppm). TSP also allows for simple algebraic determination of concentration for all peaks present in the solution by proton weighted normalization of peak areas compared to the area of the TSP peak. TSP, however, has been reported to bind non-specifically with some proteins reducing the peak signal and allowing for errors to be made in the determination of concentration of constituents in samples containing protein [24]. A solution of equal weighted TSP and sodium formate peaks was prepared. Spectra of the two reference solutions alone and in conjunction with media revealed that the TSP was likely binding to albumin or some other constituent of the media solution causing systemic errors in calculation of concentration. Because this error was non-specific and had a relatively large standard deviation, sodium formate was determined to be the better reference for the NMR studies conducted from that time forward.

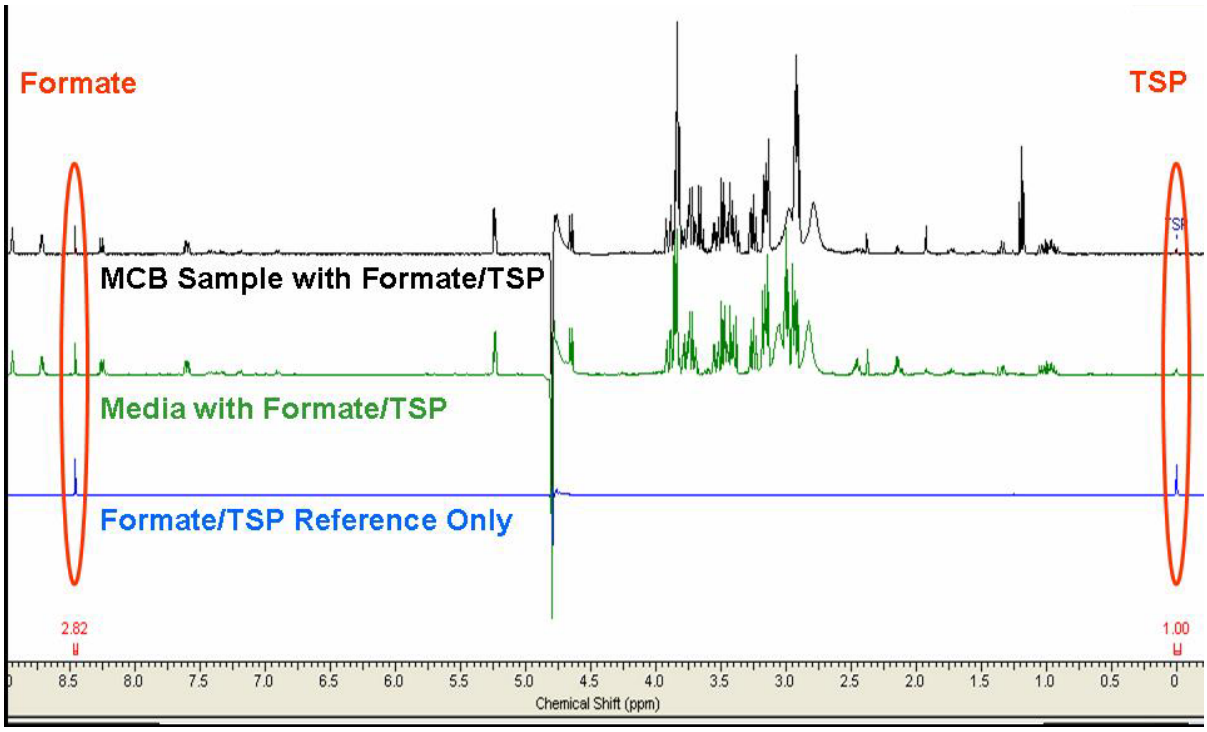

Figure 2-12
Comparison of spectra with TSP and formate references

2.3.5.4.3 Pulse Sequence

The metabolomics assay was performed on a Varian 400 megahertz (MHz) magnet. The NOESY (Nuclear Overhauser Effect Spectroscopy) pulse sequence was used with 32 transients per sample and a D1 time of 10 seconds. The NOESY pulse sequence was selected for its ability to produce narrow peak widths and excellent solvent (H_2O) suppression. A graphical interpretation of the pulse sequence can be found in Figure 2-13. Transmitter power level was maintained at 56 for all samples.

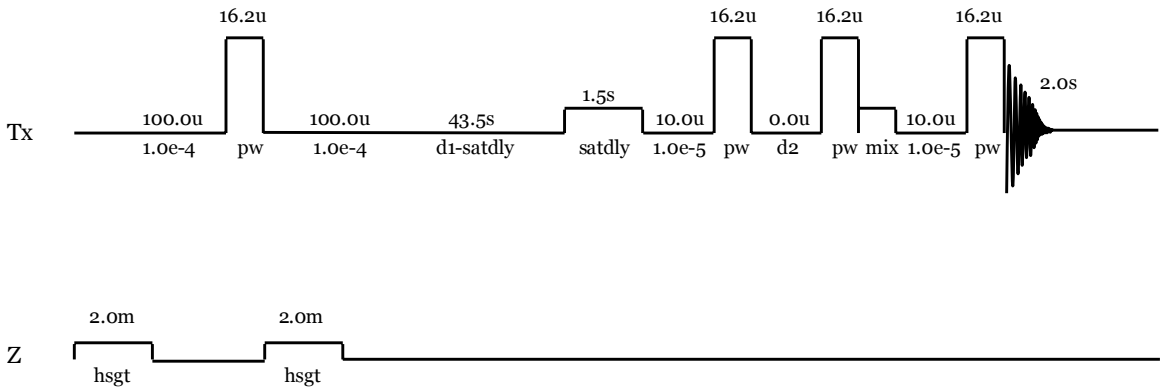

Figure 2-13
NOESY pulse sequence

2.3.5.5 Biolyzer Techniques

Media samples from experimental and control bioreactors as well as 2D control plates were analyzed using the Kodak Biolyzer Rapid Analysis System (Rochester, NY). All samples were frozen at -80˚C prior to analysis. All samples were processed in accordance with Kodak standard protocols.

2.4 Results

2.4.1 Microscopy Data

2.4.1.1 Light Microscopy

Light microscopy was employed to determine whether or not encapsulations had uniform spherical geometry. Early experiments demonstrated the need to adjust both voltage and pump flow rate to produce spherical beads. Through the use of 35 mm culture dishes with a small volume of media, encapsulations would settle to the bottom of the dish allowing for any perturbation in geometry to be observed as the encapsulations would settle to positions having the lowest energy which would routinely result in the exposure of irregular protruding features when viewed or digitally photographed using light microscopy.

2.4.1.2 Electron Microscopy

2.4.1.2.1 Transmission Electron Microscopy

Encapsulated and free cell samples were prepared as described earlier and imaged using a LEO 910 EM Transmission Electron Microscope. Many of the cells imaged in thin sections from encapsulations demonstrated grainy, poorly-defined ultra-structure suggestive of necrosis. This finding suggests that either the encapsulated cells could not survive either the initial encapsulation technique or subsequent fixation process. However, cells demonstrating more definitive

mitochondria were found representing less than 10% of the cells observed in thin sections of encapsulations.

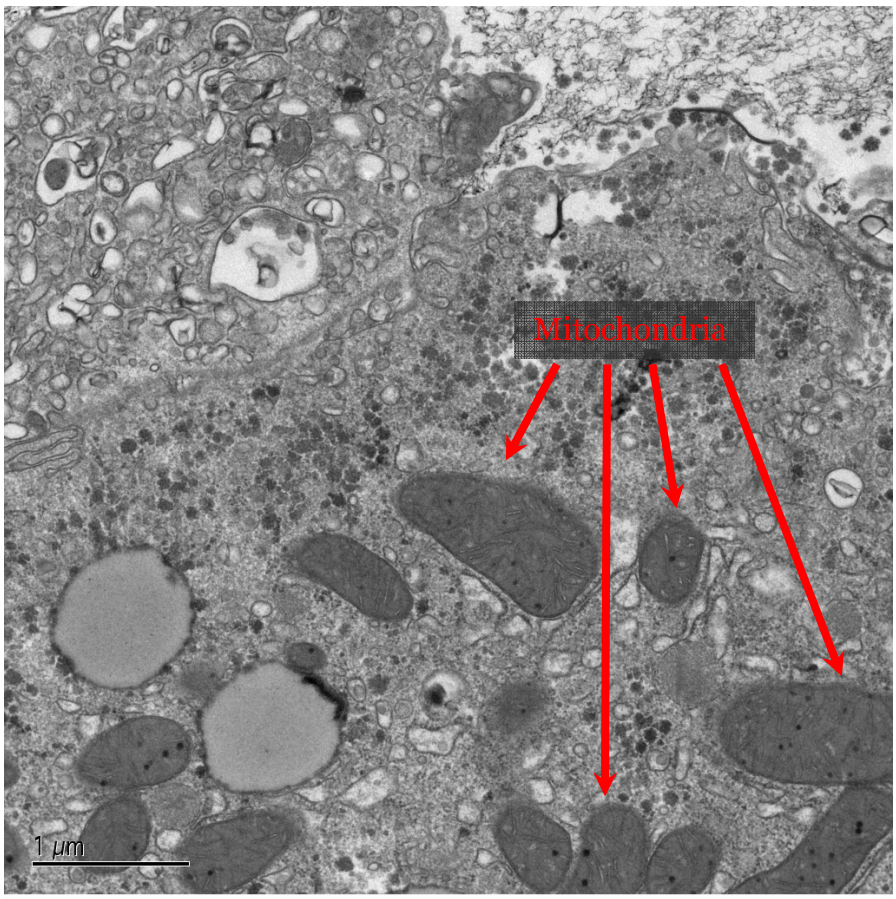

Figure 2-14
TEM of encapsulated cell showing mitochondria

Concern regarding cell death due to the encapsulation process was dismissed following the positive results of both confocal microscopy and NMR metabolic validation described later in this work. These findings suggested that the necrosis may be due to the fixation process being slowed by the encapsulation matrix allowing for cells with the encapsulation to succumb to necrotic death. A method was developed using sodium citrate to disrupt the encapsulations to free the cells.

This allowed for the free cells to be taken from an encapsulation and fixed. These freed cells were then compared to control cells taken from same study but not subjected to either the encapsulation technique or the sodium citrate encapsulation reduction. TEM of the control cells found well-defined ultra-structure with distinct intra-cellular features and crisp plasma membrane (Figure 2-15).

Figure 2-15
TEM of control cell (non-encapsulated)

2.4.1.2.2 Scanning Electron Microscopy

SEM allowed for the preparation of entire encapsulations without the need for thin sectioning. This allows the advantage of interrogating the entire external surface of an encapsulation. The findings from this line of study demonstrated that the exterior of observed encapsulations had a dramatic topographical surface with alternating peaks and valleys running along nearly parallel longitudes of the encapsulation.

Figure 2-16
SEM of alginate encapsulation observed at 575x magnification

This observation was in stark contrast to the expectation of a smooth exterior to the encapsulations. This finding was suggestive of systemic dehydration resulting from sample processing with ethanol gradient staged dehydration. However, such dehydration which would result in the shrinking and wrinkling of encapsulation surfaces might also occur at earlier steps in the process. Review of other images uncovered one sample that did show signs of possible superficial wrinkling. A series of encapsulations had been observed confocally that show similar surface characteristics. Due to the thin section viewing associated with confocal microscopy, the surface topography is considerably less apparent and was initially dismissed as a feature associated with a flaw in the angiocatheter used during the encapsulation process.

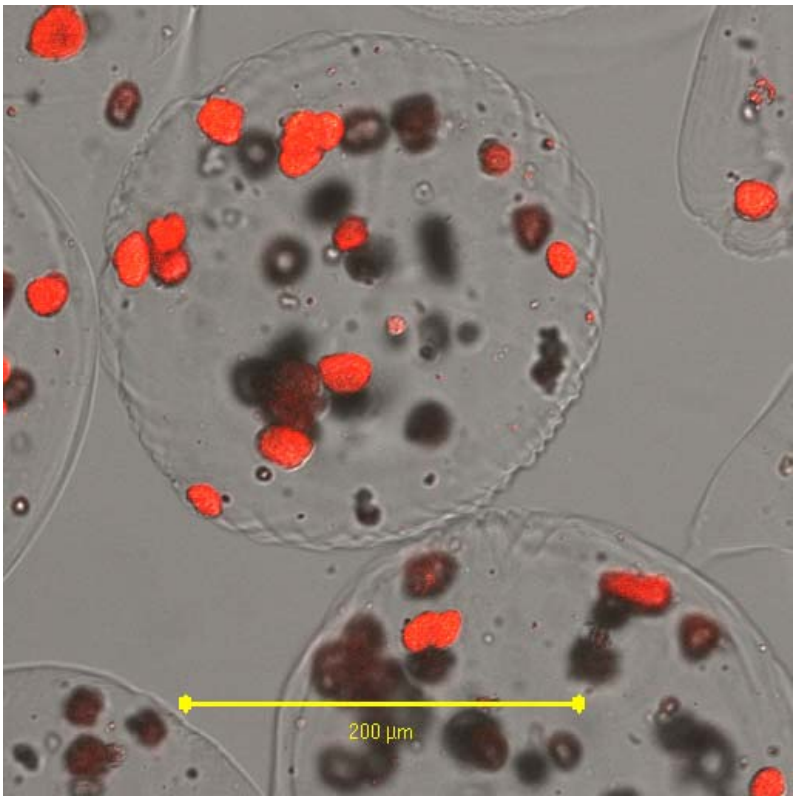

Figure 2-17
Confocal slice of encapsulation showing possible dehydration deformations of the exterior surface

It is important to note that the cells contained in the encapsulations of Figure 2-17 register as alive by fluorescence observance. This prompted an intensive interest in ensuring that all processing occurred in isotonic solutions to diminish the opportunity for variations in salt concentrations to damage encapsulations and contained cells.

2.4.1.3 Confocal Microscopy

Encapsulations were visualized using a Zeiss LSM-510 inverted confocal microscope to assess cellular viability distribution with in the three-dimensional structure of the bead. For Figure 2-18 and Figure 2-19, MitoTracker® Red as loaded into the liquid encapsulation stock at a concentration of 90 nM. Encapsulations were observed in DMEM in 35 mm glass bottom dishes.

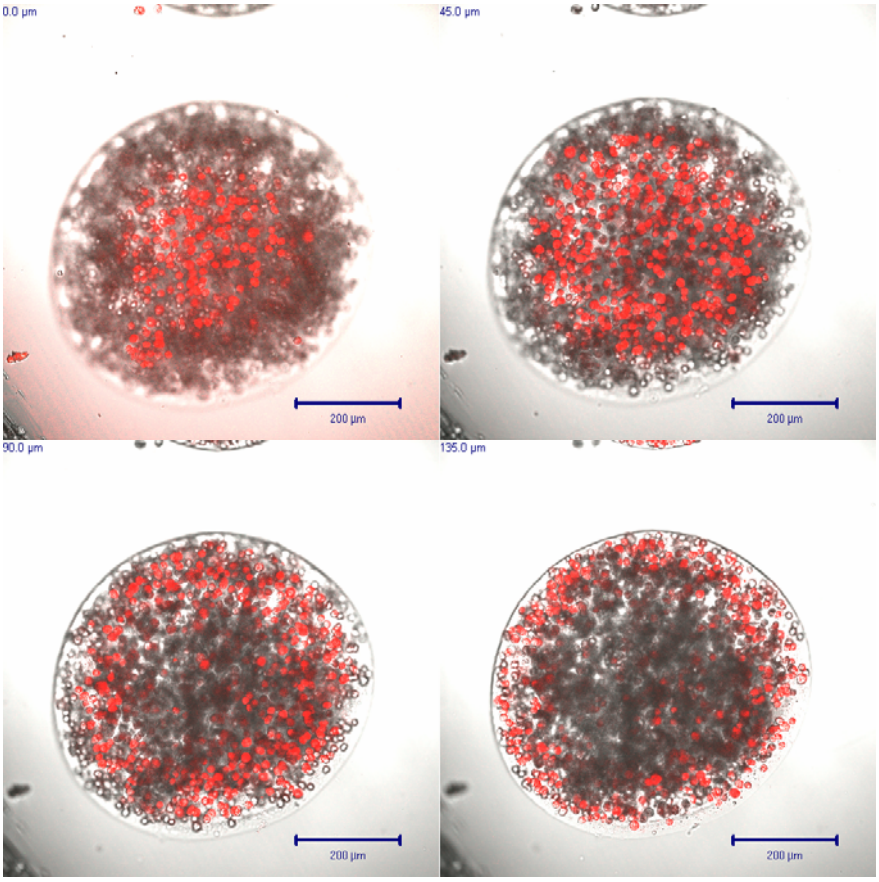

Figure 2-18
Confocal images of human UMIX® in alginate/Matrigel bead with MitoTracker® Red taken at 24 hours post encapsulation

Figure 2-18 illustrates confocal slices of an encapsulation containing human UMIX®. Because the fluorescence channel is captured confocally while the transmitted light is captured for the full sample thickness, the appearance of small cellular bodies that do not fluoresce may lead to the erroneous conclusion that the majority of cells shown in the image are dead. This, however, is not the case as only a small thickness of the encapsulation is registered on the fluorescence channel and being combined with non-fluorescing images both above and below the confocal plane. The intended effect of combining the two images is to illustrate the size of the bead, the viable cells within a narrow cross-section, and the obstructions below the

focal layer (inverted microscope) which lay between the fluorescing live cells and the microscope detector. This obstruction issue can be observed by comparing the four images and observing the density of the fluorescent signal as a function of depth. In the first image, taken just at the base of the encapsulation nearest the objective, the fluorescence is contained in the center of the bead.

Similar results were obtained with murine HPC encapsulations examined with confocal microscopy. Figure 2-19 shows a z-axis stack of confocal images penetrating into a single encapsulation. The top left block is the most superficial while the image at the lower right represents a confocal slice 90 μm into the encapsulation.

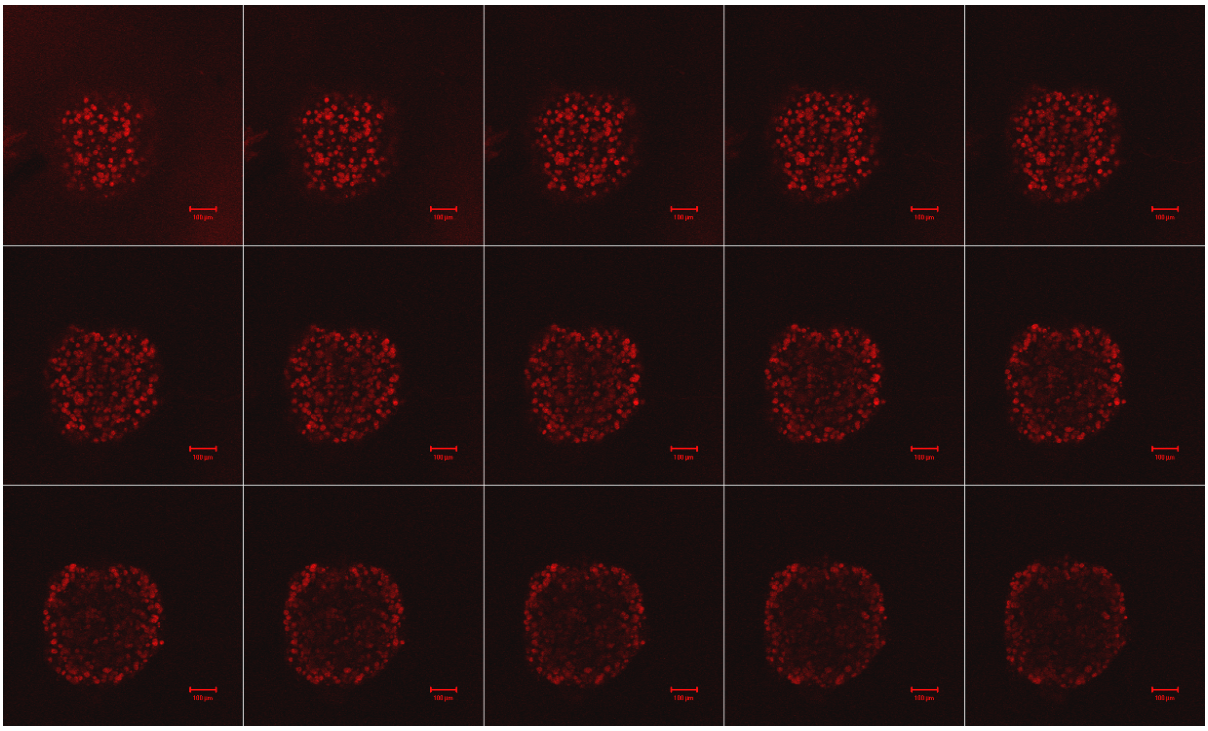

Figure 2-19
Serial confocal slices of a murine HPC encapsulation stained with MitoTracker® Red

Cross-sectioned bioreactors containing encapsulations and cells in mixed matrix were viewed using confocal microscopy as well. The bioreactors were

sacrificed 31 days after inoculation after being stained with live/dead fluoroprobe stains. Images consistently show encapsulations in the inoculated chamber adjacent one of the chamber walls or pressed against other encapsulations. In nearly every case, the spherical geometry of the encapsulations was distorted. Figure 2-20 shows the geometric perturbation but also shows increased fluorescence at the interface between two encapsulations pushed together. This is suggestive of cellular mobility within the encapsulation leading to cell aggregation.

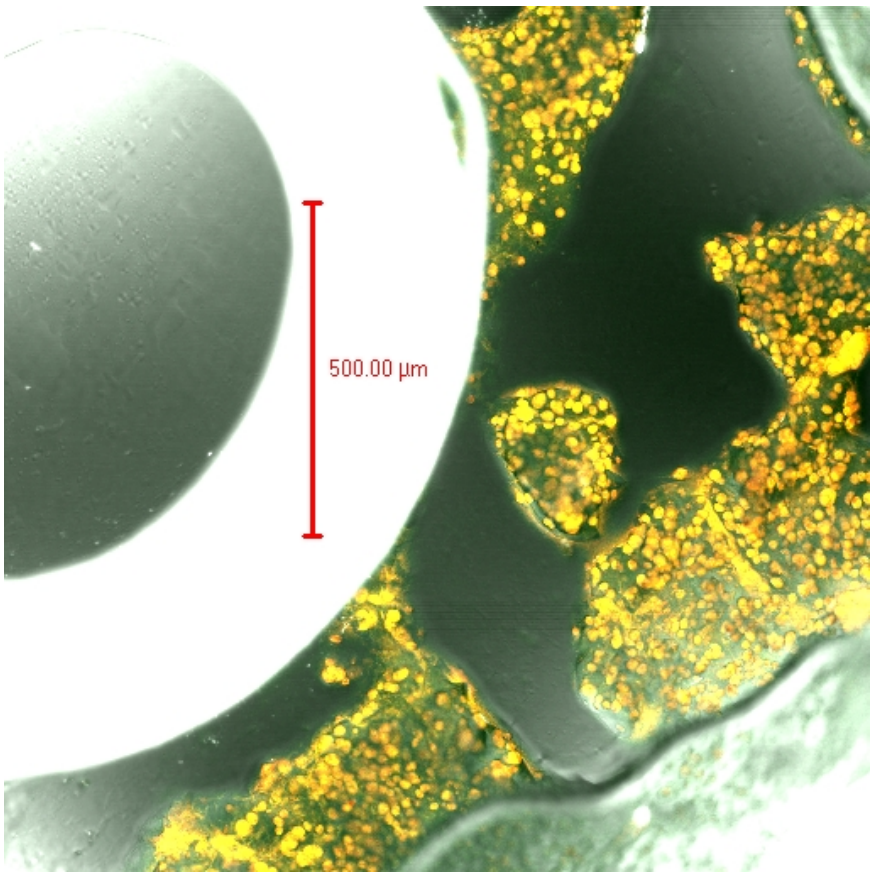

Figure 2-20
Confocal image of thin-sectioned bioreactor containing encapsulations at day 30 post inoculation (10 million cell/ml H0540)

2.4.2 NMR Data

2.4.2.1 Concerns regarding ethanol

Early in the NMR analysis process, concern arose surrounding the presence of a triplet centered at 1.18 ppm which was determined to be ethanol in the collected media samples. Initial findings from the TMS referenced studies showed erratic concentrations. It was originally thought that the switch to sodium formate referencing would reveal a more consistent trend. For the control bioreactor containing mixed gel (alginate and Matrigel) the formate referenced spectra show a decreasing concentration trend as a function of time.

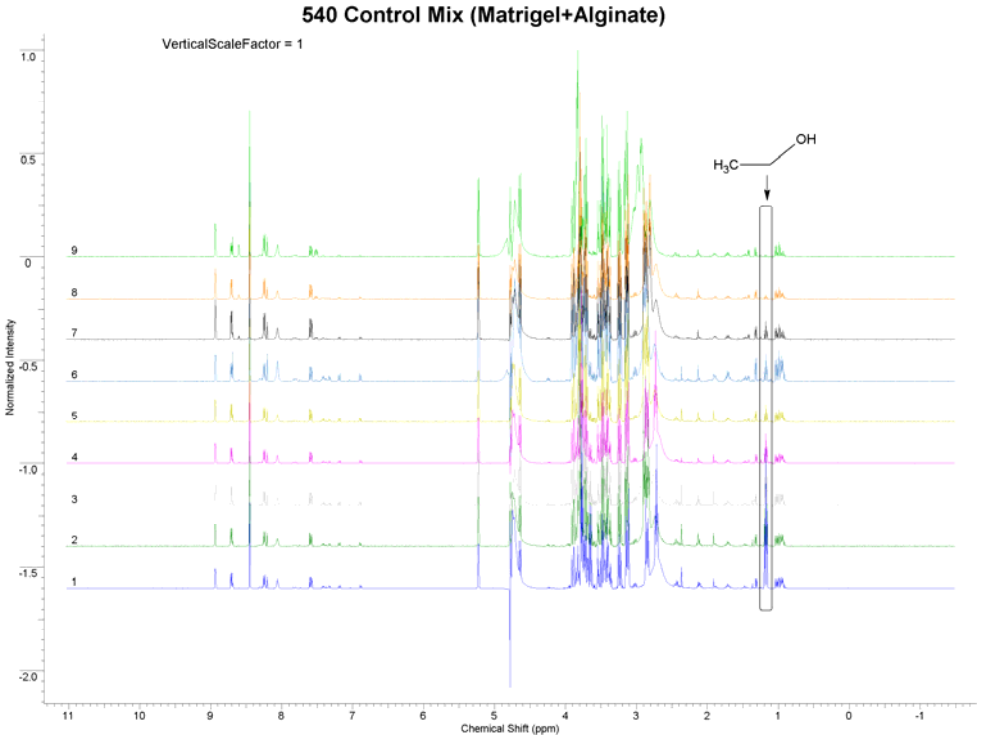

Figure 2-21
Transformed NMR FIDs for bioreactor control samples with time progressing from bottom to top

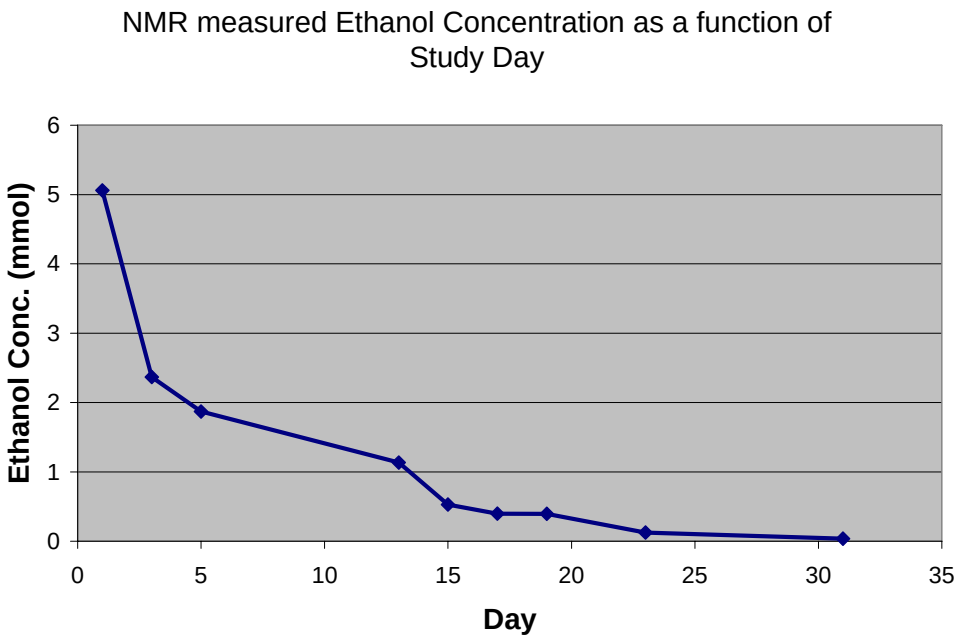

Figure 2-22
Ethanol concentration as a function of study day for control bioreactor (H0540 Study)

The diminishing trend shown in Figure 2-22 suggests that the presence of ethanol is the result of pre-study sterilization and bioreactor wetting both of which employ ethanol to prepare the bioreactor prior to inoculation with gel matrix or encapsulations.

This trend was observed in bioreactors containing cells as well. However, at certain time points, the ethanol concentration increased abruptly as shown in the red circled data point in Figure 2-23. This was originally thought to be an indication of biological contamination by bacteria, yeast, or fungus. The concentration profile for ethanol was not consistent with contamination in that the ethanol level would drop in the sample taken 48 hours later. This would suggest an analytical error or calibration error. Other chemical concentrations including glucose and acetate were monitored for use as measures of NMR stability due to the belief that these compounds would demonstrate reproducible concentrations over time points in the

study once the bioreactor had stabilized. As predicted, the concentrations for these compounds remained nearly linear supporting the stability of the method while also challenging the notion that a biological contaminant was present.

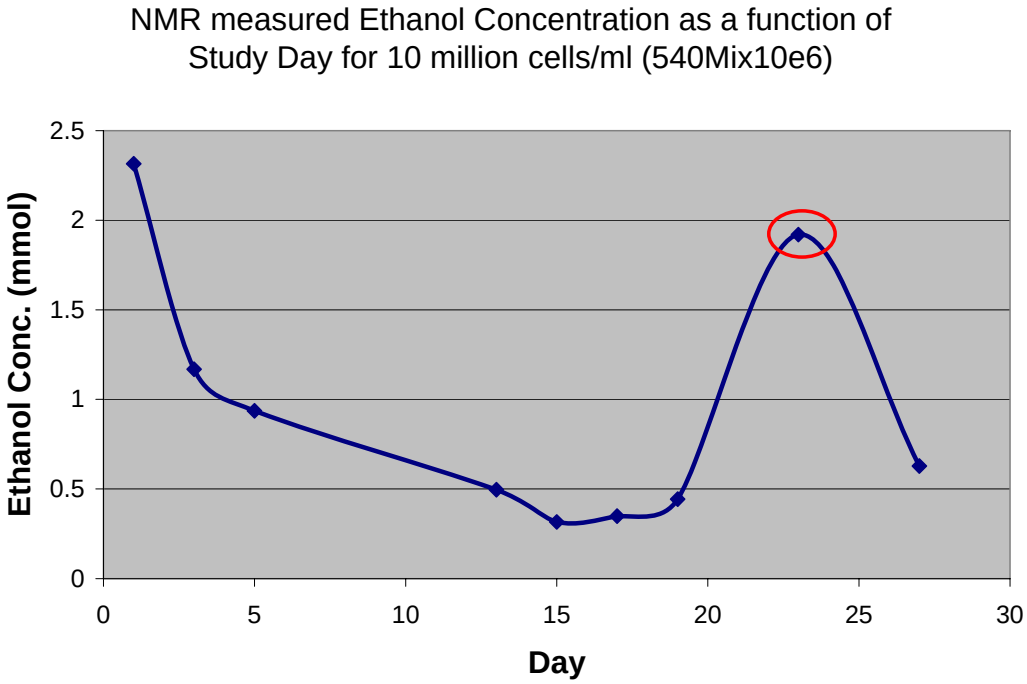

Figure 2-23
Ethanol concentration as a function of study day for mixed matrix experimental bioreactor (H0540 Study)

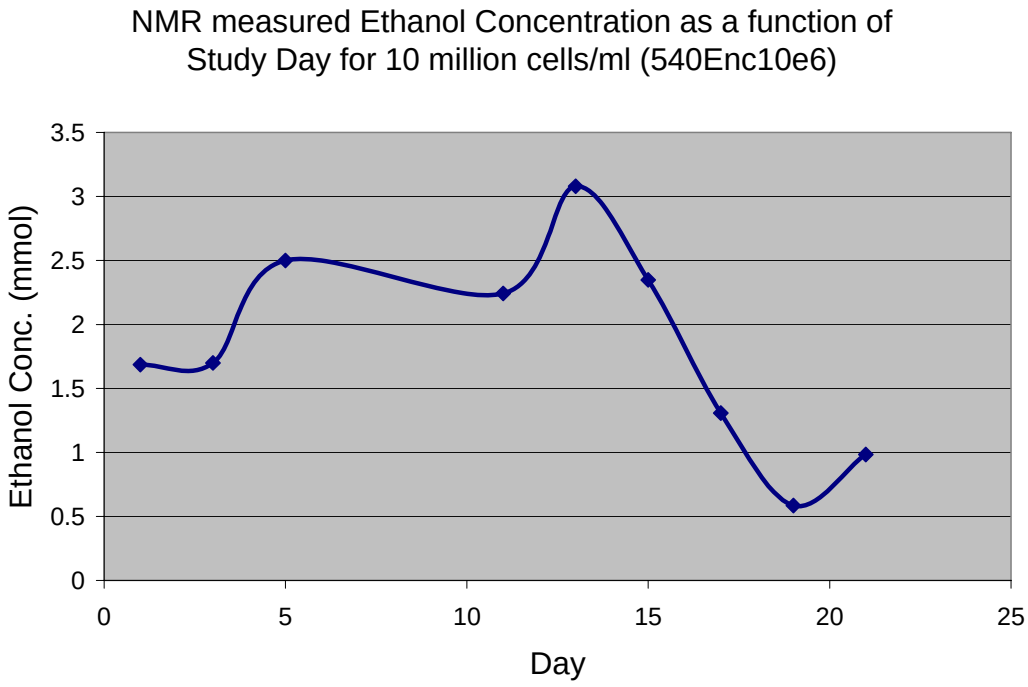

Figure 2-24
Ethanol concentration as a function of study day for encapsulation experimental bioreactor (H0540 Study)

A review of lab procedure related to collection of bioreactor media revealed the practice of swabbing a tubing port with ethanol prior to drawing samples with a syringe fitted with an 18 gauge needle. Owing to the large area of the port septum that an 18 gauge needle would cross, it is believed that the erratic behavior of the ethanol concentration is the direct result of contamination of the needle used to draw samples as it passed through the port septum. Such a finding is a clear demonstration of the sensitivity of NMR for low concentrations as well as a reminder that technicians must take care to use lab practices that minimize technique-induced errors to measurements.

2.4.2.2 Glutamine Metabolism

NMR results show that for both the mixed matrix bioreactor and encapsulation bioreactor glutamine was metabolized to completion following day five with media changes performed at 48 hour intervals. Figure 2-25 shows the results for glutamine metabolism as determined by NOESY pulse sequence NMR spectroscopy. Of particular note is the abrupt drop in glutamine in the control series following day 15. This is most likely due to the addition of 10 mmol ammonia to the media circulation at day 16 as a test to determine cellular BUN and urea response.

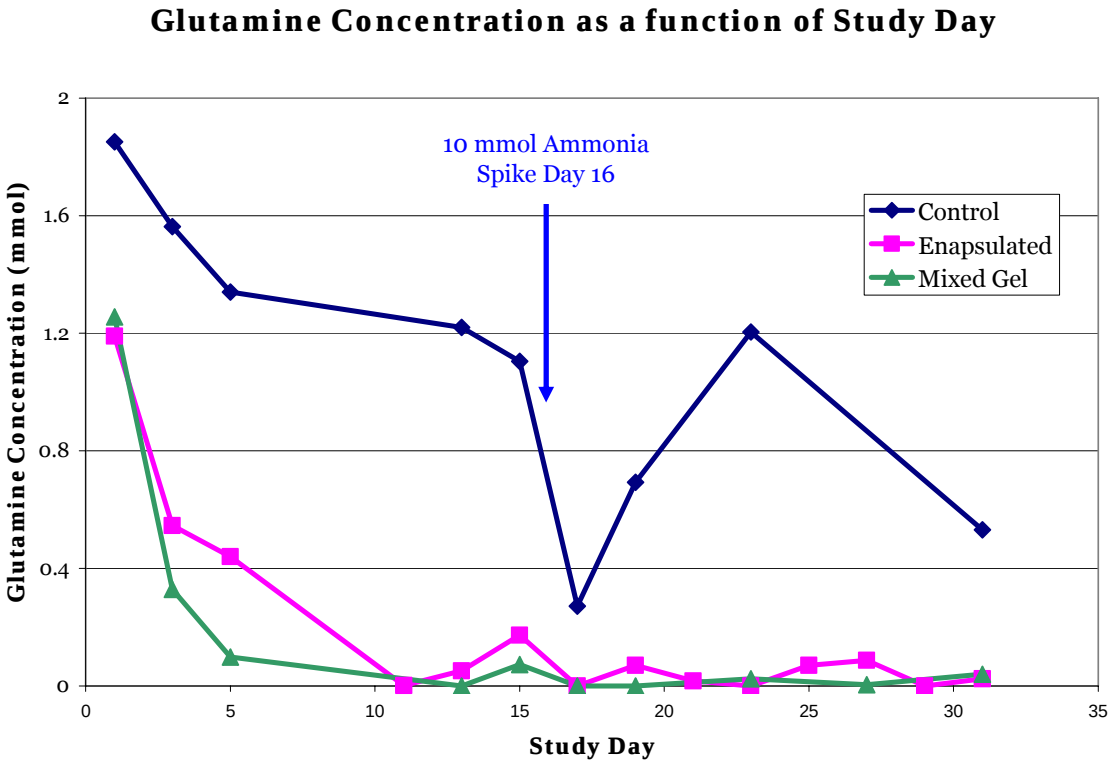

Figure 2-25
Glutamine metabolism as a function of study day for 10 million cells/ml (H0540)

2.4.2.3 Acetate Metabolism

The data for acetate concentrations as a function of time as determined by NMR measurement are shown in Figure 2-26.

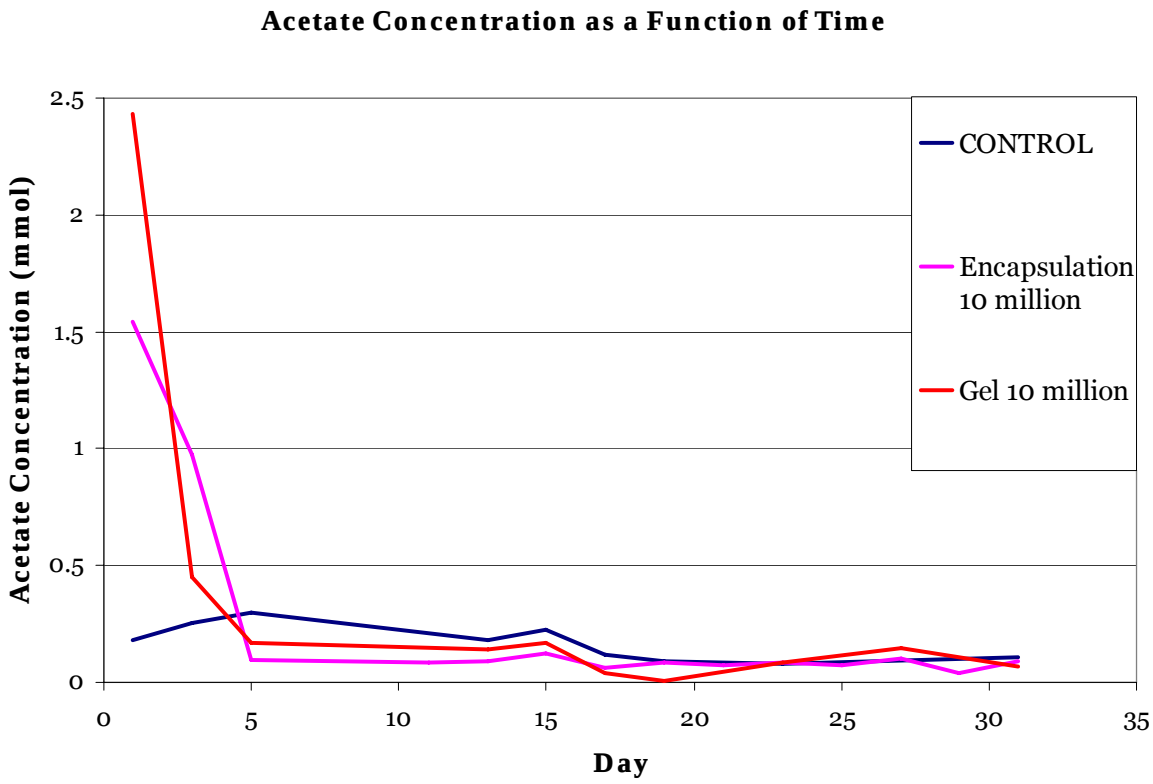

Figure 2-26
Acetate concentration as a function of time

2.4.2.4 Lactate Metabolism

The data for lactate concentrations as a function of time as determined by NMR measurement are shown in Figure 2-27.

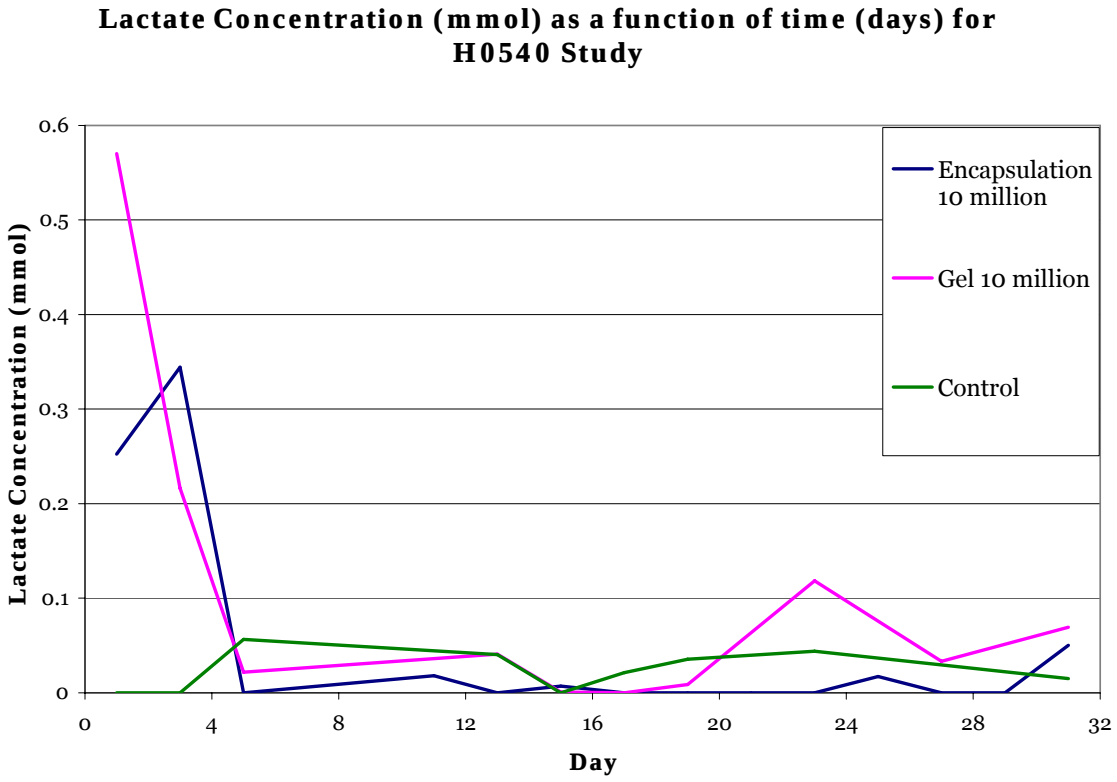

Figure 2-27
Lactate concentration as a function of time

2.4.3 Biolyzer Data

2.4.3.1 Bun/Urea Concentration

Biolyzer analysis of BUN/Urea concentrations of bioreactor media streams comparing encapsulations and cells loaded directly into Matrigel are shown in Figure 2-28. The results indicate that the BUN/Urea concentration observed in the encapsulations having 10 million cells/ml are consistently less than the concentrations for both 7 and 10 million cells/ml directly loaded in Matrigel bioreactors. The abrupt drop in concentration beyond day 15 is the result of the bioreactors being spiked with 10 mmol ammonia on day 16 of incubation.

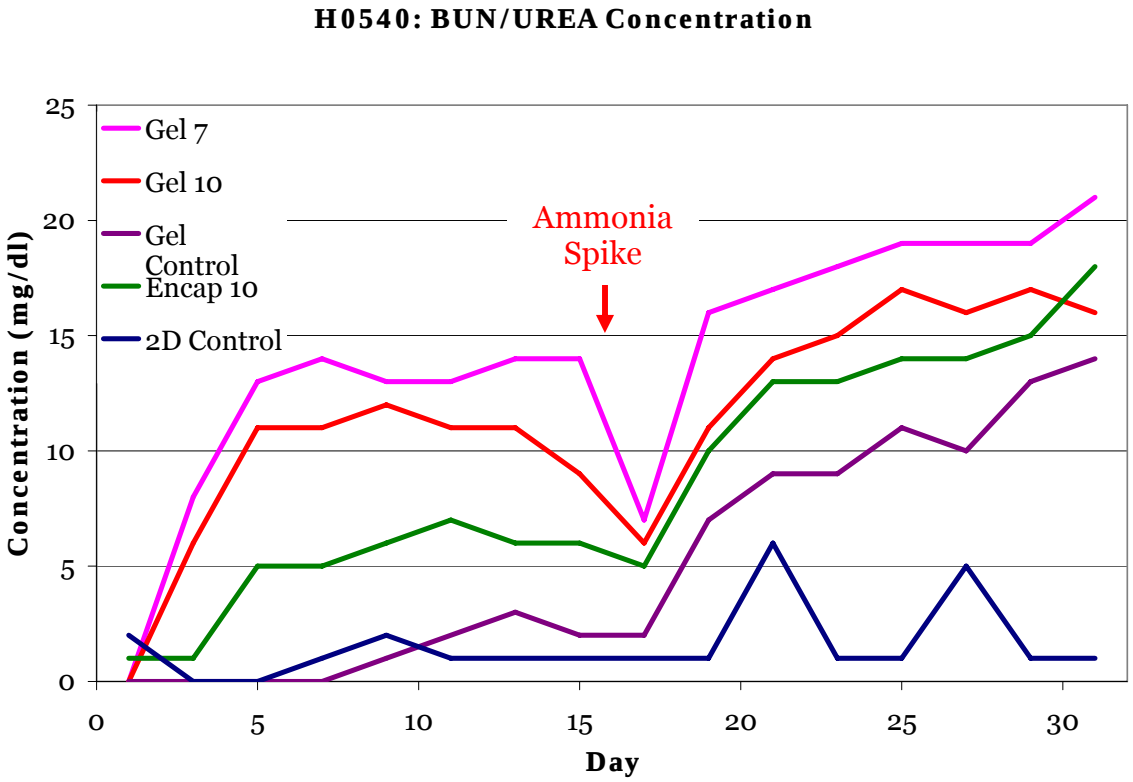

Figure 2-28
Time series BUN/Urea concentration for 7 and 10 million cells/ml gels, 10 million cells per ml, and controls

2.4.3.2 LDH Concentrations as a function of time

Biolyzer analysis of LDH concentrations of bioreactor media streams comparing encapsulations and cells loaded directly into Matrigel are shown in Figure 2-29. Of particular note is the diminishing concentration in all experimental bioreactors during the first five days.

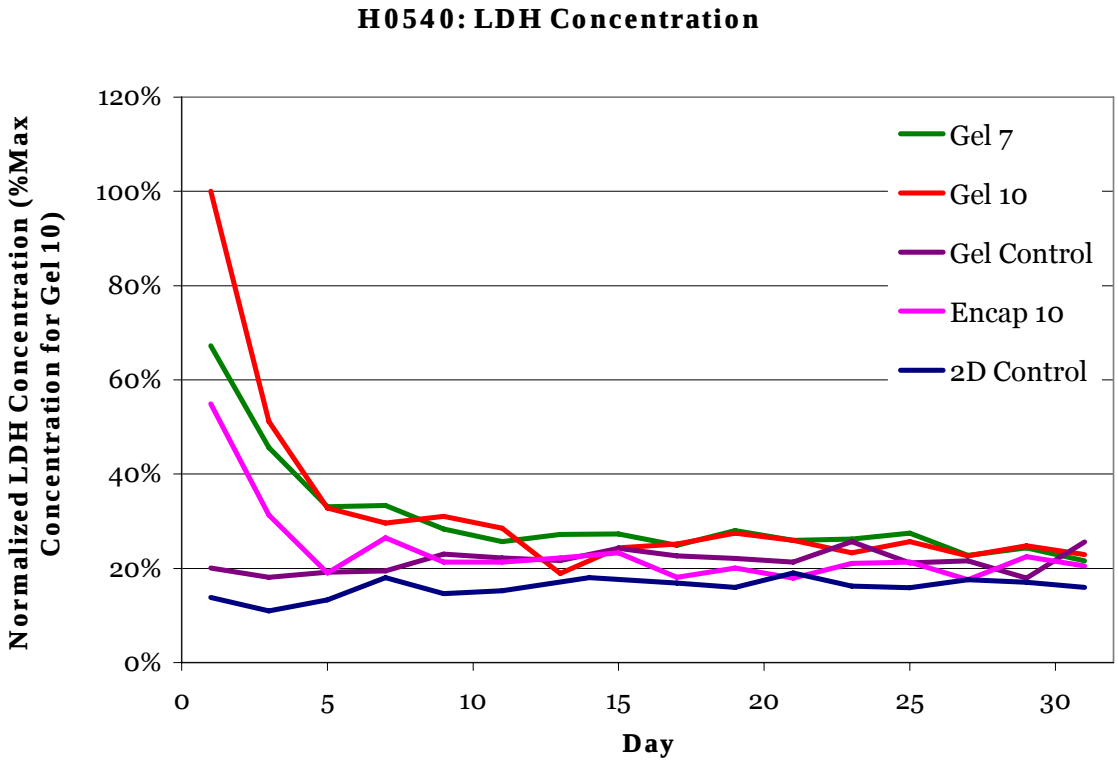

Figure 2-29
Time series LDH concentration for 7 and 10 million cells/ml gels, 10 million cells per ml, and controls

2.4.4 Cryopreservation Storage Tests

The practical utility of encapsulations will be limited by the ability to store and transport the encapsulations with relative ease. With this in mind, experiments were undertaken to explore methods for cryopreservation. An important consideration with any aqueous filled body is the expansion of water upon transition to the solid phase. An optimistic working hypothesis regarding this phenomenon was that the alginate gel would sufficiently expand to maintain spherical structure when frozen. Tests to determine geometric stability following conventional 0˚C

freezing and -80˚C freezing with thawing resulted in destruction to the integrity of the alginate encapsulations.

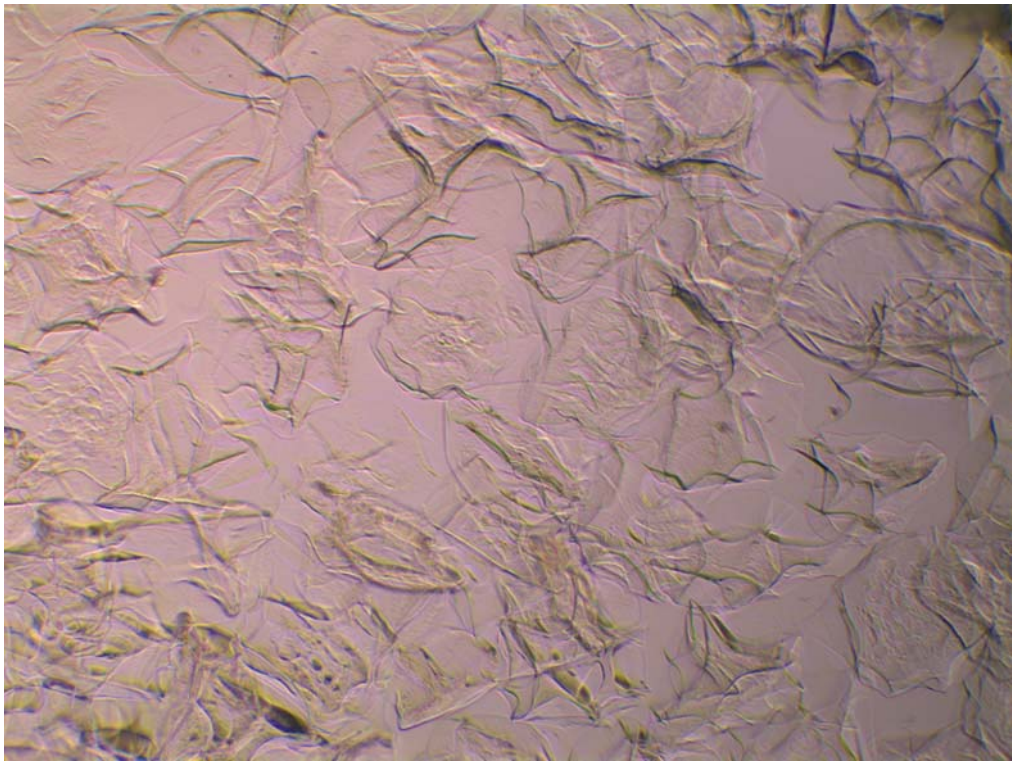

Figure 2-30
Post-thaw 10x light microscopy image of -80˚C frozen encapsulations

2.4.5 Analysis of Metabolic Findings

The LDH findings illustrate that the initial isolation and/or encapsulation causes disruption of hepatocyte function and cellular damage. Within five days, the LDH level lowers illustrating that cells have stabilized. Under the stress of isolation and encapsulation, it is likely for the cells to experience temporal hypoxia resulting in anaerobic glycolysis. This is supported with an inspection of the NMR time series analysis of lactate in which the concentration for experimental samples is elevated for the first five days of study then drops to levels consistent with the acellular

control. Similarly, the slow return of glutamine metabolism during the first five days after encapsulation supports anaerobic metabolism consistent with the other findings. Figure 2-31 illustrates the release of LDH due to cell death and the anaerobic metabolism leading to lactate.

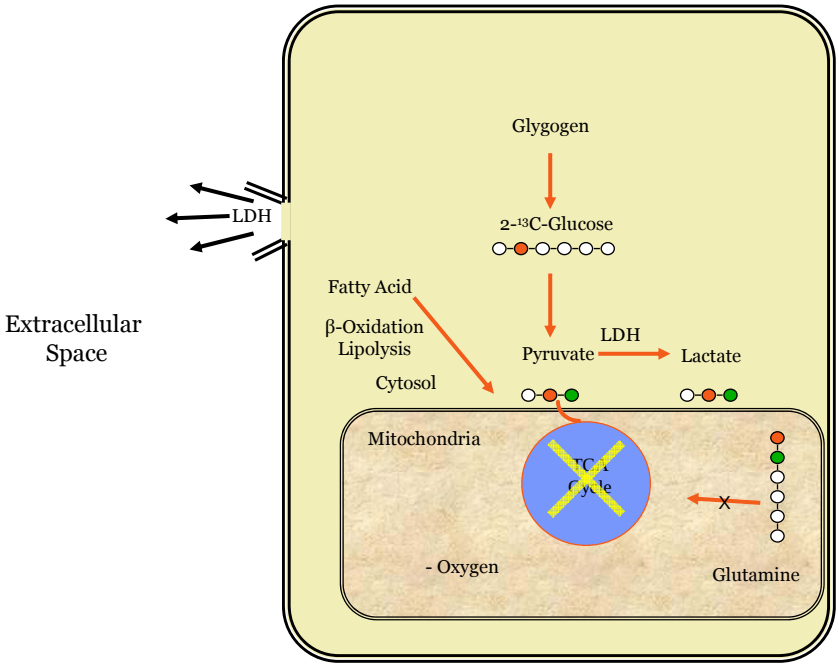

Figure 2-31
LDH release associated with cell death and anaerobic metabolism

The confocal results of sectioned bioreactors and of encapsulations incubated for up to thirty days show live cells as indicated by MitoTracker® Red. This is further supported by the consumption of glutamine to exhaustion in the bioreactor media analysis by NMR. The glutamine metabolism indicates that aerobic metabolism in the mitochondria is feeding into the TCA cycle as glyconeogenesis and gluconeogenesis are upregulated as illustrated in Figure 2-32. Similarly, the increase in BUN/urea levels in experimental bioreactors beyond day five indicates a return to protein metabolism.

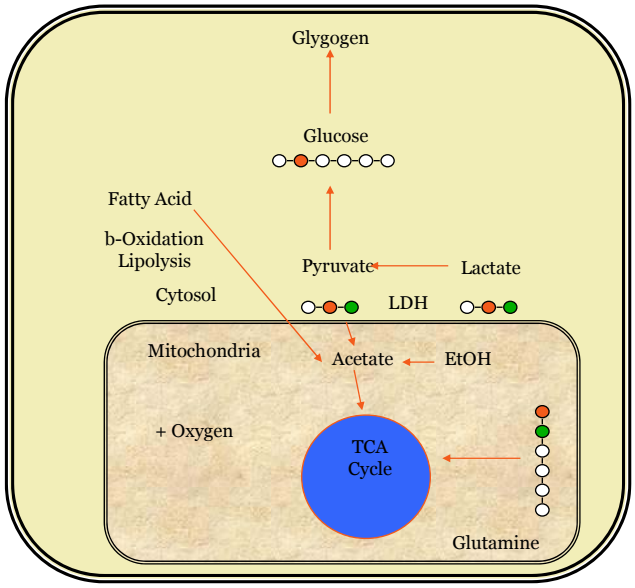

Figure 2-32
Glutamine metabolism under aerobic conditions

2.5 Endnotes

1. Glacken, M., et. al., *Large scale production of mammalian cells and their products: Engineering principles and barriers to scale-up.* Ann. New York Academy of Sciences, 1983. **413**: p. 355-372.

2. Rotem, A., Toner, M., et. al., *Oxygen uptake rates in cultured rat hepatocytes.* Biotechnology and Bioengineering, 1992. **40**: p. 1286-1291.

3. Lacy, P., Hegre, OD, et. al, *Maintenance of normoglycemia in diabetic mice by subcutaneous xenografts of encapsulated islets.* Science, 1991. **254**: p. 1782-1784.

4. Papas, K., Long, R., Sambanis A., ConstantinidisI., *Development of a bioartificial pancreas: I. Long-term propagation and basal and induced secretion from entrapped BETA TC3 cell cultures.* Biotechnology and Bioengineering, 1999. **66**(4): p. 219-230.

5. Glicklis, R., Shapiro, L., et. al., *Hepatocyte behavior within three-dimensional porous alginate scaffolds.* Biotechnology and Bioengineering, 2000. **67**(3): p. 344-353.

6. King, A., *Alginate Microcapsules for Use in Trasplantation of Islets of Langerhans*. 2001, Acta Universitatis Upsaliensis: Uppsala, Sweden. p. 43.

7. Yagi, K., Tsuda, K., Serada, M., Yamada, C., Kondoh, A., Miura, Y., *Rapid formation of multicellular spheroids of adult rat hepatocytes by rotation culture and their immobilization within calcium alginate.* Artificial Organs, 1993. **17**(11): p. 929-34.

8. King, A., Lau, J., Nordin, A., Sandler, S., Andersson, A., *The Effect of Capsule Composition in the Reversal of Hyperglycemia in Diabetic Mice Transplanted with Microencapsulated Allogeneic Islets.* Diabetes Technology & Therapeutics, 2003. **5**(4): p. 653-663.

9. Schwartz, R.E., et al., *Multipotent adult progenitor cells from bone marrow differentiate into functional hepatocyte-like cells.* J. Clin. Invest., 2002. **109**(10): p. 1291-1302.

10. Ringel, M., et al., *Hepatocytes cultured in alginate microspheres: an optimized technique to study enzyme induction*. Toxicology, 2005. **206**(1): p. 153-167.

11. Nicholson, J., Buckingham, M., Sadler, P., *High resolution H NMR studies of vertabrate blood and plasma.* Biochem. J., 1983. **211**: p. 605-615.

12. Sumner, L.W., P. Mendes, and R.A. Dixon, *Plant metabolomics: large-scale phytochemistry in the functional genomics era.* Phytochemistry, 2003. **62**(6): p. 817-836.

13. Konstantinos, J.D., Parkinson, J.A., et. al, *1H NMR spectroscopy as a tool to evaluate key metabolic functions of primary porcine hepatoctyes after cryopreservation.* NMR in Biomedicine, 2002. **15**: p. 241-250.

14. Seglen, P.O., *Preparation of isolated rat liver cells.* Methods of Cell Biology, 1976. **13**: p. 29-83.

15. Wang, J., Clark, J.B., et. al., *Proliferation and hepatic differentiation of adult-derived progenitor cells.* Cells Tissues Organs, 2003. **173**(4): p. 193-203.

16. Doyle, e.a., *Process for Making Capsules*. 1964: United States.

17. Hynes, C.R., *A Thoughtful Approach To Field-Service Grounding.* Electrostatic Discharge Journal, 1989. **1989**(Feb./Mar.).

18. U.S. Department of Health and Human Services, N.I.f.O.S.a.H., *NIOSH ALERT: Preventing fatalities of workers who contact electrical energy*. 1986. Publication No. 87-103.

19. Geddes, L.A., J.D. Bourland, and G. Ford, *The mechanism underlying sudden death from electric shock.* Medical Instrumentation, 1986. **20**(6): p. 303-315.

20. Wolfe, S.P., Hsu, E., Reid, L.M., Macdonald, J.M., *A novel multi-coaxial hollow fiber bioreactor for adherent cell types. Part 1: Hydrodynamic studies.* Biotechnology and Bioengineering, 2002. **77**(1): p. 83-90.

21. Serp, D., Cantana, E., et. al., *Characterization of an encapsulation device for the production of monodisperse alginate beads for cell immobilization.* Biotechnology and Bioengineering, 2000. **70**(1): p. 41-53.

22. *Biogeochemistry of chelating agents*, ed. B. Nowack and J. VanBriessen. 2005, Washington, D.C.: American Chemical Society. 472.

23. Bozzola, J., Russell, L.,, *Electron Microscopy Principles and Techniques for Biologists*. 2nd ed. 1999, Sudbury, Mass.: Jones and Bartlett Publishers. 670.

24. Kriat, M., Confort-Gouny, S., Vion-Dury, J., Sciaky, M., Viout, P., Cozzone, P., *Quantitation of metabolites in human blood serum by proton magnetic resonance spectroscopy. A comparative study of the use of formate and TSP as concentration standards.* NMR Biomed., 1992. **5**(4): p. 179-94.

3 High Through-put NMR Analysis of Culture Media for Bioreactors[1]

3.1 Abstract

This chapter describes a high through-put (HTP) NMR method for analysis of components in culture media. The spin-lattice relaxation (T_1) values and concentrations were measured for 19 components in culture media and two internal referencing agents, formate and 3-(trimethylsily)propionic-2,2,3,3-d_4 acid sodium salt (TSP), in pure and two-day conditioned culture media from a multi-coaxial human bioartificial liver (BAL). Pure media had the highest overall T_1 values, the longest T_1 being formate at 8.3s, while TSP had the most significant change in T_1 with addition of albumin, likely due to protein binding. Using a 400 MHz NMR spectrometer the ^{1}H NMR spectral signal-to-noise ratio for 0.16 mM alanine in media is 21 and obtained in 14 minutes , resulting in HTP automated analysis. To demonstrate the HTP ^{1}H NMR method, multicoaxial BALs were batch cultured (i.e.,

[1] This chapter is adapted from a publication entitled *High Through-put NMR Analysis of Culture Media for Quality Assurance and Metabolomics for Tissue Engineering* by Christopher Seagle, Megan A. Christie, Jason Winnike, Randall McClelland, John Ludlow, Thomas O'Connell, and Jeffrey M. Macdonald. At the time of publication of this dissertation, the article had not yet been submitted to any peer-review journal.

media changed every other day) for 15 days after inoculation with human liver cells in Matrigel™:collagen type 1 gels and compared to 2D gel cultures. The results showed that glutamine consumption was higher by day 8 in the BAL as compared to 2D culture, while lactate production was lower through the 15 day culture period. Alanine was the primary amino acids produced during the culture period and it tracked lactate or urea production. Glucose and pyruvate consumption were similar between the BAL and 2D cultures. The unbiased NMR analysis permits quality assurance of unknown potential contaminants, and a case in point is residual ethanol resulting from the bioreactor membrane 'wetting' procedure. The combination of robotic NMR sample changer and group integration of ^{1}H NMR spectra results in 14 minutes per sample using an extremely common 400 MHz NMR spectrometer. A biochemical scheme is presented to translate bioreactor metabolomic footprint results into either bioreactor operational parameters, such as media nutrient (i.e. oxygen, glutamine,…) concentration, or quality assurance issues.

3.2 Introduction

High-throughput (HTP) NMR spectroscopic analysis of media provides an unbiased determination of biochemical concentrations permitting culture protocol modifications to be rapidly implemented for optimizing culture conditions [1-3]. In combination with bioinformatic tools [4] this analytical method provides robust characterization of phenotypes for tissue engineering. Unlike analytical modalities, NMR spectroscopy does not require extensive sample preparation and is innately quantitative resulting in unbiased analysis. This makes NMR spectroscopy one of

the most powerful analytical techniques available for quality assurance which is particularly important for tissue engineering due to the multitude of operational parameters, and potential for human error and contamination. This is particularly true for engineered bioartificial liver (BAL), where clinical liver assays are used to characterize degrees of liver function and differentiation. There is a need for a more robust method of reporting the hepatic phenotype of BALs [5]. Metabolomic analysis fills this requirement [6].

The state-of-the-art method to quantify concentrations in media is HPLC and mass spectroscopy [7-9]. Media component analysis by ^{1}H NMR spectroscopy has been attempted since the 1980s [2, 3, 10-12] but has never been widely-accepted, likely because the NMR results were less sensitive than HPLC, and more importantly, the unbiased nature of NMR was not appreciated. Now with high field NMR spectrometers more common and development of multivariate statistics for metabolomics [13, 14] the unbiased strength of NMR makes it perhaps one of the most powerful techniques for phenotyping tissues especially 3D tissue constructs in tissue engineering. Although direct analysis of the tissue can be performed, the bioreactor dimensions must conform to existing NMR hardware [15] or the NMR hardware must be built around the bioreactor [16], in a similar fashion as the NMR/MRI analysis of a human tissues. Media analysis serves a similar function as monitoring the central compartment, or blood, of a human. The distinctions between the compliment of metabolites within the cells - “the fingerprint” - and from those outside the cells - “the footprint” - are given by two different metabolic profiles [17]. The fingerprint and footprint is tissue specific and depends on the degree of

metabolic differentiation, resulting from the number and capacity of transporters, and signaling and metabolic pathways.

The same problems associated with NMR spectroscopic analysis of serum apply to culture media, including differences in spin-lattice relaxation (T_1) values due to noncovalent protein binding resulting in inaccurate determination of concentrations [18]. The spin-lattice relaxation (T_1) values have never been reported for components in culture media and are necessary to insure accuracy of the NMR-derived concentrations [3]. Therefore, a HTP NMR method has been optimized whereby T_1 values of media components calculated. In addition the sample preparation conditions were optimized, and the spectral parameter identified to obtain ^{1}H NMR spectra of media within 10 minutes with bulk spectral integration to rapidly convert peak areas to metabolite concentrations. To demonstrate the application of the HTP NMR method to optimizing tissue culture protocol, we apply the method to development of a commercially-available bioartificial liver [19, 20].

3.3 Methods

NMR supplies were purchased from multiple vendors. The 5 mm tubes, deuterium oxide, sodium formate, and 3-(trimethylsily)propionic-2,2,3,3-d_4 acid were purchased from Sigma Chemical company (St Louis, MO), Cambridge Isotope Laboratories, (Andover, MA), Alfa Aesar (Ward Hill, MA), and Isotec Inc. (Miamisburg, OH), respectively. Bioreactor end pieces were machined from polypropylene tube (1 in. diameter) and assembled as previously described [16, 19]. Bioreactor life support units have been described previously [8]. Matrix supporting

the cells was made up of 1:1 (vol:vol) collagen type I and Matrigel™ from Inamed Biomaterials Inc. (Irvine, CA) and Becton Dickenson Inc. (BD, Franklin Lakes, NJ).

3.3.1 BAL Inoculation, Media, and Media Collection

The human BAL studies were performed at the ADMET Technologies Inc. (Research Triangle Park, NC) laboratory using their patented multicoaxial bioreactor [21] and using their primary human liver cells, UMIX, as described on their webpage (http://www.admettechnologies.com/). Liver cells were mixed with a 1:1 collagen-to- Matrigel™ mixture (vol:vol) and inoculated at a density of 10^7 cells/ml. The media was a hormonally-defined recipe, Kubotas media [22], using the Dulbecco's Modification of Eagle's Medium as the basal media (Mediatech 17-205-CV, Herndon, VA). The media was changed in batch mode the day after inoculation followed by every two days, and placed in a -80°C freezer until analysis, at which point it was thawed. Flow rates through the BAL were 5 ml/min, and oxygen concentration was 95% as described by McClelland and Coger [23].

3.3.2 2D Culture

Hepatocytes obtained from a single human liver were cultured immediately following isolation using the same cell and matrix mix as described in the BAL Inoculation and Media Collection methods section was plated on a pre-coated 6-well Collagen Type I plate from BD (Franklin Lakes, NJ) at a 1.25ml volume per well, or 12.5 million cells. The cell and matrix solution was placed in a 37°C humidified

incubator with 5% CO_2 for 1 hour to gel properly. Media was then added to the culture at a volume of 2 ml per well. Media was changed 24 hours after plating and every other day thereafter for all cultures.

3.3.3 3D Culture of UMIX

Figure 3-1 shows the multicoaxial bioreactor with all of the ports identified (left), and the bioreactor incorporated into the life support system (right). The bioreactor is placed inside an incubator with the reservoir, pump, and various tubings. The gas is composed of oxygen:carbon dioxide (95:5), and the gas line is inserted through the side of the incubator and attached directly to the bioreactor and dead-ending at the reservoir, which vents through a 0.2 μm pore polypropylene air filter. The temperature of the incubator is 37° C.

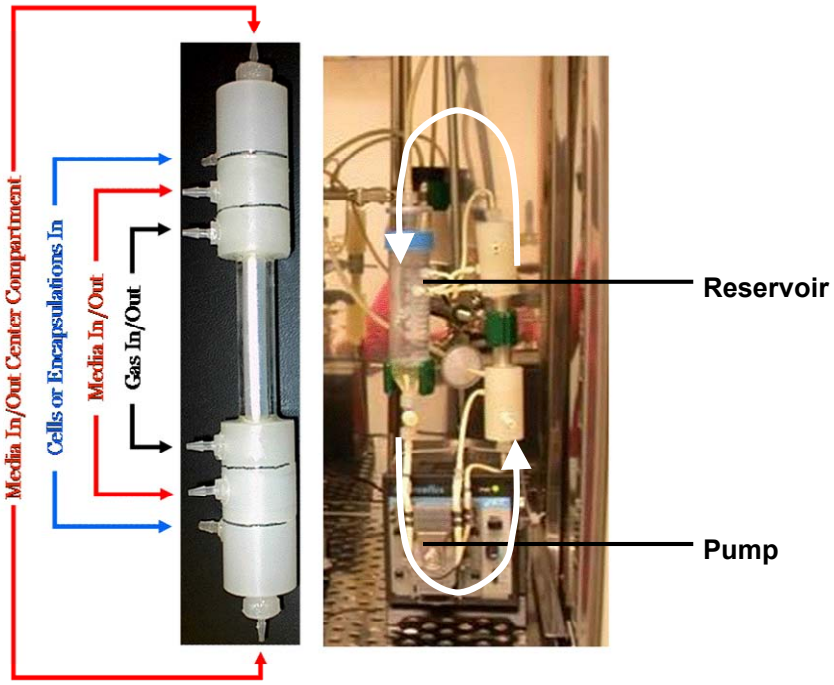

Figure 3-1
Bioreactor design and flow loops

3.3.4 Optimization of NMR Pulse Sequence for Quantification of Media Components

Four pulse sequences were compared for maximum signal-to-noise ratio, the ^{1}H one-pulse with presaturation using a 45° flip angle with 2.5 T_1 delay and a 90° flip angle with 5 T_1 delay, a T_2-weighted CPMG, and a T_1-weighted 1D NOESY. Also, an inversion recovery sequence was used to obtain spectra for determining T_1 values for multiple media components and internal standards. One pure media sample and one 'conditioned' media sample were prepared with 8.15mM formate, 25 mM citrate, 143 mM imidazole and 890µM TSP. These compounds were used to observe effects of T_1 and T_2 on peak areas while citrate and imidazole served to measure paramagnetic cation effects [24] and pH respectively. Sensitivity comparisons were

made by using the ACD signal-to-noise ratio determination between the various pulse sequences.

3.3.5 ^{1}H NMR Analysis of Media

Samples were made from 540 µl of media and 60 µl of deuterium oxide containing 8.9mM TSP and 81.5mM formate (final sample concentrations 890µM and 8.15mM, respectively). A one-pulse sequence with a 4 sec presaturation pulse was used with a sweep width of 4,406.2 Hz, 32K complex datapoints, resulting in an acquisition time of 3.72 s and total repletion time of 45 s. A total of 32 transients were obtained resulting in 22 minutes per spectrum. The FIDs were processed with a 0.5 Hz exponential, zero-filled to 64K datapoints, and Fourier transformed into the frequency domain.

Absolute sample concentrations were determined using area under the curve (AUC) for selected metabolite peaks normalized to formate concentration and adjusted for the proton number associated with the peak of interest. Consumption and production rates were calculated as the millimole difference between the two-day media changes divided by the number of remaining viable hepatocytes inoculated in the BAL or 2D culture dish per hour. Evaporation differences were corrected for by normalizing formate concentrations and applying correction factors to all constituents within each individual 2-day sample.

3.3.6 NMR Peak Area Determination and Calculation of Error

ACD software (Toronto, Ontario, CA) was used to process and fit the NMR data. A macro was written to process the FIDs as described above and baseline corrected using the multi-point baseline correction option. The spectral peaks were fit with both deconvolution, where individual peaks were fit with Lorentzian line shapes, and intelligent binning with integration. The known concentration of TSP and formate were used as internal concentration standards. The accuracy of the Mettler model XS205 balance was used in determining the accuracy of the error and calculation of NMR accuracy was determined from the literature and known recipe. New bottles of formate and TSP were used for the study to insure purity. Since TSP binds to proteins and can result in reduced peak area depending on the pulse sequence [18], formate was added as a second concentration to validate the effect of TSP binding.

3.3.7 Viability and Functional Assays

Media supernatants were analyzed at 48-hour intervals to monitor liver functions, specifically lactate dehydrogenase (LDH) leakage and urea production. To determine the number of live cells remaining in culture, LDH was quantified using a Vitros DT60 II chemistry system from Johnson and Johnson (New Brunswick, NJ). A standard curve was produced using a known number of cells in a 2 ml volume of media, sonicating the cells, and measuring the LDH. Urea production was determined using a diagnostic kit purchased from BioAssay Systems (Hayward, CA).

Briefly, a chromogenic reagent forms a colored complex specifically with urea and the color was then measured at 520nm using a BioTek microplate reader (Winooski, Vermont).

3.3.8 Metabolomic Footprint Mass Balance Model

Metabolic pathway reconstruction was done by entering media components into the KEGG or Brenda metabolomic databases (http://www.genome.jp/kegg/) and generating connecting pathways [4]. Consumption or production rates were calculated based on the NMR data and metabolic mass balance schematics of the metabolomic footprint were made at the various time points representing major shifts in metabolism throughout the time course.

3.3.9 Microscopy Techniques

The morphology of the cells in 2D cultures were examined using a Leica DMIL inverted phase contrast microscope. Pictures were taken every other day, which coincided with media changes. The BAL cultures were imaged as previously described [22].

3.4 Results

Figure 3-2 is a ^{1}H NMR spectrum of the culture media (middle) showing the various resonances representing compounds found in the media (see Figure 3-2

legend for assignments). The T_1 values of the various resonant peaks in pure media are shown in the plot on the bottom of figure 2. In general, the conditioned media decreased the T_1 values, and this difference in T_1 values is shown at the bottom of the plot in Figure 3-2. There is broadening of the TSP NMR signal that is likely caused by the albumin concentration, since albumin binds TSP greatly decreasing its spin-spin relaxation values [18]. Therefore, formate was used as a concentration standard since its peak did not broaden nor did the T_1 value change with the addition of albumin.

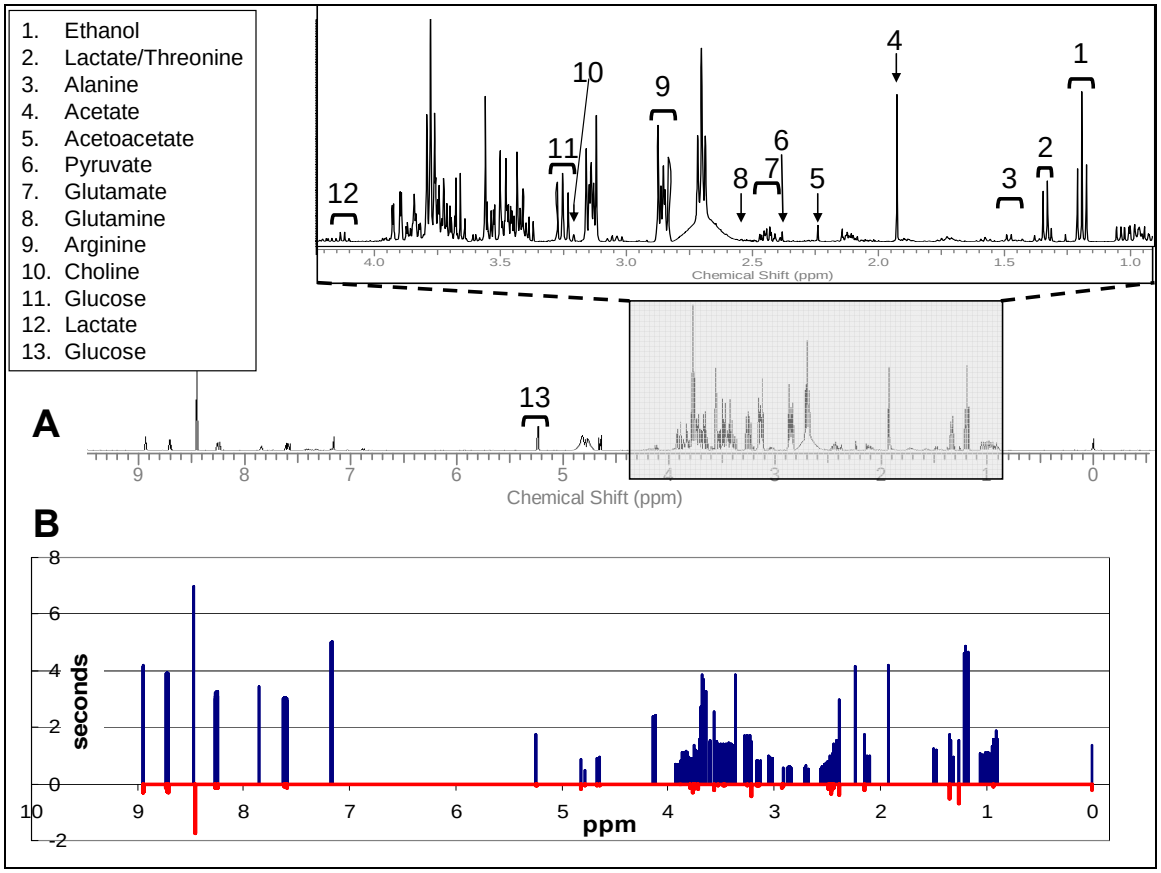

Figure 3-2
NMR metabolites and T1 values
A) 1H NMR spectra of media exposed to bioreactor containing cells, B) T1 and Delta T1 values for Fresh Bioreactor Media and Cell Exposed Bioreactor Media as a function of Chemical Shift

Further comparison of ^{1}H presaturation one-pulse, 1D NOESY (T_1-weighted), and CPMG (T_2-weighted) resulted in similar values for peak areas using either integration or deconvolution. As expected from the T_1 values shown in Figure 3-2, the T_1-weighted 1-D NOESY affected the TSP peak area, decreasing its peak area using a 100 ms mixing time (see Methods for sequence parameters). Overall, ^{1}H presaturation one-pulse spectra with a 45° or 90° flip angle had the same signal-to-noise ratio for a given time. Since the hormonally-defined or serum-supplemented media contains a tenth of the albumin as normal serum, the dramatic effects on TSP peak width observed with serum [18] were not seen with culture media. The T_2-weighted CPMG did not affect the quantification of TSP and no detectable paramagnetic load was observed as measured from citrate broadening. However, due to unforeseen effect on T_2 values caused by, for example, massive hepatocye death causing increased iron load, the simple one-pulse spectrum was chosen as the optimum pulse sequence. Therefore, a simple ^{1}H presaturation one-pulse with 90° flip angle and 45 second repetition time (five times the longest T_1 value) was determined to be the most quantitative pulse sequence. Comparison of peak fitting (i.e. deconvolution) and manual integration resulted in less than 1% difference in concentration measures for well resolved peaks. However, it is critical to manually examine the bins from each sample to insure that there are no contaminating peaks resulting from unforeseen compounds.

One interesting discovery due to the use of external standard was a dilution factor in the bioreactor in the first media change due to dilution of culture media components with the phosphate buffered saline (PBS) rinse procedure. As described

in the methods, the bioreactor membrane was 'wetted' with ethanol and then rinsed two times with PBS, and once with media prior to a final media change before inoculation.

Figure 3-4B shows calculated viable cells by measure of the cumulative media LDH, a measure of mortality, over the course of culture (15 days). In general, the LDH activity was slightly higher in 3D bioreactor as compared to the 2D control culture. By measuring the LDH level of seven aliquots of hepatocytes obtained from the same isolation used in the bioreactor experiments ranging in cell density from 65,000 cells/ml to $4.16x10^6$ cells/ml, a calibration line was developed to calculate the cell death for each 48 hour media change (Figure 3-3).

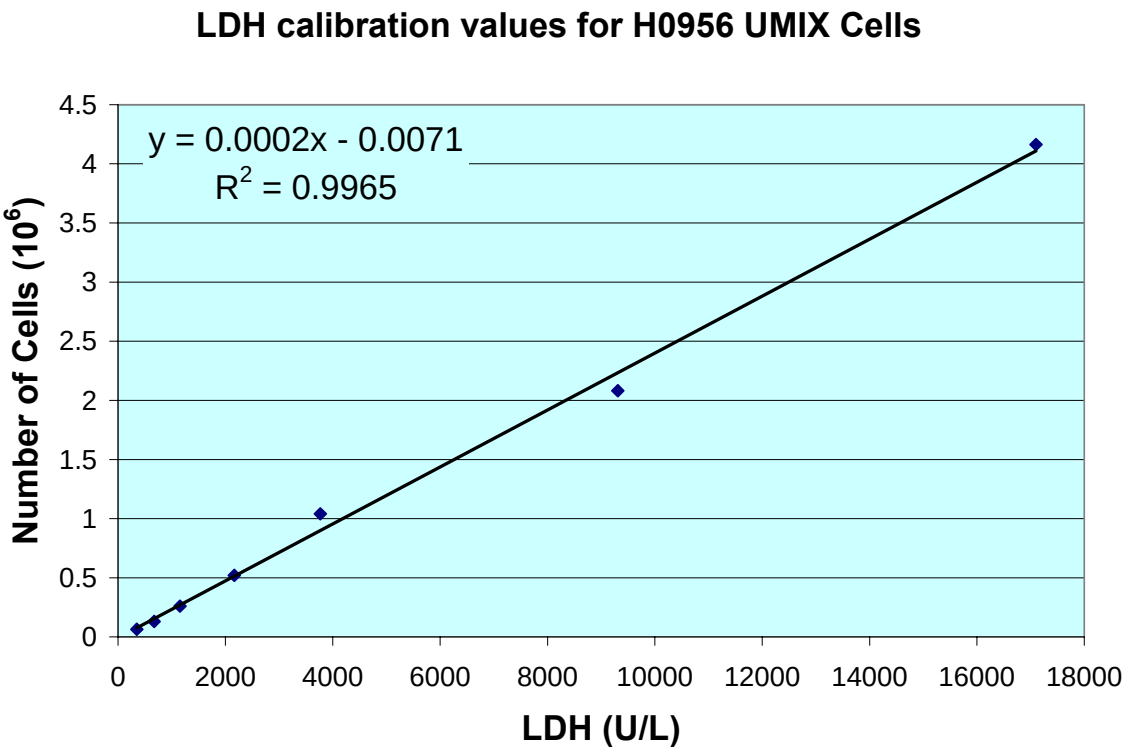

Figure 3-3
LDH calibration plot

The summation of these LDH values was taken and used to determine the total viable cell number and the percent cumulative cell death (Figure 3-4B) based upon the equation determined by the calibration plot (Figure 3-3). These mortality values were used to calculate the consumption and production rates of the 3D and 2D culture as a function of viable cells rather than initial inoculation number. The primary difference other than dimensionality was the oxygen concentration, with 95% and 20% for the 3D and 2D cultures, respectively.

A

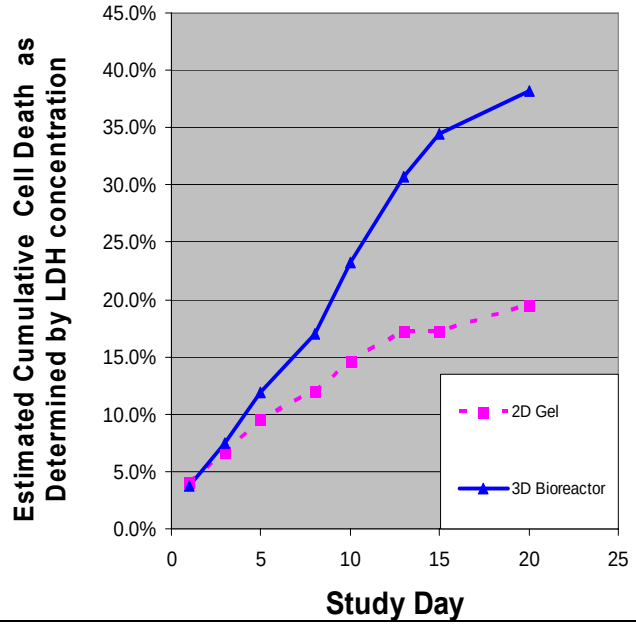

B

Estimated Live Cell Count (millions)		
Study Day	2D Gel	3D Bioreactor
0	12.5	12.5
1	11.99	12.04
3	11.66	11.56
5	11.31	11.01
7	11.00	10.38
9	10.67	9.60
11	10.35	8.66
13	10.35	8.19
15	10.06	7.73

Figure 3-4
A) Estimated cumulative cell death as a function of study day, B) Estimated viable cells

Figure 3-5 displays the time courses of the major nutrients, glucose (A), pyruvate (B), and glutamine (C) consumption rates and lactate production rate (D) for the 3D bioreactor and 2D control cultures. In comparing 2D and 3D culture

systems, the glucose and pyruvate consumption rate are fairly similar throughout the 15 days of culture. Of particular interest is the difference between glutamine consumption rates and lactate production rates as these nutrients are consumed and produced by aerobic and anaerobic metabolism, respectively. Glutamine enters directly into the TCA cycle as α-ketoglutarate. The 3D bioreactor ceases to produce lactate by day 5, while continuously consuming glutamine throughout the culture, indicating a shift to aerobic metabolism with the TCA cycle dominating energy production. On the other hand, the 2D control has increasing production of lactate, demonstrating that the majority of the hepatocytes were relying on anaerobic glycolysis.

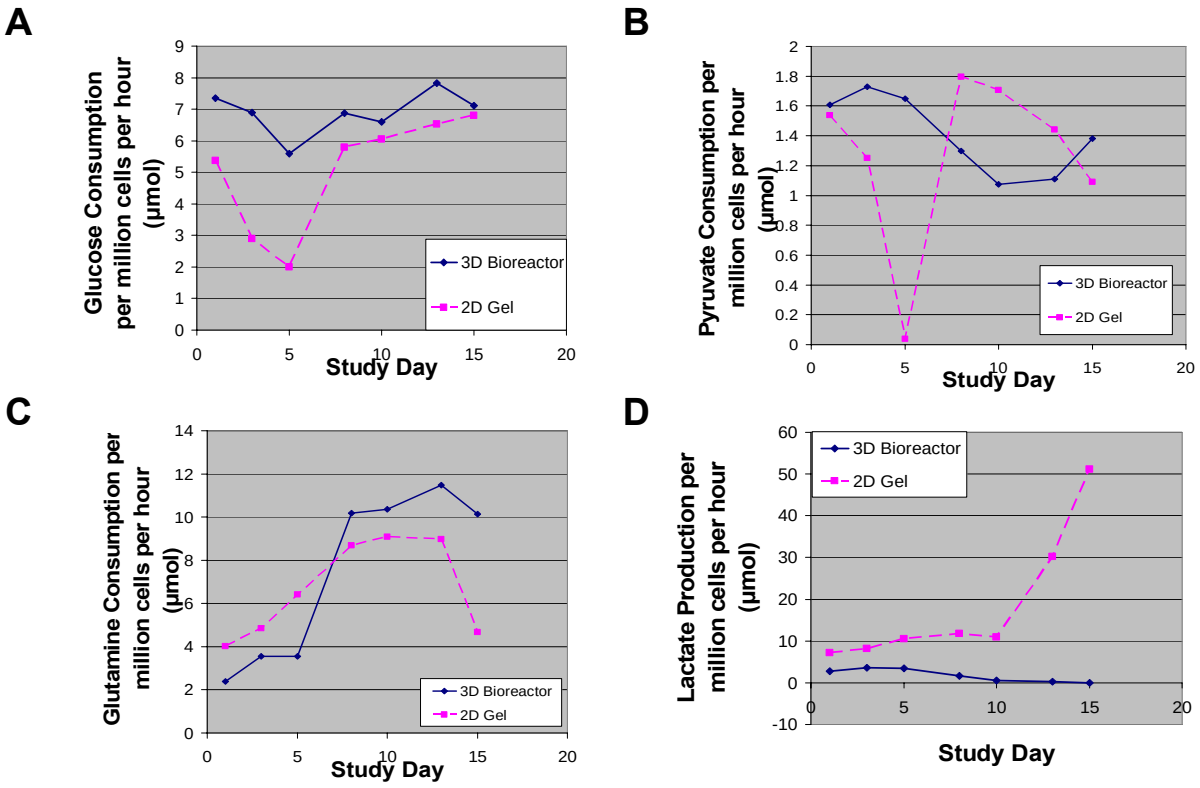

Figure 3-5
Time course of Glucose, Pyruvate, and Glutamine Consumption (A-C), and Lactate Production (D)

Figure 3-6 are the urea (A) and alanine (B), production rates in 3D bioreactor and 2D control cultures. The alanine production tracks the urea production and will generate ammonia for the urea cycle [25], and after day 8 of culture alanine in fact, is consumed. Alanine also tracks lactate production and is produced in conjunction with lactate during anaerobic glycolysis via transamination of pyruvate with glutamate [25].

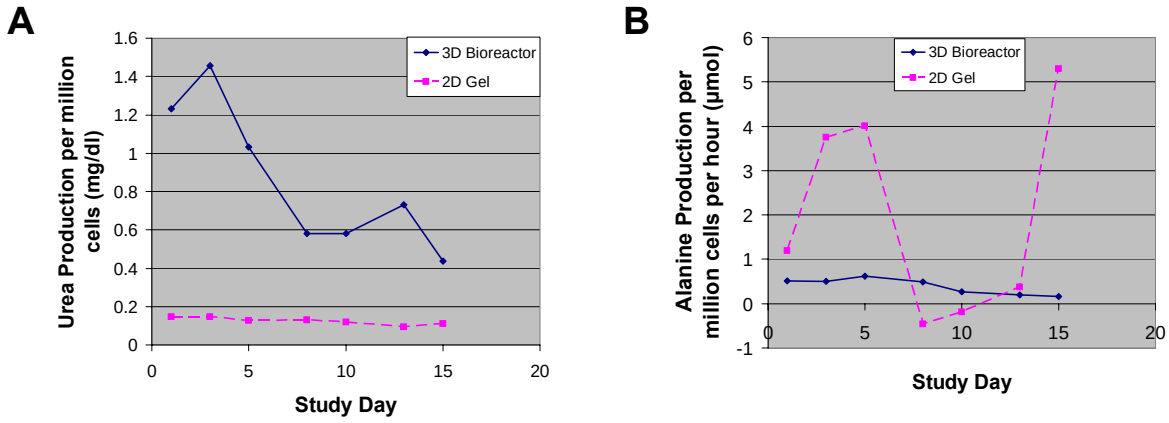

Figure 3-6
Timecourse of Urea and Alanine Production (A,B)

Figure 3-7 are the ethanol concentration (A) and acetate production (B) time courses for the 3D bioreactor and 2D control cultures. Ethanol is discovered in the 3D bioreactor due to the membrane 'wetting' procedure described in the Methods section. The middle hollow fiber is made of polypropylene and require ethanol wetting to induce water permeability. Clearly there should be additional rinsing steps with PBS to wash out residual ethanol. The hepatocytes actively metabolize the ethanol to acetate by alcohol dehydrogenase and aldehyde dehydrogenase. Interestingly, there is a spike in acetate levels by day 7 in 2D control cultures. This could be due to ethanol metabolism, but there is nearly two orders of magnitude less

ethanol in the 2D culture than the amount of acetate that would be created from this ethanol. Under normal physiological conditions, acetate accumulates during fasting due to the beta-oxidation of lipids, resulting in two carbon units of acetate.

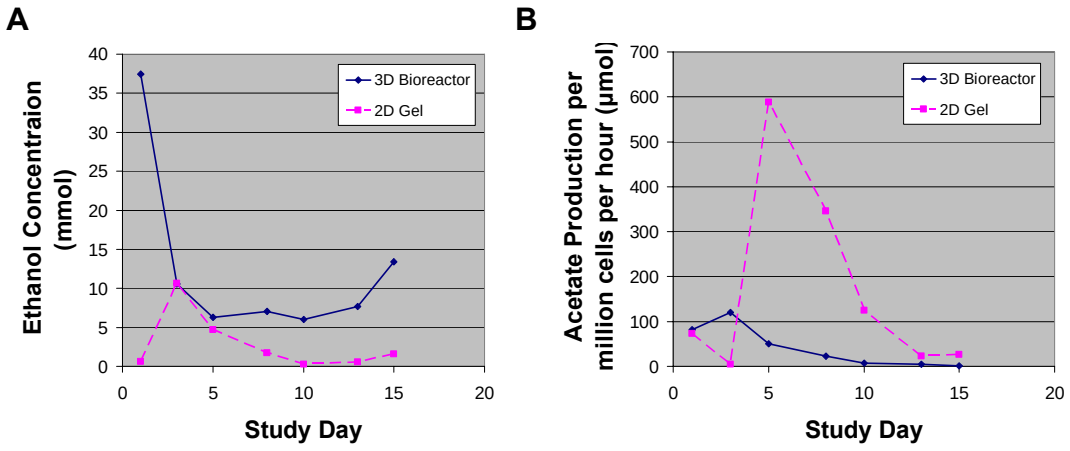

Figure 3-7
Timecourse of Ethanol Concentration (A), Acetate Production (B)

The various amino acid and nicotinamide did not significantly change over the course of the experiment.

3.5 Discussion

Although previous NMR 'footprinting' studies of cell culture have been performed [1, 3, 8, 12, 17] this is the first example of demonstrating the HTP, unbiased nature of NMR spectroscopic analysis especially for tissue engineering. Co-resonation of sample compounds can introduce errors that arise when concentration measures are performed on spectra that may include contributions within a single visible peak that actually arise from two peaks superimposed on each

other. Accurate concentration measures may also be challenged by sample contamination, macromolecular content pH, and ionic strength.[26]. Furthermore, accuracy and precision issues may arise over the course of a multi-sample study due to variation in these same four sample parameters, as well as instrument stability. Because the difference in measured concentrations for select compounds in standardized media samples was less than 1% for measurements made using deconvolution verses manual integration, batch manual integration was used exclusively in this study. The observed difference between these two methods of concentration quantification is consistent with reported best practices.[27] In combination with the use of a robotic sample changer, batch binned spectra resulted in a high throughput methodology allowing for multiple samples to be rapidly processed in a reproducible manner without the need for intensive operator scrutiny associated with individual spectrum deconvolution methods.

The primary obstacle in tissue engineering is the inability of using the most common analytical tool of the cell biologist, the microscope, because of the opaque properties of the artificial materials used in tissue engineering [22, 28]. Therefore, the indirect characterization of tissue function through cell culture media analysis is the primary means for tissue engineers to demonstrate bioartificial organ functions. The HTP ^{1}H NMR method of media analysis results in an unbiased metabolomic 'footprint' leading to well-informed tissue engineering optimization. The method permits quantitative analysis of extracellular milieu in constant contact with the cell culture, which is converted to production or consumption rates. Although the rates shown herein have been used for years in biochemical engineering [29], entering this data into a simple biochemical scheme is rarely done and permits an easy

interpretation of the complex metabolomic footprint results. This basic bioenergetic scheme of metabolism converts relative mass balance results derived from the consumption and production rates to the thickness of arrows along with the rates within the biochemical network, giving a rapid overview of carbon flow in the bioreactor, similar to other macrokinetic models

Systemic metabolic changes are evident over the time course of the experiment. In particular, Figure 3-8 is a biochemical schematic representation incorporating the consumption and production rates of the 3D and 2D culture systems across the two week period. Initially for the 3D bioreactor (Figure 3-8A), the primary energy source was glucose (Figure 3-5). The bioreactor system appears to be less reliant on glutaminolysis for energy during this initial week of culture (Figure 3-5). Glutamine is the primary carbon source for energy in proliferative cells in culture [30]. Interestingly there was less build up of lactate which indicates aeroebic glycolysis (Figure 3-5). However, ethanol was discovered in the media (Figure 3-7) which is likely an artifact of the initial bioreactor membrane wetting process. Therefore, the details of metabolism are complicated by this high concentration of ethanol in the media.

Ethanol is known to form acetate through the combined actions of ethanol dehydrogenase and aldehyde dehydrogenase. Acetate also increases in the starved state, whereby fatty acids undergo β-oxidation increasing the mitochondrial acetate concentration [25]. High mitochondrial acetate concentrations inhibits pyruvate dehydrogenase (PDH) and increases the activity of pyruvate carboxylase (PC) resulting in glucose-derived pyruvate forming oxaloacetate rather than acetyl-CoA [31]. This inhibition of pyruvate metabolism by ethanol may have been the cause of

the decrease in glucose consumption during this period, as pyruvate is the end product of glycolysis and the first step, hexose kinase is inhibited by ATP, which would be sufficiently supplied by acetate metabolism [31]. In addition, urea production was elevated during this period (Figure 3-6), indicating an abundance of ammonia present, likely due to transamination reactions. The increased glucose-derived intracellular pyruvate due to PDH inhibition by ethanol-derived AcetylCoA would drive the formation of alanine and could be the reason for increased alanine production.

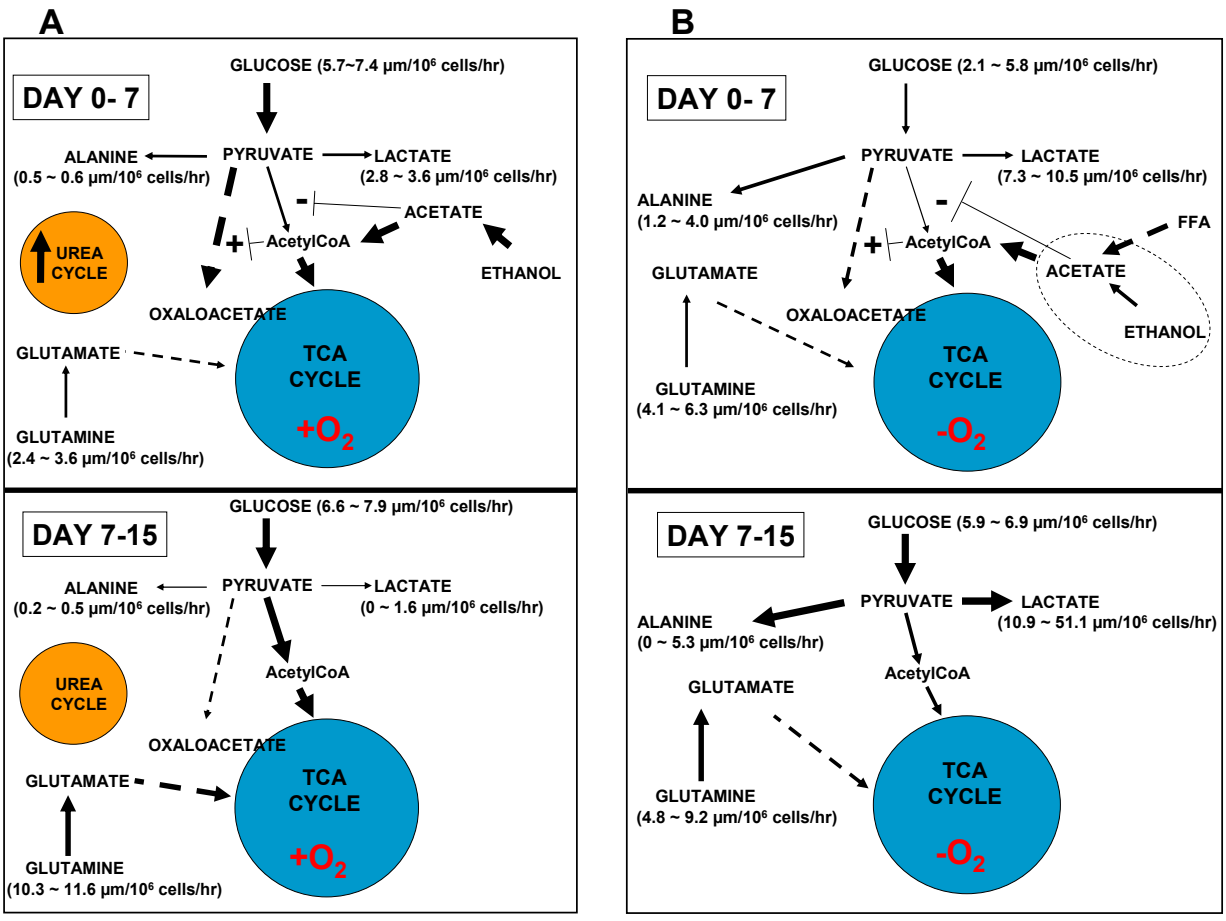

Figure 3-8
A) Metabolic scheme for 3D bioreactor, B) Metabolic scheme for 2D gel culture

During the second phase of the bioreactor footprint (Figure 3-8A), the primary energy source was both glucose and glutamine (Figure 3-5). There was no accumulation of lactate, indicating aeroebic glycolysis (Figure 3-5). Ethanol and acetate had disappeared by day 7 in the media (Figure 3-7) and glucose metabolism increased, which would ultimately produce intracellular pyruvate. This could explain why pyruvate remained elevated in the media and the apparent pyruvate consumption decreased. In addition, urea production diminished during this period (Figure 3-6).

The primary energy source for the 2D cultures proved to also be glucose during the first three time points measured after culturing (Figure 3-5). Lactate production during this initial phase of the study was elevated as compared to the 3D bioreactor indicative of anaerobic metabolism. Again, ethanol was discovered in the media (Figure 3-7) due likely to a process or technician error associated with media change. Lipids likely accumulated as the result of cell debris in the culture dish. Metabolism of these membrane breakdown products by the surviving hepatocytes resulted in increased acetate levels. In addition, urea production was observed to be nominally above the level of detection during this period (Figure 3-6), however transamination reactions were active as production of alanine was observed (Figure 3-6). Alanine formation from pyruvate is considered an ammonia detoxication in the absence of the urea cycle [25].

While glucose was the principal energy source during the second phase of the 2D culture footprint, unlike the bioreactor, anaerobic glycolysis dominated with massive production of lactate (Figure 3-5). Similar to the bioreactor though, ethanol and acetate concentrations diminish over time in the 2D culture (Figure 3-7). Urea

production was consistently low (just above detectable limits) throughout both phases of the 2D culture study (Figure 3-6) while alanine production, while erratic, was on average greater than that observed in the bioreactor.

This study demonstrated the power of unbiased NMR spectroscopic analysis of culture media for metabolomic phenotyping and experimental quality control in tissue engineering. [32]. It is unbiased because all compounds in the media containing a ^{1}H will be detected with a 100 μM limit, as long as one of the compounds NMR resonances are resolved, resulting in discovery of unexpected metabolites—such as ethanol and acetate. Ethanol and its hepatic metabolite acetate would have gone undetected by standard chromatography or spectroscopic methods.

Critical to the success of this type of study is the use of hormonally defined media rather than media using calf serum or other blood products as media supplements as such serum-based products cannot offer consistent or reliable knowledge of media additives without additional testing. This lack of reproducible initial conditions associated with classic serum-enriched culture media prevents precise measurement of consumption and production measures from culture systems thus illustrating the significant advantage afforded by hormonally defined media in metabolomic studies.

Metabolomic interpretation of these data can be used to improve the experimental conditions, specifically, oxygen concentration of the mixed gases, microenvironmental heterogeneity, and experimental oversights. The most obvious experimental difference that resulted in metabolic effects was oxygen tension. In 3D culture systems 95% oxygen is used versus 20% oxygen (i.e., air) in the 2D culture system. Quality assurance issues that were identified included ethanol rinsing of

bioreactor, technician effects, and evaporation associated with the use of dry gases. Other areas of tissue culture quality monitoring that may be served by this method include detection of low level contaminations by yeast or bacteria, media composition consistency, and media component stability. This ^{1}H NMR method of analyzing culture media can be used to obtain near real-time readings of metabolism allowing for more rapid optimization of tissue engineered culture conditions.

3.6 Endnotes

1. O'Leary, D.J., Hawkes, S.P., Wade, C.G., *Indirect monitoring of carbon-13 metabolism with NMR: analysis of perfusate with a closed-loop flow system*. Magn. Reson. Med., 1987. **5**(6): p. 572-7.

2. Bell, J., Brown, JC, Sandler, PJ, *NMR studies of body fluids*. NMR Biomed., 1989. **2**(5-6): p. 242-56.

3. Dabos, K.J., Parkinson, J.A., Hewage, C., Nelson, L.J., Sadler, I.H., Hayes, P.C., Plevris, J.N., *H NMR spectroscopy as a tool to evaluate key metabolic functions of primary porcine hepatocytes after cryopreservation*. NMR in Biomedicine, 2002. **15**(3): p. 241-250.

4. Mendes, P., *Emerging bioinformatics for the metabolome*. Briefings in Bioinformatics, 2002. **3**(2): p. 134-145.

5. Allen, J., Hassanein, T, Bhatia, SN, *Advances in bioartificial liver devices*. Hepatology, 2001. **34**(3): p. 447-455.

6. Holmes, E., et al., *Chemometric Models for Toxicity Classification Based on NMR Spectra of Biofluids*. Chem. Res. Toxicol., 2000. **13**(6): p. 471-478.

7. Pham-Tuan, H., et al., *Method development in high-performance liquid chromatography for high-throughput profiling and metabonomic studies of biofluid samples*. Journal of Chromatography B, 2003. **789**(2): p. 283-301.

8. Kell, D.B., *Metabolomics and systems biology: making sense of the soup*. Current Opinion in Microbiology, 2004. **7**(3): p. 296-307.

9. Allen, J., Davey, HM, Broadhurst, D, Heald, JK, Rowland, JJ, Oliver, SG, Kell, DB, *High-throughput classification of yeast mutants for functional genomics using metabolic footprinting*. Nat. Biotechnol., 2003. **21**(6): p. 692.6.

10. Kuesel, A.C., Graschew, G., Hull, W., Lorenz, W. Thielmann, H.W., *31P NMR studies of cultured human tumor cells. Influence of pH on phospholipid metabolite levels and the detection of cytidine 5'-diphosphate choline*. NMR Biomed., 1990. **3**(2): p. 78-89.

11. O'Leary, D.J., Hawkes, S.P., Wade, C.G., *Indirect monitoring of carbon-13 metabolism with NMR: analysis of perfusate with a closed-loop flow system*. Magn. Reson. Med., 1987. **5**(6): p. 572-577.

12. Bubb, W., Wright, LC, Cagney, M, Santangelo, RT, Sorrell, TC, Kuchel, PW, *Heteronuclear NMR studies of metabolites produced by Cryptococcus*

neoformans in culture media: Identification of possible virulence factors. Magnetic Resonance in Medicine, 1999. **42**(3): p. 442-453.

13. Nicholson, J.K., J.C. Lindon, and E. Holmes, *'Metabonomics': understanding the metabolic responses of living systems to pathophysiological stimuli via multivariate statistical analysis of biological NMR spectroscopic data.* Xenobiotica, 1999. **29**(11): p. 1181-1189.

14. Holmes, E., J.K. Nicholson, and G. Tranter, *Metabonomic Characterization of Genetic Variations in Toxicological and Metabolic Responses Using Probabilistic Neural Networks.* Chem. Res. Toxicol., 2001. **14**(2): p. 182-191.

15. Gillies, R.J., *Nuclear Magnetic Resonance and its Applications to Physiological Problems.* Annual Review of Physiology, 1992. **54**(1): p. 733-748.

16. Macdonald, J.M., Grillo, M., Schmidlin, O., Tajiri, D.T., James, T.L., *NMR spectroscopy and MRI investigation of a potential bioartificial liver.* NMR in Biomedicine, 1998. **11**(2): p. 55-66.

17. Kell, D., et al., *Metabolic footprinting and systems biology: the medium is the message.* Nat Rev Micro, 2005. **3**(7): p. 557-565.

18. Kriat, M., Confort-Gouny, S., Vion-Dury, J., Sciaky, M., Viout, P., Cozzone, P., *Quantitation of metabolites in human blood serum by proton magnetic resonance spectroscopy. A comparative study of the use of formate and TSP as concentration standards.* NMR Biomed., 1992. **5**(4): p. 179-94.

19. Wolfe, S.P., Hsu, E., Reid, L.M., Macdonald, J.M., *A novel multi-coaxial hollow fiber bioreactor for adherent cell types. Part 1: Hydrodynamic studies.* Biotechnology and Bioengineering, 2002. **77**(1): p. 83-90.

20. MacDonald JM, W.S., Roy-Chowdhury I, Kubota H, Reid LM., *Effect of Flow Configuration and Membrane Characteristics on Membrane Fouling in a Novel Multicoaxial Hollow-Fiber Bioartificial Liver.* Ann NY Acad Sci, 2001. **944**(1): p. 334-343.

21. Macdonald, J.M., Wolfe, S.P., *Bioreactor design and process for engineering tissue from cells*. 2005, University of North Carolina at Chapel Hill: USA. p. 13.

22. Macdonald, J.M., et al., *Liver Cell Culture and Lineage Biology*, in *Methods of Tissue Engineering*, A. Atala and R.P. Lanza, Editors. 2002, Academic Press: Boston. p. 151-195.

23. McClelland, R.E., Coger, R.N., *Effects of Enhanced O2 Transport on Hepatocytes Packed within a Bioartificial Liver Device.* Tissue Engineering, 2004. **10**(1-2): p. 253-266.

24. Gadian, D.G., *NMR and Its Applications to Living Systems*. 2nd ed. 1995, New York: Oxford University Press. 283.

25. Lehninger, A.L., *Principles of Biochemistry*. 4th ed. ed, ed. D.L. Nelson, Cox, M.M. 2005, New York: W.H. Freeman and Company. 1119.

26. Weljie, A.M., et al., *Targeted Profiling: Quantitative Analysis of ¹H NMR Metabolomics Data.* Anal. Chem., 2006. **78**(13): p. 4430-4442.

27. Maniara, G., et al., *Method Performance and Validation for Quantitative Analysis by 1H and 31P NMR Spectroscopy. Applications to Analytical Standards and Agricultural Chemicals.* Anal. Chem., 1998. **70**(23): p. 4921-4928.

28. MacDonald, J.M., et al., *Bioartificial livers*, in *Cell Encapsulation Technology and Therapeutics*, W. Kuhtreiber, R.P. Lanza, and W.L. Chick, Editors. 1998, Birkhauser: Boston.

29. Bailey, J.E., Ollis, D.F., *Biochemical Engineering Fundamentals*. 2nd ed. 1986, New York: McGraw-Hill. 984.

30. Mancuso, A., Sharfstein, S.A., Fernandez, E.J., Clark, D.S. Blanch, H.W., *Effect of extracellular glutamine concentration on primary and secondary metabolism of a murine hybridoma: An in vivo 13C nuclear magnetic resonance study*. Biotechnology and Bioengineering, 1998. **57**(2): p. 172-186.

31. Lieber, C.S., *Metabolism of alcohol.* Clin Liver Dis, 2005. **9**(1): p. 1-35.

4 Protein Sequestration—a novel solution for protein folding NMR studies[2]

4.1 Introduction

An evolving area in biochemical research exists in the area of protein conformation determination using NMR [1, 2]. Recent studies have demonstrated that many intracellular proteins have structure which is different from the same protein when studied in dilute solution [3-5]. Historically, most protein studies have been performed in pure isolate and *in vivo* conditions allowing for protein conformation to change in the absence of the dense milieu of cytoplasmic compounds. Most dilute solution studies are performed at protein concentrations of less than 10 g/l when in-cell concentrations can surpass 400 g/l [6]. Understanding *in vivo* conformation under such "crowded" or concentrated conditions is critical in testing pharmacokinetics, ligand/receptor interaction, and drug metabolism [7].

NMR studies differ from other structural determination methods, such as x-ray crystallography, in that NMR is a non-destructive method which can be used to

---

2 Images and technical support during some portions of the work described in this chapter were obtained through cooperative work with Lisa Charlton from the Gary J. Pielak laboratory, UNC-CH

target specific compounds when experiments are designed with appropriate isotopic nuclei in media constituents for eventual inclusion in protein synthesis. In particular, ^{15}N and ^{13}C can be introduced into nucleic acids which are then incorporated into proteins produced by cells which are then observed using NMR. Using Heteronuclear Single Quantum Correlation (HSQC), two-dimensional spectra can be obtained providing ^{1}H information on one axis and either ^{15}N or ^{13}C information on the other axis. Correlation between these two axes can be used to determine protein structure. In particular, ^{15}N HSQC provides unique chemical shifts for all amino acids with the exception of proline (the only amino acid having no amide proton). These chemical shifts arise from transference of magnetic polarization, applied first to the protons of the sample, to the next adjacent nuclei (either ^{15}N or ^{13}C). The first chemical shift evolves from the ^{15}N or ^{13}C nuclei during which a 180° pulse is applied to protons. The magnetization is then transferred from the ^{15}N or ^{13}C nuclei back to the covalently bonded proton after which the proton free induction decay is captured while a soft pulse (decoupler) is applied to the non-proton nuclei to disrupt magnetic coherence [8, 9]. Figure 5.1 illustrates a schematic for the HSQC pulse sequence in which the X nuclei channel would be either ^{15}N or ^{13}C.

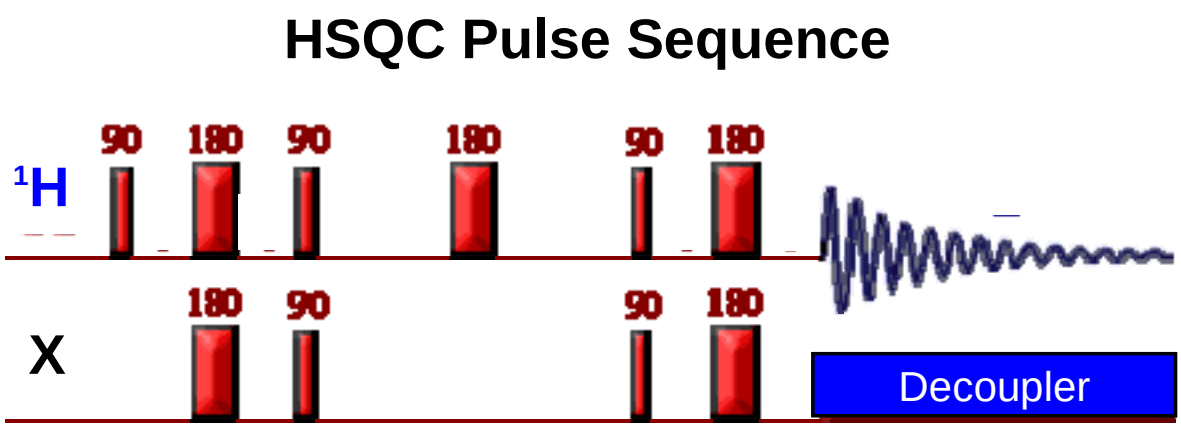

Figure 4-1
HSQC pulse sequence

4.2 Statement of problem

This dissertation does not seek to solve the in-cell conformation of a protein through using NMR but instead addresses a challenge that arises in the nature of the experiment. The problem with *in vivo* NMR occurs when synthesized proteins pass out of the cytoplasm and into the extracellular space. When this occurs, the protein conformation may alter as the local environment about the protein is less densely concentrated with other agents as compared to the cytoplasmic environment. When this protein "leaking" occurs, two different spectra may arise from the same protein based upon the location of the two populations of the protein. These spectra, however, are not truly discrete, but are collected simultaneously confounding researchers as to the true conformation of the in-cell protein.

4.3 Hypothesis

Because of the comparatively large molecular size, both in terms of sterics and molecular weight, it is a reasonable hypothesis to explore whether proteins behave differently in alginate encapsulation as compared to the more dynamically moving low molecular weight metabolites previously discussed. A possible outcome that might arise through encapsulation of cells synthesizing a protein of interest is that the encapsulate would prevent proteins released out of the cells to reach the surrounding liquid media outside the encapsulates. The sequestration of proteins in the alginate would therefore have the trapped protein behave as a solid bound protein rather than a protein dissolved in liquid phase. This has particular significance for NMR spectroscopy as line broadening occurs for compounds bound in hydrogel environments [10]. This line broadening is due the decrease in T2 times associated with solid-phase bound analytes. In short, line broadening can be viewed with the following equation:

$$\text{Line width at peak half height} \propto \frac{1}{T2}$$

This equation explains how a reduction in T2 results in substantial line broadening. Line broadening of this sort can be so complete as to diminish the magnitude of individual peaks below the ambient noise observed in the spectra.

With this in mind, a possible solution using the encapsulation process emerges. Encapsulated cells may release protein from the cytoplasm with the protein being retained either permanently or temporally within the hydrogel of the

alginate encapsulation. If the size of the protein is sufficiently large, the diffusion of a temporally bound molecule may be so diminished as to render the molecule invisible for the typical multi-hour experiment required in protein NMR.

Figure 4-2 shows three time points for an NMR experiment in which *E. coli* expressing chymotrypsin inhibitor 2 (CI2)—the inhibitor of chymotrypsin which is a digestive enzyme synthesized in the pancreas of numerous mammals and an oft studied molecule in the field of protein folding due to its relatively small and manageable size of 7.3 kilodaltons (kDa) [11-13]. The left most two images show a ^{1}H spectra (top) and 2D ^{1}H-^{15}N spectra (bottom) for media sampled at the beginning of the experiment during inoculation of *E. coli* into an NMR tube. The expectation would be that the media would show no signs of the protein. However, the spectral signatures observed are consistent with the in-cell spectra taken at 1 hour and the media extract taken at 2 hours. In all three cases, CI2 is present revealing the leak of protein from within the cytoplasm to the extracellular space.

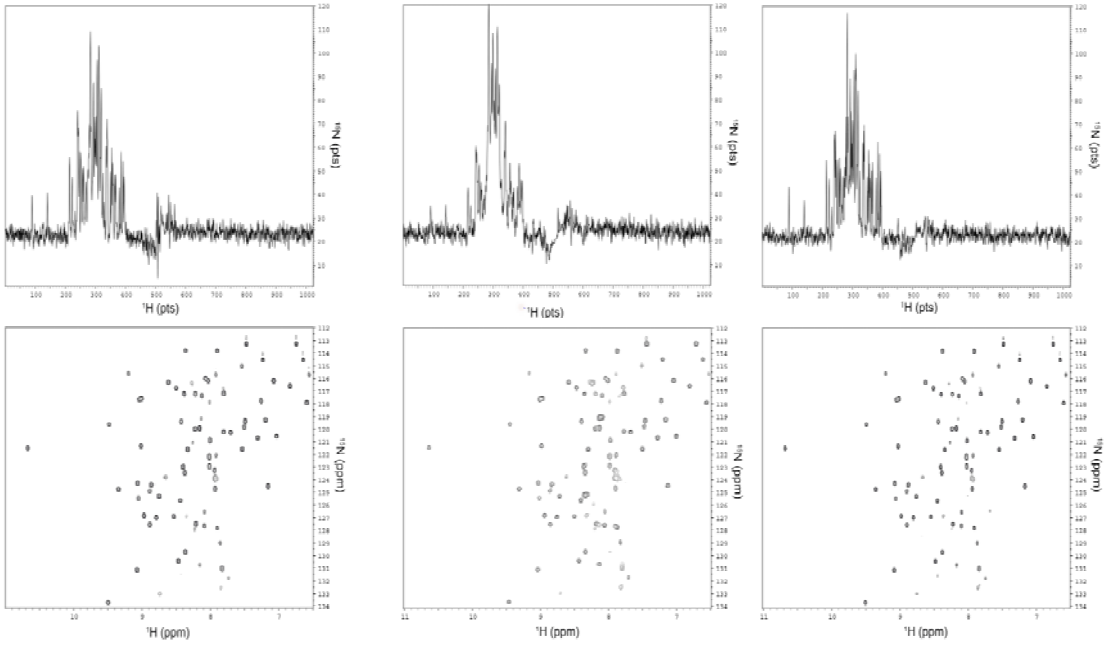

Figure 4-2
1D and 2D spectra showing CI2 leak into media

4.4 Methods

To determine the effectiveness of encapsulation as a protein sequestration solution, the following experiments were required:

1. Determine whether electrostatic encapsulation process disrupts protein synthesis in *E. coli* transformed with CI2 plasmid.
2. Determine whether encapsulated protein produces NMR resonances. If the encapsulated protein does not produce NMR resonances,

determine whether NMR signature can be regained by disruption of encapsulates to return the protein to the liquid dissolved state.

3. Determine whether encapsulated induced cells expressing ^{15}N enriched protein and introduced into an NMR study with the resultant spectra displaying no signatures associated with the protein.

Electrostatic encapsulation was performed in the manner previously described in prior chapters. Alginate stock solutions were prepared in Hanks' Balanced Salt Solution (HBSS) due to the absence of any divalent cations that would initiate polymerization of alginate and also due to the relative ease with which 2% alginate-HBSS solution passes through 0.22 micron filtration—a necessary step to remove solids from the stock including biological contaminants larger than the specified pore size.

A second-generation electrostatic encapsulation system was designed building on the experiences of three years of studies on the first system previously described. The new encapsulation system differed in two areas only. The power supply used in the system was reduced from a maximum output of 30 kV to 8kV with digital controls for improved power management as compared to the relatively challenging analog voltage needle on the Spellman RHR30PF30 used in the first system due to the small operational range of voltages employed in the process. The new Spellman SL8PN10 power supply also provided an additional measure of safety as this unit has a current limit setting which controls the maximum current that the power supply will output. By setting the current ceiling to 50 microamps (μA), this power source is considerable less dangerous than the non-limited output current which is provided by the Spellman RHR30PF30.

The second improvement to the encapsulation system was the introduction of a flexible, braided ground wire for immersion in the receiving bath. The prior system employed a solid copper wire that was difficult to maneuver due to the rigidity of the wire. In both cases, the ground wires were rated at 600 volts (V) at 5 ampere (A).

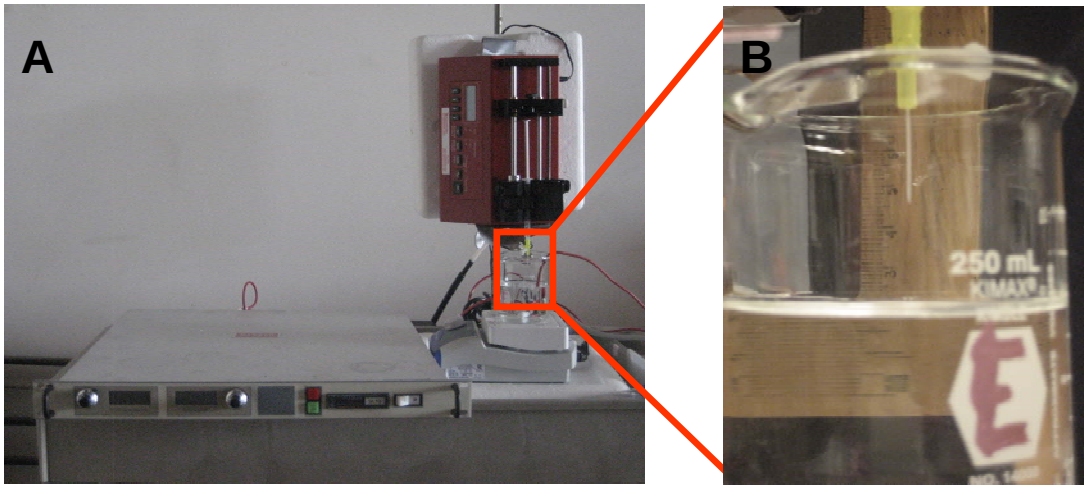

Figure 4-3
2nd Generation encapsulator
A) High voltage system with Z-axial pump
B) 24 gauge angiocatheter shown at 22 mm casting distance

NMR studies were performed on a Varian 600 MHz spectrometer using 5 mm tubes.

Samples were maintained in Luria broth—a widely used nutrient suspension appropriate for bacteria propagation and function. Cultures were treated with ^{15}N enriched amino acid Luria broth for the purpose of inclusion in expressed proteins. Cultures were centrifuged to allow for collection of cell pellets and to allow for standard Luria broth (non-enriched) to be added to cultures prior to NMR studies. This step reduces spurious signals that may arise from unused amino acid groups in

the broth and proteins bearing isotopic nuclei that may have escaped into the broth during culture incubation. Additionally, magnet shimming on the NMR was performed using Luria broth samples.

In all NMR studies using *E. coli* encapsulates, the bacteria slurry was treated with 2.5 μg/ml chloramphenicol. Chloramphenicol is an antibiotic that inhibits protein synthesis in bacteria. At a concentration of 2.5 μg/ml, chloramphenicol is non-lethal to *E. coli* but instead presents inhibitory effects on propagation [14]. Chloramphenicol disrupts the ability of effected bacteria to synthesize proteins. This results in a culture which can not propagate or replace damaged essential proteins. For the short temporal nature of the NMR experiments used in these studies, the loss of protein expression is not detrimental as the incubation which precedes encapsulation allows for over-expression of the protein of interest to the effects of the *lac* operon induction described below. The effects of chloramphenicol are reversible by removal of the agent from culture media [15]. The use of chloramphenicol is important for encapsulation studies involving highly proliferative bacterial cells to ensure that expansion of cells within an encapsulate does not burst the encapsulate and release encapsulated contents into media.

To improve the signal of proteins of interest while simultaneously limiting other innate protein synthesis, protein expression induction was used. In instances where protein expression was induced, isopropyl-β-D-thiogalactosidase (IPTG) was added to cultures. Once introduced into culture, IPTG is not metabolized by bacteria and serves to de-activate the *lac* repressor which was included as a segment in the DNA introduced into recombinant DNA (rDNA) transformed into the *E. coli* coding for the expression of target proteins. Using restriction enzymes to cleave target

protein DNA and *lac* operon DNA, the regulatory DNA found on the 5' end of the *lac* operon can be annealed with DNA coding for a specific protein. The resultant rDNA is regulated by the *lac* repressor which prevents RNA polymerase from transcribing the DNA on the 5' end of the regulatory operator. IPTG binds to the *lac* repressor and disables the binding or the repressor to the regulatory operator allowing for the RNA polymerase to transcribe numerous copies of the messenger RNA (mRNA) resulting in consistent and predictable over-expression of the protein of interest [16-18].

4.5 Bacteria viability and function test

Bacteria were passed through a 24 gauge angiocatheter by syringe pump displacing 0.714 ml/min while exposed to 3.75 kV of electrostatic force applied across a 2.2 cm distance. Rather than using alginate as a gelling material and $CaCl_2$ solution as a receiving bath, *E. coli* were maintained in Luria broth in the syringe and passed into a Luria broth receiving bath. Cells were not induced prior to the sham encapsulation. After the bacteria were collected from the receiving bath using centrifugation, IPTG was added to the experimental (sham encapsulation) cohort. The bacteria were incubated for 24 hours then treated with sodium dodecyl sulfate (SDS) to lyse the bacterial cell wall. Proteins were collected from a control sample through SDS lysis and were run on a poly polyacrylamide gel electrophoresis (PAGE) preparation along with the SDS sample from the sham encapsulation. Gels were stained with Coomassie Blue stain to reveal electrophoretically separated proteins consistent with practices described by Scopes [19].

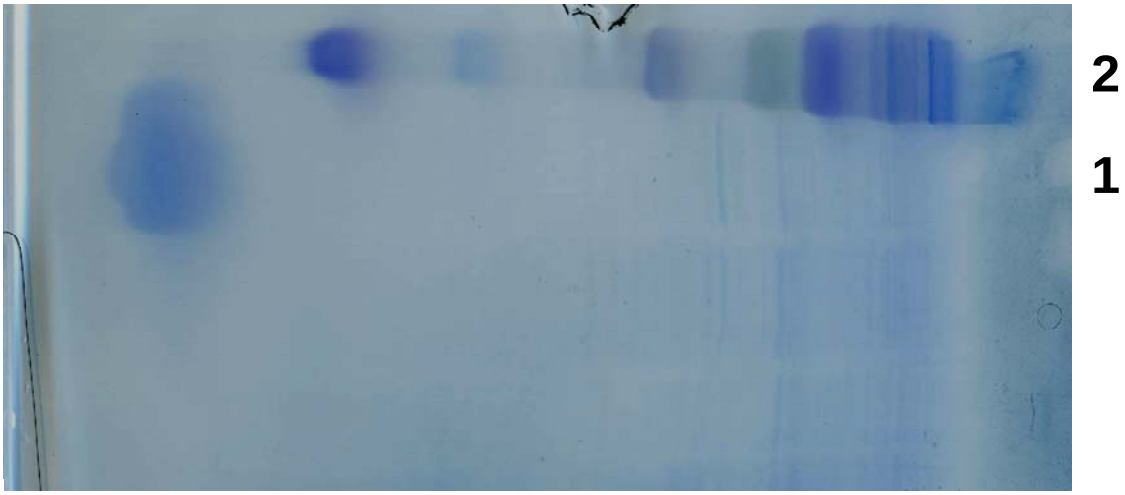

Figure 4-4
SDS-PAGE for *E. coli* + CI2
1)Control (no induction)
2) Sham Encapsulation + IPTG

Figure 4-4 demonstrates that bacteria can not only survive the encapsulation process, but also can be subsequently induced by IPTG to express proteins when the rDNA sequence for the target protein is associated with the *lac* operon. In lane 1, the large blur on the left represents stain retained in the start well of the control sample. Dim striping can be observed as tightly spaced parallel lines indicative of basal expression of proteins when the *lac* operon is engaged by the repressor. By contrast, lane 2 shows bright lines down the link of the lane consistent with robust protein synthesis following *lac* operon induction due to the deactivation of the repressor in response to IPTG treatment. Because IPTG is a low molecular weight modified sugar (MW = 238.31 g/mol), it should be capable of diffusing into encapsulations. Alternatively, IPTG can be co-encapsulated with cells or cells can be induced prior to encapsulation.

4.6 Pure protein sequestration study

Encapsulates of ^{15}N CI2 were prepared using a 1:1 mix of 2% HBSS-based alginate stock and pure protein dissolved in Luria broth under 3.77 kV electrostatic potential. The intent of this preparation was to observe whether an HSQC pulse sequence could detect an enriched protein contained in an alginate encapsulation but not contained within the cytoplasm of a cell. The predicted outcome for this experiment would be the observance of no signal for NMR spectra taken with encapsulated protein followed by the return of peaks to spectra taken after encapsulates were disrupted and the protein contained within returns to the liquid dissolved state.

The HSQC performed on the encapsulates of pure CI2 protein did not demonstrate any of the peaks typical of CI2. Encapsulates were treated next with 400 µl of 500 mM ethylene diamine tetraacetic acid (EDTA). EDTA, like sodium citrate as previously described, chelates divalent cations such as Ca^{+2} [20]. The chelation of calcium results in the disintegration of encapsulates which returns the ^{15}N enriched CI2 to the liquid dissolved state. In this study, the anticipated peaks associated with CI2 were not detected using HSQC with 256 transients. This experiment was repeated three times and never achieved the predicted outcome. The CI2 was tested using SDS-PAGE. The CI2 demonstrated the classic banding associated with CI2 in the PAGE. However, SDS-PAGE is insensitive to the difference between nuclei differing only by one neutron. Therefore, SDS-PAGE cannot be trusted to positively identify a protein as being ^{15}N enriched. At the time

of this publication, pure protein sequestration experiments were still being performed.

4.7 In-cell NMR of α-synuclein using alginate encapsulates

If the findings of the bacteria functional tests and pure protein sequestration study are reliable, encapsulates of bacteria induced to express an enriched protein should produce HSQC resonances that are associated with the in-cell protein only. Any protein that leaks out of the cytoplasm of the bacteria and into the surrounding encapsulate should not produce resonances as predicted by the previously observed outcomes.

To test these predictions, *E. coli* transformed to express α-synuclein and induced with IPTG were encapsulated in alginate and allowed to incubate for 24 hours in ^{15}N enriched Luria broth. The choice of α-synuclein as the study protein is significant in that this protein is expressed in neuronal cells and aggregates to form fibrils and Lewy bodies in dopaminergic neurons which can evolve into Parkinson's disease [21-23]. At 140 amino acid residues and 14 kDa, α-synuclein is noteworthy for the variety of conformations that the molecule can assume especially when missense mutations which can contribute to early onset Parkinson's are considered [24]. This leads to the consideration of possible therapeutics for Parkinson's based on corrupt versions of α-synuclein or similar peptides which inhibit the formation of fibrils and Lewy bodies [25, 26].

Following incubation in enriched media, encapsulates were loaded into an NMR tube with non-enriched Luria broth. An HSQC was conducted on the

encapsulates. Figure 4-5A shows the 2D HSQC spectrum for the encapsulated *E. coli*. The HSQC spectrum clearly shows resonances consistent with previously recorded α-synuclein spectra.

Because the HSQC transfers magnetic polarization from protons to covalently bonded ^{15}N and then back to the proton, a 1D proton spectra extracted from the HSQC is sufficient to observe the presence or absence of resonances arising from a single chemical entity. Figure 4-5B shows the first increment of the HSQC which is a 1-D proton spectrum of the supernatant taken 26 hours after encapsulates were inoculated into the NMR tube. This spectrum shows only slight downfield peaks which would indicate minute loss of enriched protein into the supernatant. These downfield peaks are only slightly above background noise and would contribute signal to the in-cell spectrum that would be insignificant when compared to the highly retained in-cell protein. As the evolution of signal in the supernatant study is positively correlated with time, experiments conducted more rapidly would experience supernatant contributed signal in the HSQC in proportion to the experiment duration.

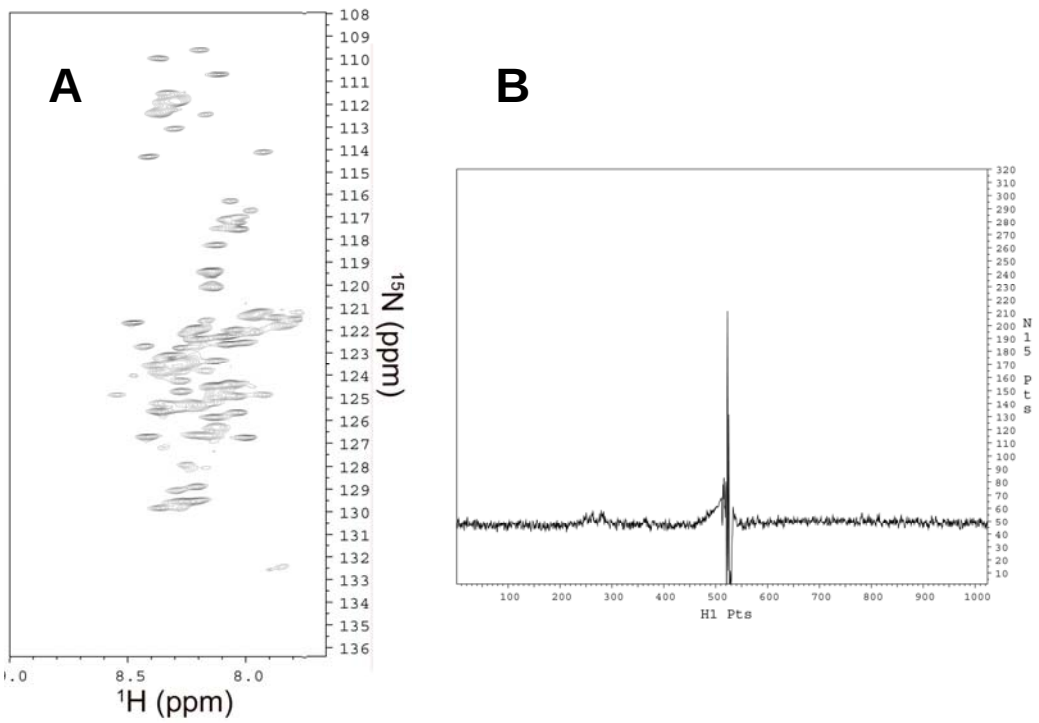

Figure 4-5
NMR spectra for in-cell α-synuclein *E. coli* study
A) Encapsulated HSQC
B) Supernatant at 26 hours

The experiment was performed again using *E. coli* transformed to express CI2. The *E. coli* were induced and incubated in ^{15}N enriched Luria broth prior to encapsulation and transferred to standard (non-enriched) Luria broth for the NMR studies. Figure 4-6A shows the proton spectrum taken from the HSQC study performed on the encapsulated *E. coli*. The resonances observed in the 5 – 6 ppm region are associated with water which is irregular due to the inhomogeneity of the sample—encapsulates immersed in Luria broth presenting solid hydrogels blended with an aqueous liquid. Figure 4-6A does not show peaks associated with CI2 in the first increment. The predicted outcome for this experiment was that classic CI2

peaks would be observed from the enriched intracellular protein within the encapsulates.

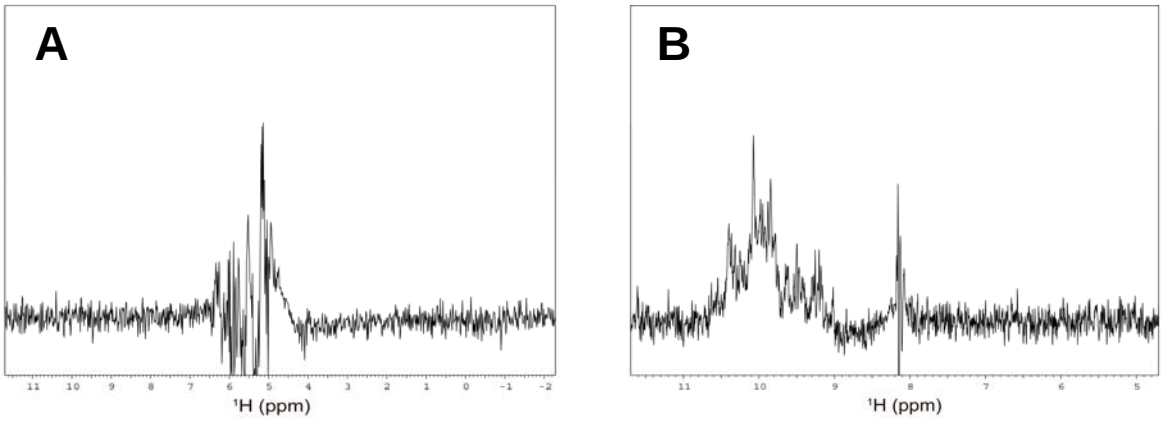

Figure 4-6
Proton spectrum for in-cell CI2 *E. coli* study
A) Encapsulated protein
B) Post-EDTA treatment

Figure 4-6B shows a similar proton spectrum taken from the first increment of an HSQC study performed on the same sample as in Figure 4-6A following removal of liquid media and treatment of encapsulates with 400µl of 500 mM EDTA. The pronounced downfield peaks arise from the intracellular CI2 following the release of bacteria from the alginate encapsulates.

In this demonstration, resonances were not observed for intracellular enriched CI2 contained in alginate encapsulates but were restored by removing the alginate encapsulates from around the contained bacteria. This result is in opposition to the previously described α-synuclein study. Continuing studies will be required to fully characterize the observed phenomena and the application of these findings to in-cell protein conformation determination using NMR.

4.8 Discussion

In summary, for large proteins, alginate encapsulation in conjunction with in-cell NMR may be a robust solution for reducing or removing extracellular or "leaked" protein contributions to NMR spectra. At the time of this publication, however, confounding experimental outcomes to assess such utility are inconclusive. An additional opportunity for in-cell experiment refinement can be achieved using alginate encapsulations in conjunction with superfused media. Because *E. coli* has an elongated cylindrical architecture with the long axis being 2 μm and the diameter measuring approximately 500 nm, free bacteria floating in solution could not be maintained in a flow environment. Encapsulation would allow for the bacteria to be held static in position while the moving media would maintain uniform pH and respiratory substrates while providing for removal of metabolic wastes. This flow would also carry off any proteins that slipped past the sequestration provided by encapsulates virtually eliminating signals that would otherwise arise from the leaked proteins.

4.9 Endnotes

1. Wuthrich, K., *Protein structure determination in solution by NMR spectroscopy*. J. Biol. Chem., 1990. **265**(36): p. 22059-22062.

2. Liu, G., et al., *NMR data collection and analysis protocol for high-throughput protein structure determination.* PNAS, 2005. **102**(30): p. 10487-10492.

3. Charlton, L.M. and G.J. Pielak, *Peeking into living eukaryotic cells with high-resolution NMR.* PNAS, 2006. **103**(32): p. 11817-11818.

4. Sina Reckel, F.L., Volker Dötsch,, *In-Cell NMR Spectroscopy*. ChemBioChem, 2005. **6**(9): p. 1601-1606.

5. Selenko, P., et al., *Quantitative NMR analysis of the protein G B1 domain in Xenopus laevis egg extracts and intact oocytes.* PNAS, 2006. **103**(32): p. 11904-11909.

6. Bryant, J.E., et al., *Protein Dynamics in Living Cells.* Biochemistry, 2005. **44**(26): p. 9275-9279.

7. Sun, C., , Huth J. R., Hajduk, P.J.,, *NMR in Pharmacokinetic and Pharmacodynamic Profiling.* ChemBioChem, 2005. **6**(9): p. 1592-1600.

8. Bodenhausen, G. and D.J. Ruben, *Natural abundance nitrogen-15 NMR by enhanced heteronuclear spectroscopy*. Chemical Physics Letters, 1980. **69**(1): p. 185-189.

9. Bax, A., et al., *Comparison of different modes of two-dimensional reverse-correlation NMR for the study of proteins.* Journal of Magnetic Resonance (1969), 1990. **86**(2): p. 304-318.

10. Hechter, O., et al., *Modification of the Structure of Water in Agar Gels.* PNAS, 1960. **46**(6): p. 783-787.

11. Niemann, C., *Alpha-Chymotrypsin and the Nature of Enzyme Catalysis.* Science, 1964. **143**(3612): p. 1287-1296.

12. Daggett, V. and A. Fersht, *The Present View Of The Mechanism Of Protein Folding.* Nature Reviews Molecular Cell Biology-Nat Rev Mol Cell Biol, 2003. **4**(6): p. 497-502.

13. Fersht, A. and V. Daggett, *Protein Folding and Unfolding at Atomic Resolution.* Cell, 2002. **108**(4): p. 573-582.

14. Gottlieb, D., et al., *Some Properties of an Antibiotic Obtained from a Species of Streptomyces.* J. Bacteriol., 1948. **55**(3): p. 409-417.

15. Edlin, G. and P. Broda, *Physiology and genetics of the "ribonucleic acid control" locus in escherichia coli.* Bacteriol Rev., 1968. **32**(3): p. 206-226.

16. Bockamp, E., et al., *Of mice and models: improved animal models for biomedical research.* Physiol. Genomics, 2002. **11**(3): p. 115-132.

17. Kercher, M.A., P. Lu, and M. Lewis, *Lac repressor--operator complex.* Current Opinion in Structural Biology, 1997. **7**(1): p. 76-85.

18. Alberts, B., et al., *Molecular Biology of the Cell*. Fourth Edition ed. 2002: Garland. 1463.

19. Scopes, R.K., *Protein Purification, Principles and Practice, Third Edition*. Third ed. 1994, New York: Springer-Verlag. 380.

20. *Biogeochemistry of chelating agents*, ed. B. Nowack and J. VanBriessen. 2005, Washington, D.C.: American Chemical Society. 472.

21. Jakes, R., M.G. Spillantini, and M. Goedert, *Identification of two distinct synucleins from human brain.* FEBS Letters, 1994. **345**(1): p. 27-32.

22. Trojanowski, J.Q. and V. Lee, *Aggregation of Neurofilament and {alpha}-Synuclein Proteins in Lewy Bodies: Implications for the Pathogenesis of Parkinson Disease and Lewy Body Dementia.* Arch Neurol, 1998. **55**(2): p. 151-152.

23. Clayton, D.F. and J.M. George, *The synucleins: a family of proteins involved in synaptic function, plasticity, neurodegeneration and disease.* Trends in Neurosciences, 1998. **21**(6): p. 249-254.

24. Uversky, V.N., *Protein folding revisited. A polypeptide chain at the folding--misfolding--nonfolding cross-roads: which way to go?* Cellular and Molecular Life Sciences, 2003. **60**(9): p. 1852-1871.

25. Bodles, A.M., et al., *Inhibition of fibril formation and toxicity of a fragment of [alpha]-synuclein by an N-methylated peptide analogue.* Neuroscience Letters, 2004. **359**(1-2): p. 89-93.

26. Paleologou, K.E., G.B. Irvine, and O.M. El-Agnaf, *a-Synuclein aggregation in neurodegenerative diseases and its inhibition as a potential therapeutic strategy.* Biochemical Society Transactions, 2005. **33**: p. 1106-1110.

5 Continuing Studies & Opportunities for Future Development

Further work will need to explore the significant contributions that extracellular matrices (ECM) have on metabolic functionality. While alginate is well tolerated by recipients of implants, it may not provide the best physiological match for hepatocytes especially when compared to collagens and other native matrices. Methodologically though, the electrostatic process should continue to be the encapsulation method for future studies due to its ability to reproducibly generate uniform encapsulations while exposing the cells contained in the gelling media to low shear stress—a feature that is particularly important for hepatocytes.

5.1 NMR Compatible Bioreactors

Continuing improvements in electrostatic encapsulations will provide several opportunities for further development in both basic research and clinical applications. In the area of basic research, cell encapsulations may be introduced into NMR compatible bioreactors for use in real-time metabolic studies. Experiments of this variety would allow for cells to be exposed to chemical stress while metabolic functionality is monitored by NMR interrogation over a period of time. The cells in encapsulations would be held in a fixed volume region of an NMR

tube while a superfusion system would allow for media flow to be delivered across the encapsulate matrix.

NMR compatible bioreactor experiments will allow for the detection of metabolites within the cell. This is of particular importance because some charged species cannot pass from the cytoplasm into the extracellular space thereby preventing detection in media-only analysis. The media analysis can demonstrate viability and functionality but a more complete understanding of metabolic outcomes will require NMR analysis of *in vitro* cell preparations.

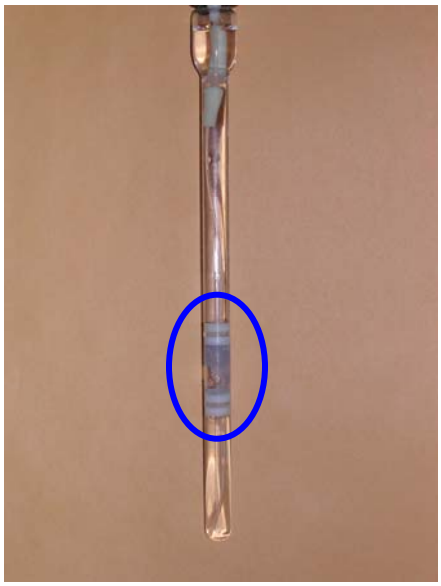

Figure 5-1
First generation NMR compatible bioreactor

Improved NMR compatible bioreactor designs have already emerged and as of this publication are being tested for use in ^{1}H and ^{31}P studies.

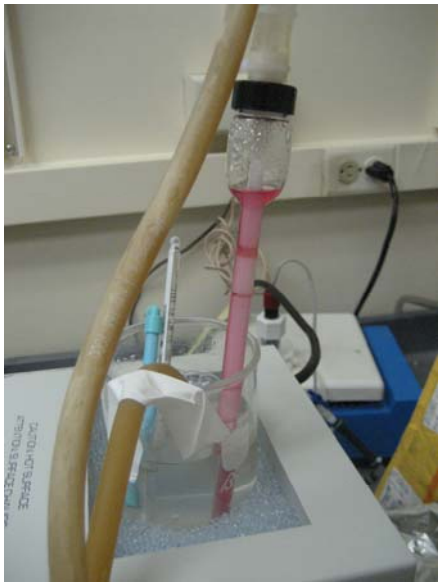

Figure 5-2
Second generation NMR compatible bioreactor

5.2 Encapsulate survival studies for NMR compatible bioreactors

While incell NMR has yet to produce successful spectra, studies to determine cell viability and effects of flow environments on encapsulate architecture have been performed. Confocal microscopy was used to image encapsulates of murine hepatocytes at 1 day, 5 day, and 10 day times points. Encapsulates were kept incubated in DMEM with 10% fetal bovine serum (FBS), penicillin, streptomycin, and dexamethasone. Images were prepared using an LSM 510 microscope. Tetra-methyl rhodamine methyl ester perchlorate (TMRM) was used to image cells containing mitochondria having a membrane potential [1]. Figure 5-3A shows an equatorial confocal slice of several encapsulates with cells nearest the alginate boundary fluorescing. Confocal stacks reveal that at all confocal planes residing

between the objective and the equator of encapsulates fluoresce suggesting that the absence of uniform fluorescence is due to either excitation light or emission light being obscured by cells laying between a given confocal plane and the detector. At a cell density of 20 million cells/ml, this type of optical phenomenon is to be expected and explains why interior cells are not observed to fluoresce as observed and discussed previously. Figure 5-3B shows the grainy interior of a single hepatocyte contained within an encapsulate. Of particular importance is the uneven intracellular distribution of the emission which is consistent with discrete mitochondria maintaining an electric potential. The image also reveals the typical geometry of mitochondria to be elliptical.

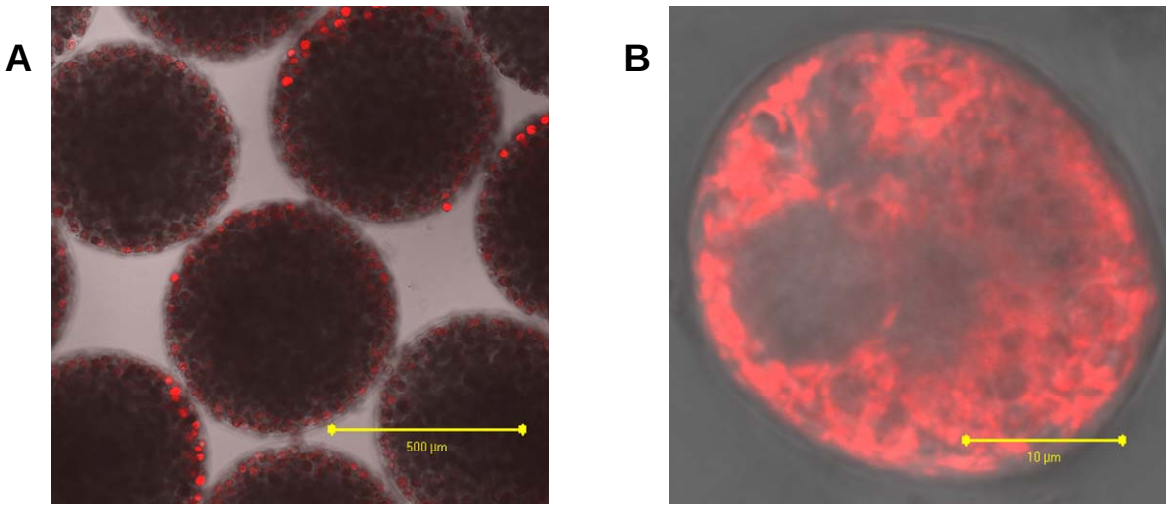

Figure 5-3
A) Encapsulates at 24 hours (10x)
B) Encapsulated cell at 24 hours (63x)

Encapsulates were inspected on day 5 of the study to observe the macro structure of encapsulates and cell viability using TMRM. Figure 5-4 presents images that are indicative of encapsulates (A) and viable cells (B) that are in tact without significant change in either shape or size.

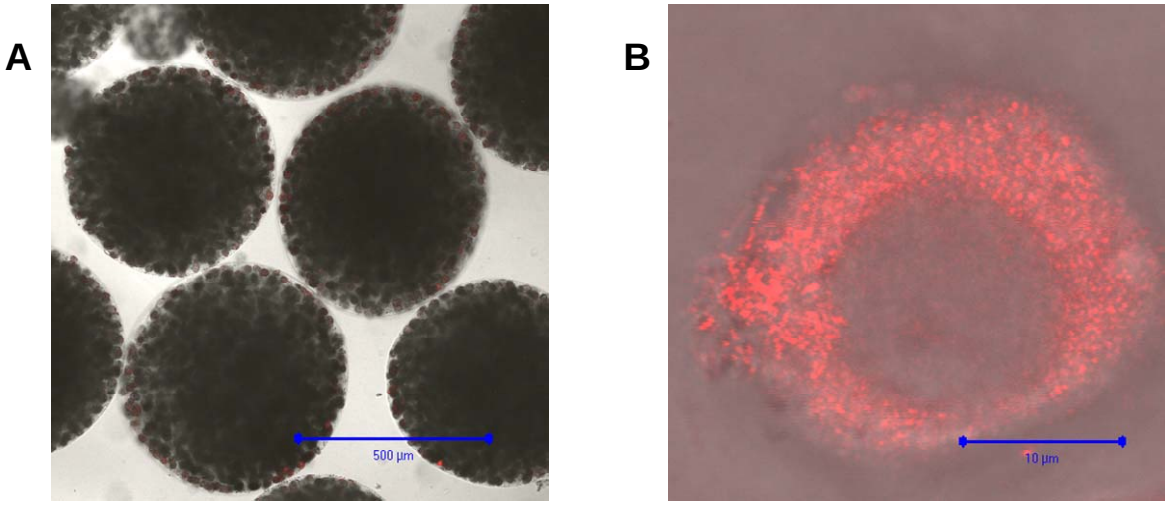

Figure 5-4
A) Encapsulates at 5 days (10x)
B) Encapsulated cell at 5 days (63x)

Encapsulations were divided into two groups on day 5. The first group was returned to standard incubation while the second group was introduced into the second generation NMR compatible bioreactor. The bioreactor system was comprised of a closed loop pump which delivered DMEM (consistent with the formulation described above) at a rate of 2ml/min. The flow passed through a gas exchange module (GEM) in which a separate closed loop recirculating water bath brought the media temperature to 37 C while allowing gas exchange across a spiraling length of silastic tubing. Figure 5-5 illustrates the GEM with labeled parts. The system was established with 125 ml of media and set for recirculation of the media during the experiment. Approximately 2.5 ml of encapsulates at a density of 20 million murine cells/ml were inoculated into the 10 mm bioreactor tube and were retained there throughout the experiment by filter baffles which allow for media flow but retain the encapsulates fixed in place within the tube.

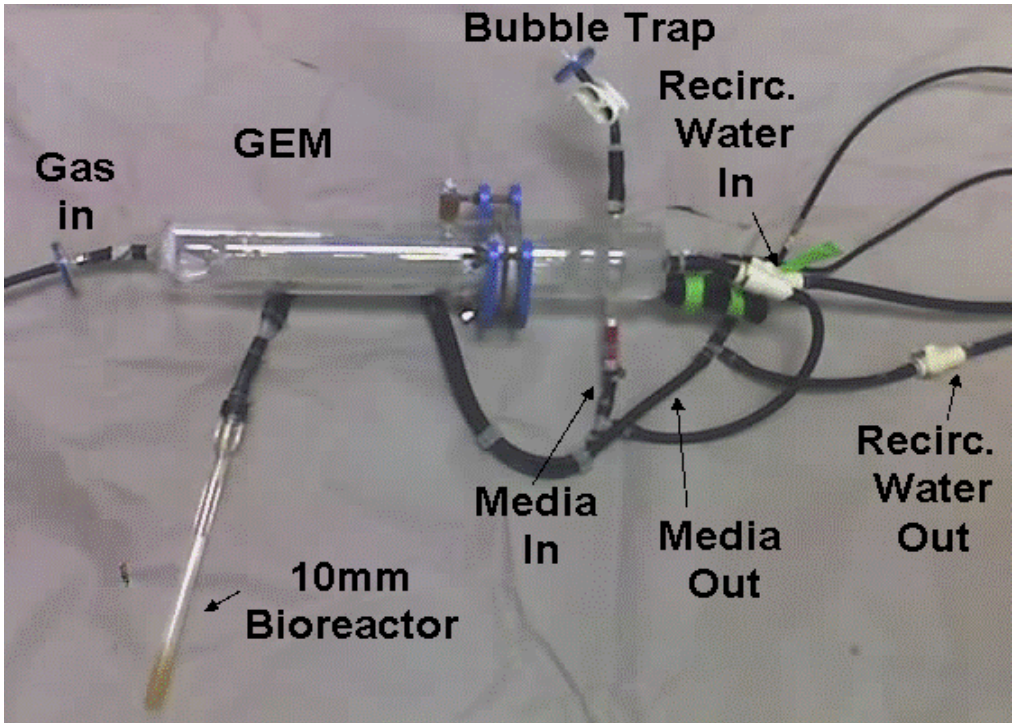

Figure 5-5
Bioreactor with Gas Exchange Module

Five days after bioreactor inoculation, encapsulates were recovered from the 10 mm bioreactor tube and were imaged confocally along with encapsulates that remained in incubation (control). Figure 5-6 shows images of the 10 day incubated encapsulates (A) and the bioreactor inoculated encapsulates which were maintained in an incubator for days 1-5 then transferred to the bioreactor for days 6-10 (B).

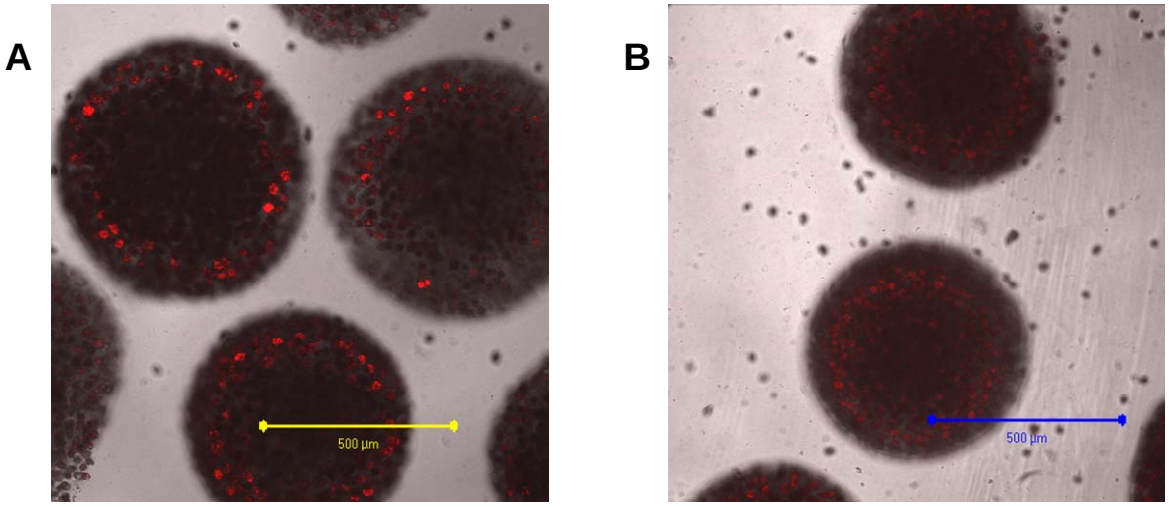

Figure 5-6
Day 10 images (10x)
A) Control B) Bioreactor

Images of individual cells taken on day 10 show uneven distribution of TMRM in both the control and bioreactor samples. In some instances, mitochondria in the control encapsulates were observed to be enlarged and round in shape rather than elliptical in shape. Figure 5-7 shows typical cells as observed on day 10 using a 63x objective.

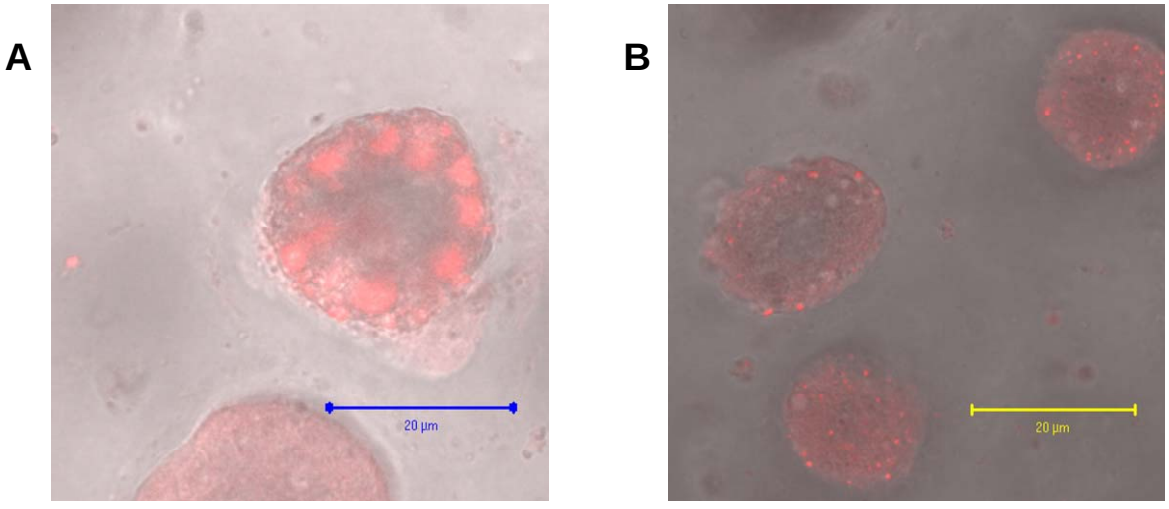

Figure 5-7
Day 10 images (63x)
A) Control B) Bioreactor

To verify the TMRM observed response, MitoTracker® Green (Molecular Probes, M7514, Eugene, OR) was applied to bioreactor encapsulates on day 10. A sample of these encapsulates was then added to non-labeled encapsulates to allow for fluorescent signals arising from fluoroprobe emissions to be differentiated from auto-fluorescence which is a common challenge for hepatocyte imaging. Figure 5-8A shows a labeled encapsulate to the left of the image in a frame containing numerous auto-fluorescing encapsulates as observed by the difference in emission intensity. The individual cells observed in Figure 5-8B show discrete mitochondria verifying the TMRM observations.

These images collectively show that the encapsulated cells can be maintained in stable encapsulates for up to five days while subjected to constant flow. This is the first demonstration of both the long term encapsulate architectural integrity and the viability of hepatocytes within encapsulates under flow conditions. Both of these findings are important steps in the development of NMR compatible bioreactor experiments which will require multi-hour or multi-day study times to acquire ^{31}P signals and other isotopically labeled compounds due to the challenges associated with capturing spectra with lower signal-to-noise measurements.

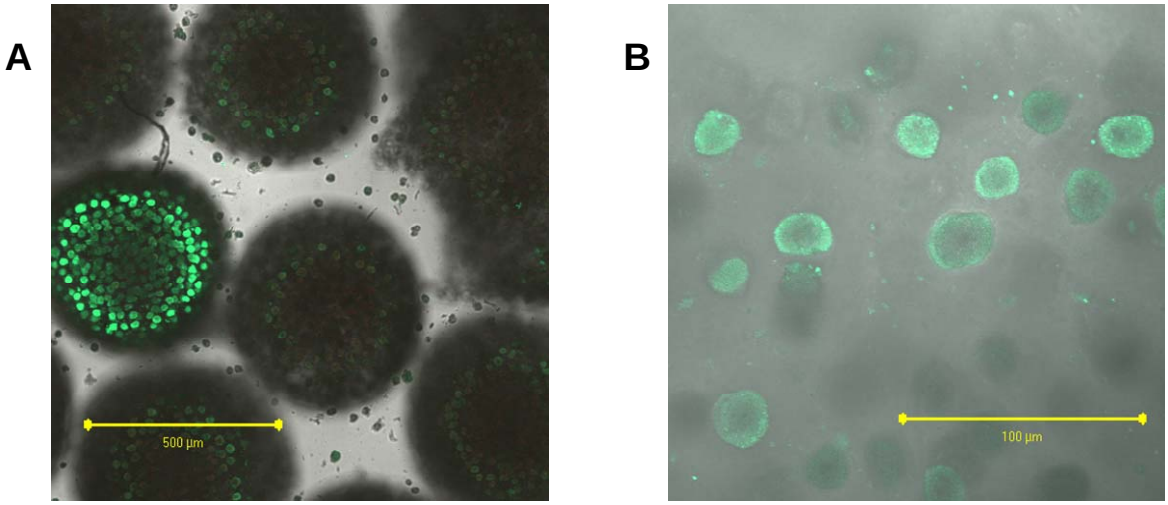

Figure 5-8 Day 10 images
A) Bioreactor (10x)
B) Bioreactor (63x)

In an effort to improve signal-to-noise quality of the spectra arising from in-cell NMR studies while limiting sample time required for each experiment, it is important to maximize the cell density within encapsulates to provide maximum signal. Such measures must be taken while simultaneously ensuring that cell viability within densely packed encapsulates is not sacrificed. At the time of this publication, uniform spherical encapsulates having a cell density of 35 million cells/ml encapsulation stock had been achieved. Figure 5-9 shows a fifteen frame series of confocal images taken 24 hours after encapsulation using 1.1 µM TMRM. Continued research should be carried out to determine viability duration and function for encapsulates at such high cell densities.

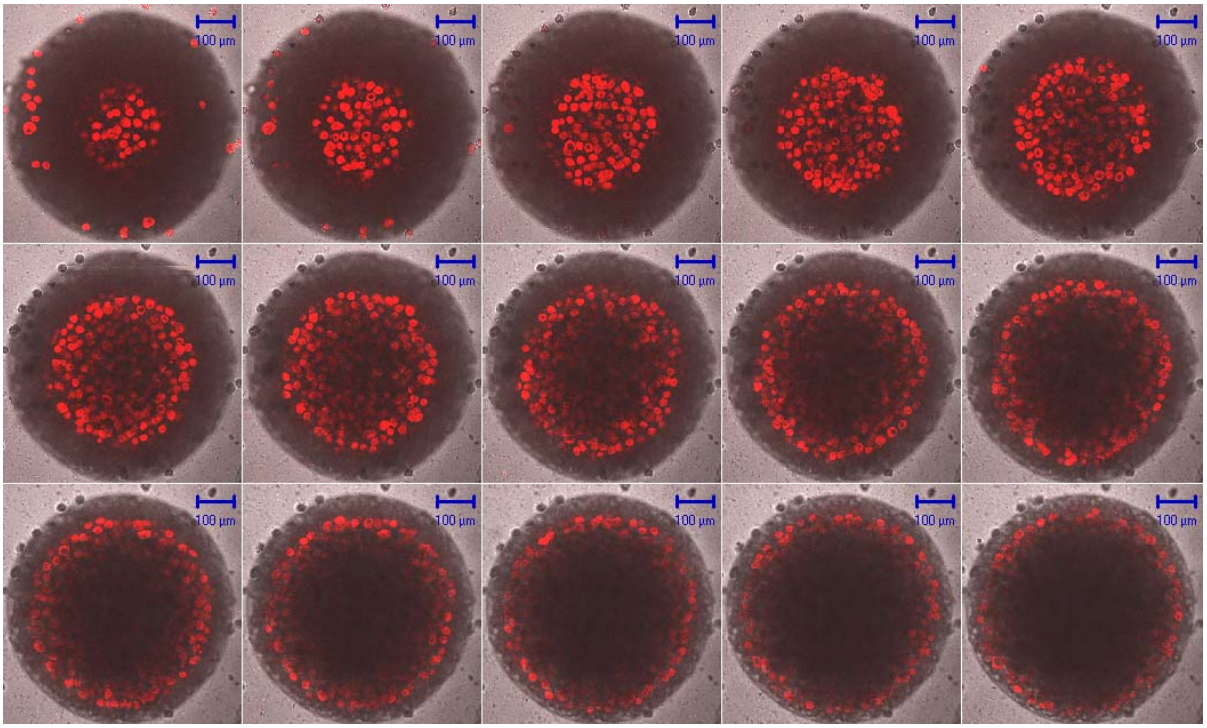

Figure 5-9
Murine Encapsulates (20x)

Figure 5-10 illustrates the spatial difference between encapsulates prepared at 20 million cells/ml and 35 million cells/ml. Both images were obtained using a 20x objective and 1.1 µM TMRM. While both samples were prepared using the same voltage (3.7 kV) and the same preparations of alginate, storage media, and $CaCl_2$ stock, the average diameter of the encapsulates differed by 3.7%. The encapsulates prepared with 20 million cells/ml had an average diameter of 599 µm while the encapsulates prepared with 35 million cells/ml had an average diameter of 622 µm. This difference is due to the viscosity or thickening of the stock which occurs as the cell density is increased. Future projects utilizing encapsulates should take care to consider encapsulation diameter effects induced by cell density. An increase in electrostatic voltage which reduces encapsulate diameter can correct for this difference.

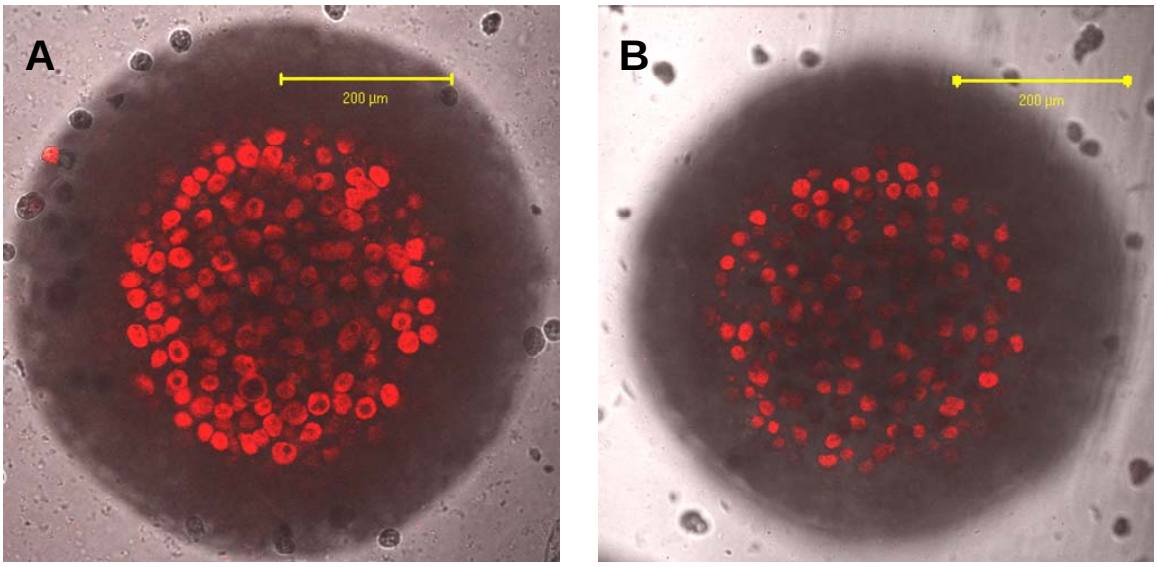

Figure 5-10
A) 35 million cells/ml
B) 20 million cells/ml

Increasing cell density should continue to be a priority in this field of study as NMR signal doubles as cell density doubles while noise is diminished by the square-root of the number of transients (n) which can be thought of as time. Therefore, a doubling of cell density improves signal-to-noise such that an equivalent experiment can be performed in one-quarter the time. Such signal-noise-improvements have profound implications for accurately measuring dynamic metabolic events and on total experimental cost.

5.3 Cryopreservation Methodology Development

Additional work in the area of cryopreservation of encapsulations should be explored. Techniques using vitrification solutions to reduce the damage due to water expansion during freezing may be employed in a manner consistent with methods

used to cryopreserve embryos. Such methods would replace water with glycerol and ethylene glycol solutions through a gradient process as a prelude to freezing [2].

5.4 Mass Transfer Studies

Questions regarding mass transfer in encapsulations should be further explored through modeling and compared to conventional gels. Furthermore, such findings will play an important role in determining the practical utility of the NMR compatible bioreactor shown above.

5.5 Metabolic Studies using Isotopic Labeled Media Components

Through the use of media constituents such as glucose or glutamine labeled with isotopic nitrogen or carbon atoms (^{15}N or ^{13}C), metabolic products can be discretely tracked from the original source through a metabolic pathway using isotopic based NMR. This method may also by used to observe changes in ATP over the time course of experiments by using. Similar tracking using non-isotopic labeling can be achieved by using fluorine replacement of protons on a compound of interest added to the media followed by fluorine NMR.

5.6 Microscopy and Histology Studies

Further microscopy and histological work should focus attention on the migration of cells within encapsulations and in adjacent encapsulations resulting in proximal cell-to-cell signaling. Determination of benefits derived from these interactions may serve to advance both clinical and basic research opportunities in the future.

5.7 Endnotes

1. Haugland, R., *Handbook of Fluorescent Probes and Research Products, 9th Edition*. 2002, Molecular Probes, Inc.: Eugene, OR.

2. Kasai, M., Mukaida, T., *Cryopreservation of animal and human embryos by vitrification*. Reproductive BioMedicine Online, 2004. **9**(2): p. 164-170.

Cited Works

Alberts, B., et al., *Molecular Biology of the Cell*. Fourth Edition ed. 2002: Garland. 1463.

Allen, J., Davey, HM, Broadhurst, D, Heald, JK, Rowland, JJ, Oliver, SG, Kell, DB, *High-throughput classification of yeast mutants for functional genomics using metabolic footprinting.* Nat. Biotechnol., 2003. **21**(6): p. 692.6.

Allen, J., Hassanein, T, Bhatia, SN, *Advances in bioartificial liver devices.* Hepatology, 2001. **34**(3): p. 447-455.

Arkadopoulos, N., et. al., *Liver assist systems: state of the art.* Int. J. Artif. Organs, 1998. **21**(12): p. 781-787.

Astegiano, M., Sapone, N., Demarchi, B., Rossetti, S., Bonardi, R., Rizzetto, M., *Laboratory evaluation of the patient with liver disease.* Eur Rev Med Pharmacol Sci, 2004. **8**(1): p. 3-9.

Bailey, J.E., Ollis, D.F., *Biochemical Engineering Fundamentals*. 2nd ed. 1986, New York: McGraw-Hill. 984.

Bax, A., et al., *Comparison of different modes of two-dimensional reverse-correlation NMR for the study of proteins.* Journal of Magnetic Resonance (1969), 1990. **86**(2): p. 304-318.

Bell, J., Brown, JC, Sandler, PJ, *NMR studies of body fluids.* NMR Biomed., 1989. **2**(5-6): p. 242-56.

Bockamp, E., et al., *Of mice and models: improved animal models for biomedical research.* Physiol. Genomics, 2002. **11**(3): p. 115-132.

Bodenhausen, G. and D.J. Ruben, *Natural abundance nitrogen-15 NMR by enhanced heteronuclear spectroscopy*. Chemical Physics Letters, 1980. **69**(1): p. 185-189.

Bodles, A.M., et al., *Inhibition of fibril formation and toxicity of a fragment of [alpha]-synuclein by an N-methylated peptide analogue.* Neuroscience Letters, 2004. **359**(1-2): p. 89-93.

Bollard, M., Stanley, E., Lindon, J., Nicholson, J., Holmes, E., *NMR-based metabonomic approaches for evaluating physiological influences on biofluid composition.* NMR in Biomedicine, 2005. **18**(3): p. 143-162.

Bozzola, J., Russell, L.,, *Electron Microscopy Principles and Techniques for Biologists*. 2nd ed. 1999, Sudbury, Mass.: Jones and Bartlett Publishers. 670.

Bryant, J.E., et al., *Protein Dynamics in Living Cells.* Biochemistry, 2005. **44**(26): p. 9275-9279.

Bubb, W., Wright, LC, Cagney, M, Santangelo, RT, Sorrell, TC, Kuchel, PW, *Heteronuclear NMR studies of metabolites produced by Cryptococcus neoformans in culture media: Identification of possible virulence factors.* Magnetic Resonance in Medicine, 1999. **42**(3): p. 442-453.

Butcher, E.C., *Can Cell Systems Biology Rescue Drug Discovery?* Nature Reviews Drug Discovery, 2005. **4**(6): p. 461-467.

Charlton, L.M. and G.J. Pielak, *Peeking into living eukaryotic cells with high-resolution NMR.* PNAS, 2006. **103**(32): p. 11817-11818.

Clayton, D.F. and J.M. George, *The synucleins: a family of proteins involved in synaptic function, plasticity, neurodegeneration and disease.* Trends in Neurosciences, 1998. **21**(6): p. 249-254.

Dabos, K.J., Parkinson, J.A., Hewage, C., Nelson, L.J., Sadler, I.H., Hayes, P.C., Plevris, J.N., *H NMR spectroscopy as a tool to evaluate key metabolic functions of primary porcine hepatocytes after cryopreservation.* NMR in Biomedicine, 2002. **15**(3): p. 241-250.

Daggett, V. and A. Fersht, *The Present View Of The Mechanism Of Protein Folding.* Nature Reviews Molecular Cell Biology-Nat Rev Mol Cell Biol, 2003. **4**(6): p. 497-502.

Dixit V, G.G., *Artificial liver support: state of the art.* Scand J Gastroenterol Suppl., 1996. **220**: p. 101-114.

Doyle, e.a., *Process for Making Capsules*. 1964: United States.

Edlin, G. and P. Broda, *Physiology and genetics of the "ribonucleic acid control" locus in escherichia coli.* Bacteriol Rev., 1968. **32**(3): p. 206-226.

Fersht, A. and V. Daggett, *Protein Folding and Unfolding at Atomic Resolution.* Cell, 2002. **108**(4): p. 573-582.

Fremond, B., et. al., *Cell-based therapy of acute liver failure: the extracorporeal bioartificial liver.* Cell Biol. Toxicol., 1996. **12**(4-6): p. 325-329.

Gadian, D.G., *NMR and Its Applications to Living Systems*. 2nd ed. 1995, New York: Oxford University Press. 283.

Geddes, L.A., J.D. Bourland, and G. Ford, *The mechanism underlying sudden death from electric shock.* Medical Instrumentation, 1986. **20**(6): p. 303-315.

Gerlach, J., Schnoy, N., et. al., *Comparison of hollow fibre membranes for hepatocyte immobilisation in bioreactors.* Int. J. Artif. Organs, 1996. **19**(10): p. 610-616.

Gerlach, J., Ziemer, R., Neuhaus, P., *Fulminant liver failure: relevance of extracorporeal hybrid liver support systems.* Int. J. Artif. Organs, 1996. **19**(1): p. 7-13.

Gillies, R.J., *Nuclear Magnetic Resonance and its Applications to Physiological Problems.* Annual Review of Physiology, 1992. **54**(1): p. 733-748.

Gitlin, N., Serio, K., *Ischemic hepatitis: widening horizons.* Am J Gastroenterol, 1992. **87**(7): p. 831-836.

Glacken, M., et. al., *Large scale production of mammalian cells and their products: Engineering principles and barriers to scale-up.* Ann. New York Academy of Sciences, 1983. **413**: p. 355-372.

Glicklis, R., Shapiro, L., et. al., *Hepatocyte behavior within three-dimensional porous alginate scaffolds.* Biotechnology and Bioengineering, 2000. **67**(3): p. 344-353.

Gottlieb, D., et al., *Some Properties of an Antibiotic Obtained from a Species of Streptomyces.* J. Bacteriol., 1948. **55**(3): p. 409-417.

Grabowski, H., *Are the Economics of Pharmaceutical Research and Development Changing? Productivity, Patents and Political Pressures.* PharacoEconomics, 2004. **22, Suppl. 2**: p. 15-24.

Guyton, A.C., Hall, J.E., *Textbook of Medical Physiology*. 10 ed. 2000, Philadelphia: W.B.Saunders. 1064.

Haugland, R., *Handbook of Fluorescent Probes and Research Products, 9th Edition*. 2002, Molecular Probes, Inc.: Eugene, OR.

Hechter, O., et al., *Modification of the Structure of Water in Agar Gels.* PNAS, 1960. **46**(6): p. 783-787.

Holmes, E., et al., *Chemometric Models for Toxicity Classification Based on NMR Spectra of Biofluids.* Chem. Res. Toxicol., 2000. **13**(6): p. 471-478.

Holmes, E., J.K. Nicholson, and G. Tranter, *Metabonomic Characterization of Genetic Variations in Toxicological and Metabolic Responses Using Probabilistic Neural Networks.* Chem. Res. Toxicol., 2001. **14**(2): p. 182-191.

Hughes, R., Williams, R., *Use of bioartificial and artificial liver support devices.* Semin. Liver Disease, 1996. **16**(4): p. 435-444.

Hynes, C.R., *A Thoughtful Approach To Field-Service Grounding.* Electrostatic Discharge Journal, 1989. **1989**(Feb./Mar.).

Ichihara, A., Nakamura, T., Tanaka, K., *Biochemical functions of adult rat hepatocytes in primary culture.* Ann. New York Academy of Sciences, 1980. **349**: p. 77-84.

Ijima, H., et. al., *Development of a hybrid artificial liver using a polyurethane foam/hepatocyte-spheroid packed-bed module.* Int. J. Artif. Organs, 2000. **23**(6): p. 389-97.

Jakes, R., M.G. Spillantini, and M. Goedert, *Identification of two distinct synucleins from human brain.* FEBS Letters, 1994. **345**(1): p. 27-32.

Kasai, M., Mukaida, T., *Cryopreservation of animal and human embryos by vitrification.* Reproductive BioMedicine Online, 2004. **9**(2): p. 164-170.

Kell, D., et al., *Metabolic footprinting and systems biology: the medium is the message.* Nat Rev Micro, 2005. **3**(7): p. 557-565.

Kell, D.B., *Metabolomics and systems biology: making sense of the soup.* Current Opinion in Microbiology, 2004. **7**(3): p. 296-307.

Kercher, M.A., P. Lu, and M. Lewis, *Lac repressor--operator complex.* Current Opinion in Structural Biology, 1997. **7**(1): p. 76-85.

King, A., *Alginate Microcapsules for Use in Trasplantation of Islets of Langerhans.* 2001, Acta Universitatis Upsaliensis: Uppsala, Sweden. p. 43.

King, A., Lau, J., Nordin, A., Sandler, S., Andersson, A., *The Effect of Capsule Composition in the Reversal of Hyperglycemia in Diabetic Mice Transplanted with Microencapsulated Allogeneic Islets.* Diabetes Technology & Therapeutics, 2003. **5**(4): p. 653-663.

Knight, J., *Liver Function Tests: Their Role in the Diagnosis of Hepatobiliary Diseases.* Journal of Infusion Nursing, 2005. **28**(2): p. 108-117.

Konstantinos, J.D., Parkinson, J.A., et. al, *1H NMR spectroscopy as a tool to evaluate key metabolic functions of primary porcine hepatoctyes after cryopreservation.* NMR in Biomedicine, 2002. **15**: p. 241-250.

Kriat, M., Confort-Gouny, S., Vion-Dury, J., Sciaky, M., Viout, P., Cozzone, P., *Quantitation of metabolites in human blood serum by proton magnetic resonance spectroscopy. A comparative study of the use of formate and TSP as concentration standards.* NMR Biomed., 1992. **5**(4): p. 179-94.

Kuesel, A.C., Graschew, G., Hull, W., Lorenz, W. Thielmann, H.W., *31P NMR studies of cultured human tumor cells. Influence of pH on phospholipid metabolite levels and the detection of cytidine 5'-diphosphate choline.* NMR Biomed., 1990. **3**(2): p. 78-89.

Lacy, P., Hegre, OD, et. al, *Maintenance of normoglycemia in diabetic mice by subcutaneous xenografts of encapsulated islets.* Science, 1991. **254**: p. 1782-1784.

Lehninger, A.L., *Principles of Biochemistry*. 4th ed. ed, ed. D.L. Nelson, Cox, M.M. 2005, New York: W.H. Freeman and Company. 1119.

Lieber, C.S., *Metabolism of alcohol.* Clin Liver Dis, 2005. **9**(1): p. 1-35.

Liu, G., et al., *NMR data collection and analysis protocol for high-throughput protein structure determination.* PNAS, 2005. **102**(30): p. 10487-10492.

MacDonald JM, W.S., Roy-Chowdhury I, Kubota H, Reid LM., *Effect of Flow Configuration and Membrane Characteristics on Membrane Fouling in a Novel Multicoaxial Hollow-Fiber Bioartificial Liver.* Ann NY Acad Sci, 2001. **944**(1): p. 334-343.

MacDonald, J.M., et al., *Bioartificial livers*, in *Cell Encapsulation Technology and Therapeutics*, W. Kuhtreiber, R.P. Lanza, and W.L. Chick, Editors. 1998, Birkhauser: Boston.

Macdonald, J.M., et al., *Liver Cell Culture and Lineage Biology*, in *Methods of Tissue Engineering*, A. Atala and R.P. Lanza, Editors. 2002, Academic Press: Boston. p. 151-195.

Macdonald, J.M., et. al., *Chapter 21 Bioartificial Livers*, in *Cell Encapsulation Technology and Therapeutics (Tissue Engineering)*, W.M. Kuhtreiber, Lanza, R.P., and Chick, W.L., Editor. 1999, Birkhäuser: Boston. p. 450.

Macdonald, J.M., Grillo, M., Schmidlin, O., Tajiri, D.T., James, T.L., *NMR spectroscopy and MRI investigation of a potential bioartificial liver.* NMR in Biomedicine, 1998. **11**(2): p. 55-66.

Macdonald, J.M., Wolfe, S.P., *Bioreactor design and process for engineering tissue from cells*. 2005, University of North Carolina at Chapel Hill: USA. p. 13.

Mancuso, A., Sharfstein, S.A., Fernandez, E.J., Clark, D.S. Blanch, H.W., *Effect of extracellular glutamine concentration on primary and secondary metabolism of a murine hybridoma: An in vivo 13C nuclear magnetic resonance study*. Biotechnology and Bioengineering, 1998. **57**(2): p. 172-186.

Maniara, G., et al., *Method Performance and Validation for Quantitative Analysis by 1H and 31P NMR Spectroscopy. Applications to Analytical Standards and Agricultural Chemicals.* Anal. Chem., 1998. **70**(23): p. 4921-4928.

Margulis, M., Erukhimov, E., Andreiman, L., Viksna, L., *Temporary organ substitution by hemoperfusion through suspension of active donor hepatocytes in a total complex of intensive therapy in patients with acute hepatic insufficiency*. Resuscitation, 1989. **18**(1): p. 85-94.

Matsumura, K., Guevara, G., Huston, H., Hamilton, W., Rikimaru, M., Yamasak,i G., Matsumura, M., *Hybrid bioartificial liver in hepatic failure: preliminary clinical report*. Surgery, 1987. **101**(1): p. 99-103.

McClelland, R.E., Coger, R.N., *Effects of Enhanced O2 Transport on Hepatocytes Packed within a Bioartificial Liver Device.* Tissue Engineering, 2004. **10**(1-2): p. 253-266.

McClelland, R.E., MacDonald, J.M., Coger, R.N., *Modeling O2 transport within engineered hepatic devices.* Biotechnology and Bioengineering, 2003. **82**(1): p. 12-27.

Mendes, P., *Emerging bioinformatics for the metabolome.* Briefings in Bioinformatics, 2002. **3**(2): p. 134-145.

Nicholson, J., Buckingham, M., Sadler, P., *High resolution H NMR studies of vertabrate blood and plasma.* Biochem. J., 1983. **211**: p. 605-615.

Nicholson, J.K., J.C. Lindon, and E. Holmes, *'Metabonomics': understanding the metabolic responses of living systems to pathophysiological stimuli via multivariate statistical analysis of biological NMR spectroscopic data.* Xenobiotica, 1999. **29**(11): p. 1181-1189.

Niemann, C., *Alpha-Chymotrypsin and the Nature of Enzyme Catalysis.* Science, 1964. **143**(3612): p. 1287-1296.

Nowack, B. and J. VanBriessen, *Biogeochemistry of chelating agents*, ed. B. Nowack and J. VanBriessen. 2005, Washington, D.C.: American Chemical Society. 472.

O'Leary, D.J., Hawkes, S.P., Wade, C.G., *Indirect monitoring of carbon-13 metabolism with NMR: analysis of perfusate with a closed-loop flow system.* Magn. Reson. Med., 1987. **5**(6): p. 572-577.

O'Leary, D.J., Hawkes, S.P., Wade, C.G., *Indirect monitoring of carbon-13 metabolism with NMR: analysis of perfusate with a closed-loop flow system.* Magn. Reson. Med., 1987. **5**(6): p. 572-7.

Paleologou, K.E., G.B. Irvine, and O.M. El-Agnaf, *a-Synuclein aggregation in neurodegenerative diseases and its inhibition as a potential therapeutic strategy.* Biochemical Society Transactions, 2005. **33**: p. 1106-1110.

Papas, K., Long, R., Sambanis A., ConstantinidisI., *Development of a bioartificial pancreas: I. Long-term propagation and basal and induced secretion from entrapped BETA TC3 cell cultures.* Biotechnology and Bioengineering, 1999. **66**(4): p. 219-230.

Pham-Tuan, H., et al., *Method development in high-performance liquid chromatography for high-throughput profiling and metabonomic studies of biofluid samples.* Journal of Chromatography B, 2003. **789**(2): p. 283-301.

Quinn, P., Johnston, D., *Detection of chronic liver disease: costs and benefits.* Gastroenterologist, 1997. **5**(1): p. 58-77.

Ringel, M., et al., *Hepatocytes cultured in alginate microspheres: an optimized technique to study enzyme induction.* Toxicology, 2005. **206**(1): p. 153-167.

Rotem, A., Toner, M., et. al., *Oxygen uptake rates in cultured rat hepatocytes.* Biotechnology and Bioengineering, 1992. **40**: p. 1286-1291.

Schwartz, R.E., et al., *Multipotent adult progenitor cells from bone marrow differentiate into functional hepatocyte-like cells.* J. Clin. Invest., 2002. **109**(10): p. 1291-1302.

Scopes, R.K., *Protein Purification, Principles and Practice, Third Edition*. Third ed. 1994, New York: Springer-Verlag. 380.

Seglen, P.O., *Preparation of isolated rat liver cells.* Methods of Cell Biology, 1976. **13**: p. 29-83.

Selenko, P., et al., *Quantitative NMR analysis of the protein G B1 domain in Xenopus laevis egg extracts and intact oocytes.* PNAS, 2006. **103**(32): p. 11904-11909.

Serp, D., Cantana, E., et. al., *Characterization of an encapsulation device for the production of monodisperse alginate beads for cell immobilization.* Biotechnology and Bioengineering, 2000. **70**(1): p. 41-53.

Sina Reckel, F.L., Volker Dötsch,, *In-Cell NMR Spectroscopy.* ChemBioChem, 2005. **6**(9): p. 1601-1606.

Sumner, L.W., P. Mendes, and R.A. Dixon, *Plant metabolomics: large-scale phytochemistry in the functional genomics era.* Phytochemistry, 2003. **62**(6): p. 817-836.

Sun, C., , Huth J. R., Hajduk, P.J.,, *NMR in Pharmacokinetic and Pharmacodynamic Profiling.* ChemBioChem, 2005. **6**(9): p. 1592-1600.

Tilles, A.W., et al., *Bioengineering of liver assist devices.* Journal of Hepato-Biliary-Pancreatic Surgery, 2002. **9**(6): p. 686-696.

Trojanowski, J.Q. and V. Lee, *Aggregation of Neurofilament and {alpha}-Synuclein Proteins in Lewy Bodies: Implications for the Pathogenesis of Parkinson Disease and Lewy Body Dementia.* Arch Neurol, 1998. **55**(2): p. 151-152.

U.S. Department of Health and Human Services, F.D.A., *Innovation or Stagnation: Challenge and opportunity on the Critical Path to New Medical Products.* 2004.

U.S. Department of Health and Human Services, N.I.f.O.S.a.H., *NIOSH ALERT: Preventing fatalities of workers who contact electrical energy*. 1986. Publication No. 87-103.

Uversky, V.N., *Protein folding revisited. A polypeptide chain at the folding--misfolding--nonfolding cross-roads: which way to go?* Cellular and Molecular Life Sciences, 2003. **60**(9): p. 1852-1871.

Wang, J., Clark, J.B., et. al., *Proliferation and hepatic differentiation of adult-derived progenitor cells.* Cells Tissues Organs, 2003. **173**(4): p. 193-203.

Weljie, A.M., et al., *Targeted Profiling: Quantitative Analysis of ¹H NMR Metabolomics Data.* Anal. Chem., 2006. **78**(13): p. 4430-4442.

Wolf, C., Munkelt, B., *Bilirubin coujugation by an artificial liver composed of cultured cells and synthetic capillaries.* Transactions of the American Socity of Artificial Internal Organs, 1975. **21**: p. 16-27.

Wolfe, S.P., Hsu, E., Reid, L.M., Macdonald, J.M., *A novel multi-coaxial hollow fiber bioreactor for adherent cell types. Part 1: Hydrodynamic studies.* Biotechnology and Bioengineering, 2002. **77**(1): p. 83-90.

Wuthrich, K., *Protein structure determination in solution by NMR spectroscopy*. J. Biol. Chem., 1990. **265**(36): p. 22059-22062.

Yagi, K., Tsuda, K., Serada, M., Yamada, C., Kondoh, A., Miura, Y., *Rapid formation of multicellular spheroids of adult rat hepatocytes by rotation culture and their immobilization within calcium alginate.* Artificial Organs, 1993. **17**(11): p. 929-34.

Zhou, F.B., J., Zeng, A., Yuan, J., *A macrokinetic model for myeloma cell culture based on stoichiometric balance.* Biotechnol Appl Biochem, 2007. **46**(Pt 2): p. 85-95.